

**MODELING CHARCOT MARIE TOOTH 1A  
WITH HUMAN PLURIPOTENT STEM CELLS**

by

Bipasha Mukherjee-Clavin

A dissertation submitted to Johns Hopkins University in conformity with the  
requirements for the degree of Doctor of Philosophy

Baltimore, Maryland  
May 2015

## ABSTRACT

We have developed a defined protocol for the direct derivation and prospective isolation of Schwann cells from human embryonic and induced pluripotent stem cells. Potential uses of these cells include disease modeling, drug screening, and transplantation therapy, making it an exciting platform for translational research and personalized medicine. This method was applied to model CMT1A, a genetic peripheral neuropathy characterized by a 1.4 MB duplication on chromosome 14. Results from profiling CMT1A hiPSC-Schwann cells were validated using CMT1A PGD-hESC-Schwann cells and CMT1A iNC-Schwann cells. All three models displayed increased expression of the Peripheral Myelin Protein (*PMP22*) transcript, the gene believed to cause CMT1A. Two of the three models demonstrated upregulated expression of the heparan sulfate biosynthesis gene, *HS3ST3b1*, which is also located in the 1.4 MB CMT1A duplicated region, plays a rate limiting role in heparan sulfate fine structure biosynthesis, and whose specific role in Schwann cells is yet to be determined. Most interestingly, two pro-inflammatory cytokines, CXCL1 and MCP-1 proteins, were ultimately commonly overexpressed in all three models, and their overexpression was also confirmed in nerve biopsies from two CMT1A patients. It was also found that CMT1A Schwann cells of all three models could more readily recruit human THP-1 monocytes, and that this recruitment occurred in an MCP-1 dependent manner. Finally, through treatment with three small molecules previously identified to decrease *PMP22* gene expression, we found a compound (bortezomib) that decreased both *PMP22* gene

and MCP-1 protein expression in Schwann cells from hiPSCs from one patient, in an example of how hiPSC-derived Schwann cells may be used for patient-specific therapeutic studies going forward.

These results imply pro-inflammatory cytokine release may comprise an intrinsic and early property of nascent Schwann cells, and that immune dysregulation may be an early contributor to CMT1A pathogenesis, as opposed to a secondary reaction. Finally, the broadest contribution of this study is a methodological one, in which all three reprogrammed Schwann cell models were utilized to demonstrate a converged phenotype. This approach offers a technical alternative to genome editing for disease hiPSC phenotype validation, and comprises a feasible model for future studies.

Thesis readers:

Gabsang Lee, DVM/PhD (Thesis mentor)

Charlotte Sumner, MD (Thesis committee chair)

## ACKNOWLEDGMENTS

This work would not have been possible without the support and influence of many individuals. I'd first and foremost like to thank my thesis mentor, Gabsang Lee, for the opportunity to work on what I hope will become a fundamental part of our lab's portfolio. I've appreciated his keen ability to identify and address impactful scientific questions, and I hope to hone this skill going forward in my own career.

I'd also like to thank my husband, Chris, for his patient support of my scientific and academic endeavors, and for keeping me company during many nights and weekends of stem cell culture. He is one of the few people who truly understands my idealistic drive to become a physician-scientist, and while he may not fully share my somewhat masochistic tendencies, his support, advice, and encouragement has been instrumental during this journey.

My parents have also played a critical role in shaping my ideals and career goals. My mother worked tirelessly throughout childhood to ensure that I received a good education, and my father instilled in me a desire to use the resources and opportunities available to me to contribute meaningfully to society. My younger sister mostly distracted me from my studies for much of my life, but now she's a pretty great friend and confidant.

I moved from California to Baltimore six years ago, not knowing anyone on the entire Atlantic coast. Over the past several years, my classmates at the Johns Hopkins MSTP have become like an extended family of cheerleaders and supporters. Wan, Carolina, Bridget, Eliah, Chris Cashman, and many others have

been great friends and I look forward to us becoming fellow colleagues and collaborators in the future.

Finally, I'd like to thank the patients and families whose contributions make such work possible. All of this work relies upon voluntary tissue donation from patients and parents, and I am humbled to have the opportunity to participate in this effort. Biomedical research is truly a team effort, and it is my honor and privilege to be a part of that team.

## TABLE OF CONTENTS

ABSTRACT .....	i
ACKNOWLEDGMENTS .....	iii
TABLE OF CONTENTS .....	v
LIST OF FIGURES.....	vii
CHAPTER 1: INTRODUCTION .....	1
Schwann cell development and engineering.....	2
An overview of CMT1A .....	4
Rodent models of CMT1A.....	7
Comparison of CMT1A rodent models and CMT1A patients.....	9
Immunocompetence of Schwann cells.....	12
CHAPTER 2: DIRECTED DIFFERENTIATION OF HUMAN EMBRYONIC STEM CELLS INTO SCHWANN CELLS .....	16
Introduction .....	17
Methods.....	19
Results.....	24
Discussion .....	33
Conclusion.....	38
CHAPTER 3: MODELING CMT1A WITH HUMAN INDUCED PLURIPOTENT STEM CELL DERIVED SCHWANN CELLS .....	39
Introduction .....	40
Methods.....	42
Results.....	46
Discussion .....	61
Conclusion.....	67

CHAPTER 4: VALIDATION OF THE CMT1A hiPSC PHENOTYPE WITH TWO ADDITIONAL PATIENT DERIVED CMT1A MODELS .....	68
Introduction .....	69
Methods .....	72
Results.....	78
Discussion .....	96
Conclusion.....	102
CHAPTER 5: DISCUSSION AND CONCLUSIONS .....	103
Wrapping it all up: From <i>PMP22</i> to demyelination and dysmyelination.....	104
Future applications of patient-derived Schwann cells .....	113
Final perspectives.....	117
REFERENCES .....	118
APPENDIX 1: Protocol for Schwann cell differentiation from human pluripotent stem cells .....	130
APPENDIX 2: Tables of primers and antibodies .....	141
CURRICULUM VITAE .....	143

## LIST OF FIGURES

Figure 2-1: LSB2i differentiation schematic .....	<b>29</b>
Figure 2-2: LSB2i treatment yields a mixed population of Schwann cells and neurons .....	<b>30</b>
Figure 2-3: Global gene expression profiling of ES, NC, and CD49d+ Schwann cells .....	<b>31</b>
Figure 2-4: Post-FACS purification plating and culturing of CD49d+ Schwann cells .....	<b>32</b>
Figure 3-1: CMT1A hiPSC generation and Schwann cell differentiation overview...	<b>52</b>
Table 3-1: Control and CMT1A lines included in this study .....	<b>53</b>
Figure 3-2 CMT1A patient-derived hiPSCs exhibit clonal morphology and express pluripotency markers.....	<b>54</b>
Figure 3-3: CMT1A hiPSC quality control .....	<b>55</b>
Figure 3-4: CMT1A hiPSC differentiation into Schwann cells.....	<b>56</b>
Figure 3-5: Global gene expression profiling of CMT1A hiPSC-Schwann cells.....	<b>57</b>
Figure 3-6: Gene ontology and pathway analysis of CMT1A hiPSC-Schwann cell expression profiling results.....	<b>58</b>
Figure 3-7: Validation of CMT1A hiPSC-Schwann cell microarray results.....	<b>59</b>
Figure 3-8: Microarray expression of CMT1A duplicated region genes .....	<b>60</b>
Figure 4-1: Comparison of hiPSCs, hESCs, and directly converted cells .....	<b>85</b>
Figure 4-2: Use of three congruent Schwann cell models to find a converged phenotype.....	<b>86</b>
Figure 4-3: Overview of CMT1A PGD-hESC-Schwann cell generation and characterization .....	<b>87</b>
Figure 4-4: CMT1A PGD-hESC differentiation into Schwann cells .....	<b>88</b>
Figure 4-5: Validation of CMT1A hiPSC-Schwann cell microarray results with CMT1A PGD-hESC-Schwann cells .....	<b>89</b>
Figure 4-6: Overview of CMT1A iNC-Schwann cell generation and characterization .....	<b>90</b>



Figure 4-7: Validation of CMT1A hiPSC-Schwann cell microarray results with CMT1A iNC-Schwann cells..... **91**

Figure 4-8: Three congruent CMT1A models reveal a converged phenotype that is consistent with patient nerve biopsies ..... **92**

Figure 4-9: THP-1 human monocytes are more readily recruited to CMT1A Schwann cells in a MCP-1 dependent manner..... **93**

Figure 4-10: Pharmacological treatment can decrease MCP-1 and CXCL1 release in a patient derived hiPSC line..... **94**

Table 4-1: Summary of all genotypes included in this study ..... **95**

## CHAPTER 1: INTRODUCTION

## **Schwann cell development and engineering**

Schwann cells are the myelinating and non-myelinating glia of the peripheral nervous system. They are one of many derivatives of neural crest, a multipotent cell type that delaminates from the dorsal neural tube and migrates throughout the body to give rise to specialized cell types<sup>1</sup>. Neural crest along different positions on the anterior-posterior axis give rise to different cell types. Most anteriorly, cranial neural crest form the craniofacial bones, cartilage, and ganglia. Trunk neural crest give rise to the dorsal root ganglia, Schwann cells, sympathetic ganglia, adrenal medulla, and melanocytes. The cardiac neural crest generate neurons, melanocytes, fibroblasts, chondrocytes, and also play a role in cardiac septation. Finally the vagal and sacral neural crest create the enteric nervous system and parasympathetic ganglia<sup>2,3</sup>.

Schwann cell development from neural crest occurs over a number of embryonic and postnatal transitions. During embryonic gliogenesis, the neural crest first give rise to the Schwann cell precursor (seen at rat E14/15), which can be distinguished from neural crest by its expression of Myelin Protein Zero and Cadherin 19. At this stage, the Schwann cell precursors (SCPs) are associated with axons, and the neurons and SCPs are mutually dependent for survival. In particular, it appears Neuregulin 1 type III (NRG1-III) is the relevant axon-associated signal that permits Schwann cell precursor survival<sup>4,5</sup>.

Around rat E17/18, the Schwann cell precursors evolve into immature Schwann cells, and transition from merely being associated with axons to selectively ensheathing groups of axons. Then around birth, in preparation for

myelination, individual Schwann cells begin to surround large diameter axons in a 1:1 ratio, in a process known as radial sorting. These pro-myelinating Schwann cells will eventually develop into myelinating Schwann cells in a process requiring profound molecular changes, including activation of transcription factors *Oct6*, *Krox20*, and perhaps *Brn2*. In contrast to the myelinated large diameter axons, some of the smaller diameter axons remain unmyelinated in Remak bundles and are surrounded by non-myelinating Schwann cells that continue to provide metabolic and trophic support<sup>4,5</sup>.

By mimicking the *in vivo* processes orchestrating Schwann cell development, we may be able to generate Schwann cells *in vitro* as well. Major technological strides in biology now give us the ability to engineer cell types *in vitro*, either through directed differentiation from human pluripotent stem cells (hPSCs) (collectively, human embryonic stem cells and human induced pluripotent stem cells) or via direct lineage conversion from somatic cells (ie fibroblasts). Engineered or reprogrammed human Schwann cells are desirable for a number of applications including: 1) *in vitro* disease modeling, often in a patient-specific manner, 2) high throughput *in vitro* drug screening, possibly in a patient specific manner, and 3) cell transplantation therapy, possibly using patient-matched cells, although this goal is the most elusive of the three.

This thesis began four years ago, with the initial goal of developing a methodology for the efficient differentiation of Schwann cells from human pluripotent stem cells. Over the course of this thesis, another such protocol has been published with this goal in mind<sup>6</sup>, yet we believe that our methodology offers

several advantages including: use of a 2D monolayer culture system (vs a 3D embryoid body or neurosphere culture system; a monolayer culture systems allow for more homogeneity in cell fate specification), direct differentiation into Schwann cells (as opposed to a 2 step method for neural crest differentiation, followed by Schwann cell differentiation), use of defined conditions and small molecules to activate developmentally relevant pathways *in vitro*, and a method for prospective isolation of resulting Schwann cells from the non-Schwann cells.

In chapter 2, we detail that method for differentiating Schwann cells from human pluripotent cells. In chapter 3, that method is applied to CMT1A patient-derived hiPSCs, to better model the molecular pathways that may be aberrant in CMT1A patient Schwann cells. In chapter 4, our hiPSC-based results are validated using engineered Schwann cells from two additional sources: IVF-derived blastocysts with a preimplantation genetic diagnosis (PGD-hESCs) of CMT1A and CMT1A patient fibroblasts that have been directly converted into induced neural crest (iNC) and subsequently differentiated into Schwann cells. Overall this thesis makes contributions to both the stem cell and CMT1A fields through development of 1) a defined protocol for Schwann cell derivation, 2) expression profiling of CMT1A hiPSC-Schwann cells, and 3) validation of the hiPSC data with CMT1A embryonic stem cell lines and CMT1A induced neural crest-derived Schwann cells.

## **An overview of CMT1A**

Charcot Marie Tooth disease (CMT), also known as Hereditary Motor and Sensory Neuropathy (HMSN), is a genetically and clinically diverse collection of

inherited peripheral neuropathies characterized by their progressive motor and sensory deficits and muscle wasting. Combined, they affect an estimated 1 in 2500 individuals, making them the most common inherited peripheral nervous system disorder in the world<sup>7</sup>. The CMTs are categorized into various subtypes based on their genetic and clinical characteristics<sup>8</sup>. CMT1 (HMSN1) comprises autosomal dominant demyelinating peripheral neuropathies in which Schwann cells are believed to be the pathological cell type; it is caused by mutations (and duplication in the case of peripheral myelin protein 22, *PMP22*) in genes related to myelination, such as *PMP22*, myelin protein zero (*MPZ*), early growth response 2 (*EGR2*), and others. CMT2 (HMSN2) is a primarily axonal neuropathy, clinically characterized by normal nerve conduction velocities, and genetically characterized by mutations in genes critical to neuronal function, such as mitofusin 2 (*MFN2*), ras associated protein 7 (*RAB7*), transient receptor potential cation channel subfamily V member 4 (*TRPV4*), and others. HMSN3 is also known as Dejerine-Sottas Syndrome, a more rapidly progressive and severe demyelinating neuropathy than CMT1; it is also characterized by mutations in genes expressed in Schwann cells, ie *PMP22*, *MPZ*, *EGR2*, and others. CMT4 (HMSN4) is also a demyelinating neuropathy, distinguished by its autosomal recessive inheritance pattern, and is caused by mutations in a diverse set of genes, such as ganglioside-induced differentiation-associated protein 1 (*GDAP1*), myotubularin related protein 2 (*MTMR2*), myotubularin related protein 13 (*MTMR13*), sh3 domain and tetratricopeptide repeat domain 2 (*SH3TC2*), periaxin (*PRX*) and *FIG4*. Finally, CMTX is an X-linked peripheral neuropathy caused by mutations in gap junction

protein beta 1 (*GJB1*), which encodes a connexin. It is the second most prevalent form of CMT, affecting 10% of patients<sup>9</sup>.

In this thesis, we exclusively focus on modeling CMT1A. CMT1A is the most common subtype of CMT, affecting an estimated 55% of CMT patients<sup>10</sup>. It is typically characterized by normal development for the first two decades of life, and a subsequent slowly progressive demyelinating and dysmyelinating peripheral neuropathy that results in sensory loss, motor deficits, and muscle wasting. Physiological studies reveal a slowed nerve conduction velocity, and histological analysis demonstrate “onion bulb” formations, indicating repeated rounds of demyelination and remyelination. Therapeutically, CMT1A is treated exclusively through orthopedic and surgical interventions, and no targeted pharmacological therapies are currently available.

The cause of CMT1A is a 1.4 MB duplication in the short arm of chromosome 17. This region contains the gene *PMP22* (Peripheral Myelin Protein 22), which encodes a tetraspan integral membrane glycoprotein found in compact myelin<sup>11</sup>. The myelin sheath is a multi-layered membrane, unique to the nervous system, which functions as an insulator to greatly increase the velocity of nerve conduction; it is believed that overexpression of *PMP22* results in the demyelination and dysmyelination seen in CMT1A. *PMP22* is expressed predominantly in Schwann cells, but is also expressed in neural crest, neurons, and fibroblasts. In addition to *PMP22*, the CMT1A duplicated region also contains six known genes, 13 predicted genes, at least a dozen long non-coding RNAs, a microRNA, and several pseudogenes, none of which have yet been reported to play a role in CMT1A

pathogenesis<sup>12</sup> (**Figure 3-1B**). In addition, loss of one copy of *PMP22* results in another neuropathy, Hereditary Neuropathy with Liability to Pressure Palsies (HNPP), demonstrating that *PMP22* gene dosage must be tightly regulated to maintain proper nerve function.

Based on data from CMT1A patients and animal models, *PMP22* is indeed believed to be the causative gene in CMT1A pathogenesis. CMT1A patients, who have 3 genomic copies of *PMP22*, have been shown to overexpress *PMP22* mRNA in sural nerve biopsy tissue<sup>13</sup>, Schwann cells cultured from patient sural nerves<sup>f14</sup>, and dermal nerve biopsies<sup>15</sup>. Overexpression of *PMP22* in rodents leads to a severe dys- and demyelinating phenotype, leading to the conclusion that *PMP22* overexpression is sufficient to induce CMT1A pathology.

### **Rodent models of CMT1A**

In 1996 several independently created CMT1A rodent models were reported. The CMT1A transgenic rat, was created through introduction of three additional copies of *PMP22* to the endogenous genes, leading to five genomic doses total. The CMT1A rat expresses 1.6-fold more *PMP22* than controls, and exhibits dysmyelination and demyelination in its peripheral and cranial nerves. Rats display an unsteady gait, have "onion bulbs" on histology, and the histological and physiological changes precede the motor and sensory phenotypes, similar to CMT1A patients.



Additionally, several lines of CMT1A transgenic mice were developed independently, through overexpression of 4-16 genomic copies of human or murine *PMP22*<sup>16-18</sup>. These mice models appear to vary in their ability to recapitulate the CMT1A phenotype<sup>19</sup>. The TGN248 mouse with 16 copies of the *PMP22* transgene exhibits severe dysmyelination, yet actually exhibits lower *PMP22* mRNA expression than controls and lack onion bulbs, making them quite dissimilar from the molecular phenotype of CMT1A patients<sup>20</sup>.

Around the same time as the CMT1A rat and the TGN248 mouse, the C22 mouse model of CMT1A was reported by overexpressing seven copies of human *PMP22*<sup>16</sup> on a yeast artificial chromosome (YAC). The resulting mice express 2.7 fold more *PMP22* mRNA, only survive 2-10 months, and demonstrate severe gait abnormalities and/or paralysis at 6 months, dys- and demyelination, and basal lamina onion bulbs. They appear to be a more clinically relevant mouse than the TGN248 model, yet their *PMP22* expression levels, decreased lifespan, and severe clinical deficits suggest they might be modeling a more severe disease (ie, perhaps Dejerine Sottas Syndrome) than that of most CMT1A patients. This mouse was used for the ascorbic acid trials, as will be discussed shortly.

Similar to the C22 mouse with seven copies of *PMP22*, two years later the same group reported the C61 mouse created with four additional YAC copies of *PMP22*<sup>17</sup>. This mouse exhibits less dramatic *PMP22* overexpression than its C22 counterpart and there is no gross visible motor phenotype. However, upon physiological examination, there is a mild slowing of the motor conduction velocity (25 m/s in C61 mice, vs 38 m/s in wild type mice and 4 m/s in C22 mice), and on

histology some demyelination is visible. Furthermore, a side-by-side comparison of the distribution profile of myelinated and demyelinated nerve fiber sizes closely matches that of CMT1A patients<sup>21</sup>, suggesting the C61 mouse may be the best representation of the mild or early clinical phenotype. This is also the mouse used for the Martini groups studies on macrophage infiltration in CMT1A mouse nerves<sup>22,23</sup>, and will be discussed further in Chapter 3.

Whereas the C22 and C61 CMT1A mice overexpress a human isoform of *PMP22*, two additional mouse models have been created that overexpress the mouse isoform of *PMP22*. One is the MY41 mouse, made with a mouse YAC, which has a severe demyelinating peripheral neuropathy with no evidence of hypertrophy or classical onion bulbs<sup>21</sup>. Over 70% of axons have no measurable myelin and the number of Schwann cells present is three times more than usual. Another is the JP18 mouse, which has a tetracycline-OFF inducible mouse *PMP22* YAC transgene<sup>24</sup>. Essentially, *PMP22* is constitutively overexpressed in this mouse, and transgene expression is switched off by feeding the mouse tetracycline. In the absence of tetracycline, the mice are demyelinated. However, when *PMP22* overexpression is switched off in adult mice, remyelination begins to occur within a week and myelination is nearly normal with 12 weeks, suggesting that *PMP22* overexpression is sufficient to cause demyelination in mice.

### **Comparison of CMT1A rodent models and CMT1A patients**

Overall, it appears that the many rodent models of CMT1A appear to exhibit a peripheral neuropathy, with the C61 being the mildest and the TgN248, C22, and

My41 mice being the most severe, perhaps even more severe than what is typical clinically. Unfortunately, none of the models exhibit the mild early phenotype observed for the first two decades in humans, followed by a progressive long term degeneration characterized by axonal loss and onion bulbs<sup>21</sup>. In contrast, other than C61, most of the mouse models appear to show a severe demyelinating phenotype present from the onset, suggesting they may be better models of the more severe end of the CMT1A spectrum, such as Dejerine-Sottas syndrome, rather than the average clinical course. And unfortunately the C61 mouse does not develop any long term progressive deficits, even after 18 months<sup>21</sup>.

CMT1A mice also demonstrate a clear dose relationship between *PMP22* copy number and peripheral nerve deficits, though this same relationship is not as clear in humans. The dose relationship can be seen by comparing the C61 model (4 copies *PMP22*), C22 model (7 copies *PMP22*), and TgN248 (16 copies *PMP22*); increasing the genomic copy number worsens the phenotype dramatically. It can also be seen in the inducible JP18 mouse, where overexpressing *PMP22* for 8 weeks and then switching it off leads to a correction of the myelination deficit.

However, this relationship between *PMP22* gene and protein expression and myelination deficits aren't nearly as clear in CMT1A patients. Interestingly, CMT1A patients appear to exhibit a broader variation in *PMP22* protein expression levels than normal controls<sup>15</sup>, and clinical studies demonstrate that levels of *PMP22* mRNA and protein expression do not correlate significantly with clinical phenotype<sup>15</sup>. For instance, some patients with high *PMP22* expression levels actually experience the mildest phenotypes<sup>13,15</sup>. This suggests that other factors may be at play in the

human form of the disease, such as *PMP22* having slightly different functions in humans versus rodents, or that factors other than *PMP22* may contribute to human CMT1A pathogenesis. An example of factors other than *PMP22* that might play such a role could be many non-*PMP22* genes present in the CMT1A duplicated region (**Figure 3-1B**), none of which are currently included as transgenes in rodent models of CMT1A. Efforts are currently ongoing to identify such potential modifying genes using exome sequencing in clinical samples (clinicaltrials.gov Identifier NCT01193088).

Furthermore, another difference between CMT1A rodent models and humans is their response to potential pharmacologic treatments. For instance, it has been well established that ascorbic acid is important for Schwann cell basal lamina formation and induction of myelination in *in vitro* settings<sup>25,26</sup>. Consequently, trials were conducted with C22 CMT1A mice to determine the effect of ascorbic acid administration, and it was found to decrease *PMP22* expression levels, improve locomotion, improve lifespan, and remyelinate the sciatic nerve<sup>27,28</sup>. However, several follow up clinical trials conducted in both pediatric<sup>29,30</sup> and adult populations, using both low dose<sup>31,32</sup> and high dose<sup>33</sup> ascorbic acid treatments, unfortunately found little clinical improvement. This suggests that critical differences may exist between rodent models and CMT1A patients, indicating that development of novel, more patient-relevant model systems is warranted.

In this dissertation, we utilize human CMT1A patient-derived Schwann cells to model the disorder and complement existing rodent models. These human Schwann cells come from three different sources: induced pluripotent stem cells, blastocysts with a preimplantation genetic diagnosis of CMT1A, and patient

fibroblasts that have been directly converted into neural crest and then differentiated into Schwann cells. As human Schwann cells, they should be able to 1) recapitulate the *PMP22*-mediated pathology of CMT1A patient Schwann cells, 2) reflect the expression or involvement of any non-*PMP22* genes in CMT1A pathogenesis, and 3) predict response to drugs modulating expression of *PMP22* and other mediators of CMT1A.

### **Immunocompetence of Schwann cells**

Over the course of this study, a phenotype of inflammatory dysregulation was found in the CMT1A Schwann cells. Because Schwann cells are not classically considered effectors of the immune system, here we briefly review the immunocompetence of Schwann cells, much of which has been previously described by Patricia J. Armati in [The Biology of Schwann Cells: Development, Differentiation, and Immunomodulation](#).

Whereas the nervous system has long been considered an immune privileged location, there is substantial evidence to the contrary. Immune privilege is the idea that there are certain regions, the nervous system, cornea, retina, anterior chamber of the eye, testis, and liver for example, in which immune surveillance is reduced<sup>34</sup>. The idea originated in 1948 from Medagar's observations that homologous skin transplantations into the brain did not elicit the same degree of immune response as transplantations into other sites<sup>35</sup>. The theory was based on the idea that there is 1) anatomic separation between blood and neural tissue, 2) molecules required for antigen presentation are absent under normal physiological

conditions, 3) absence of lymph drainage, and 4) decreased T-cell surveillance<sup>34,36,37</sup>. While the blood nerve barrier does limit immune cell access to a certain degree, it is far from impermeable, particularly at anatomic sites like nerve roots, nerve ganglia, and motor terminals. In addition, recent work has demonstrated that Schwann cells can participate in a wide spectrum of immune activities including: antigen recognition, antigen presentation, and immune response generation<sup>36</sup>.

Antigen recognition by Schwann cells is evidenced by their expression of Toll-like receptors, which are “pattern-recognition receptors” that recognize stereotypical pathogen-associated structures; their recognition plays an important role in the acute response of the innate immune system. Evidence for Schwann cell participation in antigen recognition comes from Schwann cell expression of toll-like receptors 2, 3, and 4, and suggests they may even act as sentinel cells for the PNS<sup>38,39</sup>. In addition to potential pathogens, necrotic neuronal cells can also activate Toll-like receptors of Schwann cells and cause pro-inflammatory cytokine secretion, suggesting a role for Schwann cells TLR-signaling in mediating peripheral nerve injury<sup>40</sup>. Another study demonstrated that TLR-signaling is essential for macrophage recruitment and myelin debris clearance during Wallerian degeneration<sup>41</sup>.

Antigen presentation by Schwann cells is supported by their constitutive expression of MHC class I molecules and inflammation-induced expression of MHC class II molecules<sup>42</sup>. All nucleated cells can present MHC class I molecules to CD8+ T cells. In contrast, only professional antigen presenting cells can display MHC

class II molecules. MHC class II molecules display antigen peptides to CD4+ T-cells, and if there is a second co-stimulatory molecule, the T cell will become activated and mount an immune response. Pollard, et al, found that Schwann cells stained positive for MHC class II molecules in patients with chronic inflammatory demyelinating polyneuropathy (CIDP) and Guillain-Barre syndrome (GBS), suggesting that Schwann cells may indeed act as antigen presenting cells in inflammatory PNS disorders<sup>43,44</sup>. In addition, it's also been found that Schwann cells of CIDP patients express the co-stimulatory molecule BB-1, meaning they have all the molecular components to act as antigen presenting cells<sup>45</sup>. Although successful antigen presentation to T-cells has been demonstrated *in vitro*, the extent to which Schwann cells actually play a meaningful role in antigen presentation *in vivo* is still controversial<sup>46,47</sup>.

Generation of an immune response by Schwann cells, on the other hand, is no longer controversial. At one point it was believed that only immune cells in the nervous system could release cytokines, but now there is ample evidence that Schwann cells, microglia, astrocytes, and oligodendrocytes can all secrete cytokines upon appropriate stimulation<sup>47</sup>. Schwann cells have been shown to secrete a myriad of cytokines in various physiological and pathological conditions, including, but not limited to: IL-1, which initiates T-cell mediated immune responses<sup>48,49</sup>; IL-6, which is a monocyte chemoattractant<sup>50</sup>; TNF- $\alpha$ , which mediates multiple proinflammatory functions and can also induce cell death, proliferation, and differentiation<sup>51,52</sup>; and TGF- $\beta$ , which is a master regulator of inflammation and cell proliferation<sup>53</sup>. Whether the effects of such cytokine release by Schwann cells are beneficial or detrimental appear to be particularly context-dependent. For instance,

during Wallerian degeneration, upregulation of MCP-1, Mip1-a, and IL1-B and the subsequent recruitment of macrophage actually facilitates clearance of myelin and axonal debris, thus creating a more permissive environment for axon regeneration<sup>54,55</sup>.

In addition to secreting cytokines, Schwann cells also have some of the physical capabilities of immune effectors, such as phagocytosing myelin themselves as has been demonstrated by several studies of Wallerian degeneration. It appears that in early response to axotomy, Schwann cells de-differentiate and begin reabsorbing the lipid myelin debris, as the segmented myelin sheath and axonal debris can be seen within Schwann cell cytoplasmic vacuoles<sup>56-58</sup>. Subsequently, macrophages are recruited to the lesion and perform the bulk of myelin phagocytosis, but it is the Schwann cells that initiate the process.

Relative to their role in synthesizing myelin, Schwann cell functions in immune surveillance and immune modulation has been comparatively underappreciated. Engineered Schwann cells, such as those developed in Chapter 2, may very well model the immunomodulatory functions of endogenous Schwann cells, even if their myelination potential has yet to be demonstrated.



CHAPTER 2: DIRECTED DIFFERENTIATION OF HUMAN EMBRYONIC STEM CELLS  
INTO SCHWANN CELLS

## Introduction

Schwann cells are the myelinating glia of the peripheral nervous system. Their synthesis of myelin allows peripheral nerves to conduct sensory and motor signal with rapid efficiency and fidelity. Developmentally, they originate from neural crest, which delaminate from the neural tube and migrate extensively to give rise to a number of different cell types throughout the body. They include Schwann cells, sensory neurons, autonomic neurons, enteric neurons, and melanocytes, as well as bones, cartilage and connective tissue in the craniofacial region.

During development, Schwann cells and sensory neurons form in parallel. Through a process of radial sorting, each Schwann cell selectively associates with one neuron and forms a single segment of compact myelin. Disrupting this peripheral myelin results in numbness, tingling, difficulty moving, and often debilitating disability, as evidenced by disorders like Charcot Marie Tooth disease, Hereditary Neuropathy with Liability to Pressure Palsies, Guillain-Barre Syndrome, and chronic inflammatory demyelinating polyradiculopathy.

Our current understanding of these disorders is far from complete and our current treatment options leave patients much to be desired. Studying Schwann cell disorders directly through patient biopsies, while perhaps scientifically ideal, is ethically and clinically challenging as it would remove an intact nerve from a patient who has limited nerve function. Consequently, animal models are extensively used to model these disorders, study their pathology, and screen for therapeutics to reverse that pathology. These animal models, while extremely valuable as an *in vivo* and mammalian model system, also have their limitations. As non-human

models, they may not fully recapitulate the human pathophysiology, and drugs that might prove efficacious in humans may not pass screening trials in rodents, and vice versa.

This is where engineering human stem cells towards the Schwann cell lineage might prove useful. Human pluripotent stem cell technology allows us to create potentially unlimited numbers of any target cell type. Developing Schwann cells from human embryonic and induced pluripotent stem cells would allow us to better model Schwann cell disorders, perform high throughput drug screens in disease relevant cells types, and offer a source of potentially clinically transplantable Schwann cells.

By taking advantage of our lab's prior experience with human pluripotent stem cell differentiation into neural crest and its sublineages, we were able to develop a protocol for the derivation of Schwann cells from hPSCs. Although a few other such protocols have already been published (one for hPSC differentiation towards Schwann cells<sup>6</sup>; one for fibroblast conversion to Schwann cells<sup>59</sup>), we believe that our method offers several advantages. Ours uses a chemically defined method and 2D monolayer culture method to provide precise control over cell fate. It also features a FACS purification method to selectively isolate and replat Schwann cells in the absence of contaminating cell types. We believe that the resulting human Schwann cells provide an effective and impactful platform for future studies.

## Methods

### *SOX10 and OCT4 hESC reporter line generation*

The human embryonic stem cell line, H9 (also known as WA09) was modified to express *eGFP* under the *SOX10* or *OCT4* promoter, using the TALEN genome editing system, as previously described by published methods<sup>60,61</sup>. Briefly, feeder-free H9 hESCs were dissociated into single cells using Accutase and  $2 \times 10^6$  cells were resuspended in nucleofection solution V (Lonza) with 12  $\mu$ g total plasmids and nucleofected by Nucleofector™ II according to manufacturer's instructions (using B-16 program, Lonza). The nucleofected cell suspension were subsequently plated on the puromycin-resistant MEFs (DR4, Global Stem) in hESC media with 10  $\mu$ M Y-27632. Four days after nucleofection, cells that have undergone homologous recombination were selected adding 0.5  $\mu$ g/ml of puromycin in the hESC media. To verify the chromosomal aberrations, karyotype analyses were performed on the candidate clones (Cell Line Genetics, Inc.).

These lines were generated by Ho Tae Lim and Yohan Oh, both members of the Lee Lab.

### *Schwann cell differentiation*

H9 Sox10::eGFP cells were plated and differentiated into putative Schwann cells, as described extensively in Appendix 1. Briefly, colonies of pluripotent cells were rendered into single cells and plated on Geltrex, an artificial basement membrane-

like matrix. They were then treated with a combination of small molecules to induce neuronal and Schwann cell differentiation:

1. To initiate differentiation, aspirate the medium and add KSR medium containing 10  $\mu\text{M}$  SB-431542 and 500 nM LDN-193189 (day 0).
2. On day 2 of differentiation, aspirate the medium and add KSR medium containing 10  $\mu\text{M}$  SB-431542, 500 nM LDN-193189, 3  $\mu\text{M}$  CHIR 99021, 10  $\mu\text{M}$  DAPT.
3. On day 4 of differentiation, aspirate the medium and add KSR/NB (3:1) medium containing 3  $\mu\text{M}$  CHIR 99021 and 10  $\mu\text{M}$  DAPT (final concentrations are for the combined KSR/NB mixture).
4. On day 6 of differentiation, aspirate the medium and add KSR/NB (1:1) medium containing 3  $\mu\text{M}$  CHIR 99021 and 10  $\mu\text{M}$  DAPT.
5. On day 8 of differentiation, aspirate the medium and add KSR/NB (1:3) medium containing 3  $\mu\text{M}$  CHIR 99021 and 10  $\mu\text{M}$  DAPT.
6. On day 10 of differentiation, aspirate the KSR/NB and add NB medium containing 200  $\mu\text{M}$  dibutyl cAMP and 200  $\mu\text{M}$  sodium L-ascorbate.
7. On day 14 of differentiation, aspirate the NB and add NB medium containing 200  $\mu\text{M}$  dibutyl cAMP and 200  $\mu\text{M}$  sodium L-ascorbate.
8. On day 18 of differentiation, aspirate the NB and add NB medium containing 200  $\mu\text{M}$  dibutyl cAMP and 200  $\mu\text{M}$  sodium L-ascorbate.
9. Maintain in this manner until day 21-23 of differentiation, when the cells are ready for purification.

*Schwann cell purification and culture*

The FACS protocol is described extensively in Appendix 1. Briefly, Schwann cells were purified with Fluorescence Activated Cell Sorting (FACS) after 21-23 days of differentiation using a PE-conjugated antibody to the alpha4 integrin, CD49d (R&D Systems, FAB1354P). After FACS, Schwann cells were replated onto tissue culture plates treated with fibronectin (R&D Systems, 1918-FN-02M) and laminin (Cultrex, R&D Systems, 3400-010-1) coated plates. (Plates were coated with 1ug/mL laminin and 2ug/mL fibronectin in PBS for 24 hours). Cells were maintained in culture for up to 80 days post-FACS using Neurobasal medium (Life Technologies, 21103-049) supplemented with L-glutamine (Life Technologies, 25030-081), B-27 supplement (Life Technologies, 12587-070), N2 supplement (Life Technologies, cat. no. 17502-048), and 1% fetal bovine serum (Hyclone, cat. no. SH30070.03).

#### *OCT4+ embryonic stem cell purification*

H9 *OCT4::eGFP* human embryonic stem cells were maintained clonally and *OCT4::eGFP* positive pluripotent cells were FACS purified. This step was performed by Yohan Oh, a postdoctoral fellow in the Lee lab.

#### *SOX10+ Neural crest generation and purification*

H9 *SOX10::eGFP* cells were plated and as described above for Schwann cell differentiation. For differentiation towards neural crest:

1. To initiate differentiation, aspirate the medium and add KSR medium containing 10  $\mu$ M SB-431542 and 500 nM LDN-193189 (day 0).

2. On day 2 of differentiation, aspirate the medium and add KSR medium containing 10  $\mu$ M SB-431542, 500 nM LDN-193189, 3  $\mu$ M CHIR 99021.
3. On day 3 of differentiation, aspirate the medium and add KSR medium containing 10  $\mu$ M SB-431542, 3  $\mu$ M CHIR 99021.
4. On day 4 of differentiation, aspirate the medium and add KSR/NB (3:1) medium containing 3  $\mu$ M CHIR 99021 (final concentrations are for the combined KSR/NB mixture).
5. On day 6.5 of differentiation, Sox10::eGFP positive neural crest were FACS purified.

This step was performed by Yohan Oh, a postdoctoral fellow in the Lee lab.

### *Immunofluorescence*

Cells were fixed in 4% Paraformaldehyde for 20 minutes, then blocked and permeablized in 0.5%BSA and 0.1% Triton X-100 in PBS for 30 minutes. Primary antibodies were diluted 1:100 to 1:500 in 0.5%BSA and 0.1% Triton X-100 in PBS and samples were incubated overnight at 4 degrees. Secondary antibodies were diluted 1:1000 in 0.5%BSA and 0.1% Triton X-100 in PBS, and incubated 2 hours at room temperature. Primary antibodies can be found in Appendix 2. Appropriate 488, 568, and 647-conjugated Alexa fluor secondary antibodies were utilized.

### *RNA extraction, real time PCR, and microarray analysis*

Cells were homogenized in Trizol Reagent (Life Technologies, 15596-026) and manufacturer's protocols were followed to extract total RNA. 0.5 ug total RNA was

reverse transcribed into cDNA using the High Capacity cDNA Reverse Transcription Kit (Applied Biosystems, 4387406). Real time PCR was performed on an Eppendorf Realplex Mastercycler Ep gradient S. Cycling conditions are as follows: 95 degrees 2 min, 40 cycles (95 degrees 3 seconds, 60 degrees 30 seconds). Primer probes can be found in Appendix 2. For microarray analysis, total RNA from Oct4+ embryonic stem cells, Sox10+ neural crest, and CD49d+ Schwann cells were hybridized in triplicate to the Affymetrix Primeview Human Gene Expression Array by the Johns Hopkins Deep Sequencing and Microarray Core. Data analysis and visualizations were performed in Partek and Spotfire. Transcripts that were up- and down-regulated 2-fold with a p-value greater than 0.05 were further analyzed using DAVID and Ingenuity Pathway Analysis.



## Results

### *LSB2i treatment for 21-23 days yields Sox10+ Schwann cells and Tuj1+ neurons*

We plated human embryonic stem cells modified to report eGFP under the *SOX10* promoter (H9 *SOX10::eGFP* cells). The H9 human embryonic stem cell line, one of the original human embryonic stem cell lines first developed by Jamie Thompson<sup>62</sup>, was chosen as it's one of the most extensively utilized and best characterized human ES lines available<sup>63</sup>. Furthermore, its ability to be differentiated towards neuroectodermal lineages has been well established<sup>64-66</sup>.

We found that by modifying a published protocol (referred to as the LSB3i protocol, **Fig. 2-1B**) for sensory neuron differentiation<sup>67</sup>, we were able to enhance Schwann cell differentiation. The LSB3i sensory neuron differentiation protocol consists of 10 days of treatment with five small molecules. Treatment from Day 0 to Day 4 with two such small molecules (LDN-1931189 and SB431542, collectively referred to as LSB) effectively neutralize the fate of the H9 cells by inhibiting the SMAD/TGFbeta pathway<sup>68</sup>. Treatment from Day 2 to Day 10 with three additional small molecules (DAPT, CHIR99021, and SU5402, called 3i for 'three inhibitors') serves to differentiate the cells into neurons of dorsal root ganglia, as opposed to CNS neurons. Specifically, DAPT is a  $\gamma$ -secretase inhibitor that blocks Notch signaling, also neutralizing the fate of the cells. CHIR99021 is a WNT agonist that inhibits glycogen synthase kinase-3 $\beta$  (GSK-3 $\beta$ ) and stabilizes  $\beta$ -catenin, and thereby promotes a neural crest cell fate (as opposed to a CNS/neural tube fate). SU5402 inhibits the vascular epithelial growth factor (VEGF), fibroblast growth

factor (FGF) and platelet-derived growth factor (PDGF) tyrosine kinase signaling pathways<sup>67</sup>, and serves to increase the efficiency of neuron generation.

We modified this LSB3i protocol to create a new protocol (dubbed LSB2i, **Fig. 2-1C**) that is optimized for Schwann cell generation. We eliminated the use of SU5402 in order to decrease the efficiency of neuronal specification, as we wanted to maximize glial specification. After 10 days of treatment with LDN-1931189, SB431542, DAPT, and CHIR99021, we treat the cells for an additional 11-13 days with cAMP and ascorbic acid, to promote Schwann cell proliferation<sup>69-72</sup> and maturation<sup>73,74</sup>. After a total of 21-23 days of differentiation, a mixed population of cells results (**Fig. 2-2A**) and *SOX10::eGFP*+ Schwann cells can be seen in close association with TUJ1+ neurons.

#### *CD49d-PE can be used to prospectively isolate Schwann cells*

As the differentiation protocol yields a mixture of Schwann cells, neurons, and non-neuronal cell types, it is important to be able to purify the Schwann cell population. Towards this end, we have utilized CD49d as a cell surface marker that can be utilized to purify the Schwann cell population. The protein CD49d is an alpha4 integrin previously identified to be expressed on the surface of Schwann cell precursors<sup>4</sup>, the earliest member of the Schwann cell lineage. By FACS purifying differentiated H9 *SOX10::eGFP* cells for CD49d-PE, we could isolate a CD49d+ putative Schwann cell population and CD49d- putative non-Schwann cell population. As expected, the CD49d+ population also expresses a high level of eGFP (**Fig. 2-2B**), demonstrating that the *SOX10* promoter is highly active in these CD49d+ cells and supporting the idea that they are indeed Schwann cell

precursors. Furthermore, the average yield of CD49d+ cells from the H9 hESC line, as determined during FACS purification, is 13.62% (n=27) (Fig. 2-2C).

*Schwann cell lineage genes are enriched in the CD49d+ population and downregulated in the CD49d- population*

To further characterize these CD49d+ putative Schwann cells, we used qRT-PCR to evaluate Schwann cell gene expression in the CD49d+ fraction, CD49d- fraction, and in unsorted cells. Real time PCR was performed for *SOX10* (expressed on neural crest, Schwann cell precursors, and immature Schwann cells), Desert Hedgehog (*DHH*) (expressed on Schwann cell precursors and immature Schwann cells), and Cadherin19 (*CDH19*) (specific to Schwann cell precursors)<sup>4,75</sup> (**Fig. 2-2D**). Results demonstrate that these three Schwann cell genes are specifically enriched in the CD49d+ population, and are downregulated in the CD49d- population, relative to the unsorted population. This suggests that our protocol yields a cellular population that expresses Schwann cell marker genes, specifically of the Schwann cell precursor sublineage.

*OCT4+ hESCs, SOX10+ neural crest, and CD49d+ Schwann cells have distinct gene expression profiles and upregulate Schwann cell signaling pathway genes*

Whereas the data thus far demonstrates an enrichment of Schwann cell precursor gene expression in CD49d+ cells relative to CD49d- and unsorted LSB2i treated cells, here we investigate enrichment of Schwann cell genes relative to independently generated, developmentally relevant cell populations. Towards this end, we compared the global gene expression profile of CD49d+ cells against undifferentiated human embryonic stem cells and neural crest derived from human

embryonic stem cells. The human embryonic stem cells were obtained by taking H9 *OCT4::eGFP* cells and FACS-purifying the eGFP+ population. Because the *OCT4* promoter is critical for the maintenance of pluripotency, this method will yield only pluripotent stem cells. The neural crest were obtained from H9 *SOX10::eGFP* cells that were differentiated *in vitro* towards the neural crest lineage, and then FACS selected for the *SOX10::eGFP*+ neural crest population. Microarray profiling of human embryonic stem cells, neural crest, and CD49d+ putative Schwann cells reveals that the three populations have quite different gene expression profiles, as evident from the heat map representation of the data (**Fig. 2-3A**). Hierarchical clustering and the resulting dendrogram profile demonstrates that the three populations are quite distinct and, as expected, the neural crest and CD49d+ putative Schwann cell populations are more similar to each other than they are to the human ES cells.

Gene ontology and pathway analysis of the genes differentially expressed between the CD49d+ putative Schwann cell population and the *OCT4*+ hESCs found significant representation of pathways and categories critical for gliogenesis and Schwann cell development, including Erbb signaling ( $p=0.0000758$ ), Neuregulin signaling ( $p=0.000436$ ), Gliogenesis ( $p=0.000430$ ), PDGF signaling ( $p=0.0120$ ), and CNTF signaling ( $p=0.0370$ ) (**Fig. 2-3B**). This suggests that these Schwann cell development pathways are indeed activated in the CD49d+ cells, further supporting the idea that they are Schwann cells.

*Both classical and non-classical Schwann cell lineage genes are highly upregulated in CD49d+ cells*

Among the most highly upregulated genes in the CD49d+ population is *S100B*, a well-established Schwann cell marker<sup>4</sup>, and less classically, these cells also robustly express *GPR126* and *POSTN* (Periostin), all of which were confirmed by qRT-PCR (**Fig. 2-4A**). *GPR126* encodes a G-protein coupled receptor which has been shown to be essential for initiation of myelination<sup>76-78</sup>. *POSTN* (Periostin) encodes an adhesive glycoprotein that facilitates the migration of cells undergoing epithelial to mesenchymal transition during development; it is expressed in Schwann cells in addition to endocardial cushions<sup>79</sup>.

*FACS-purified cultured CD49d+ cells exhibit bipolar morphology and express classical Schwann cell proteins*

All of the above studies were performed on FACS purified CD49d+ Schwann cells. After FACS the cells can also be replated and cultured for up to 80 days in NB+1%FBS. After 20+ days post-FACS, the cells exhibit an elongated morphology stereotypical of Schwann cells and immunostain positively for several classical Schwann cell protein markers such as S100b, GFAP, and GalC (**Fig. 2-4B**), providing further evidence that they are indeed Schwann cells and also demonstrating the CD49d+ population's ability to mature *in vitro*.

*Statistical analyses*

Data was analyzed using Graphpad Prism 6. Means +/- standard deviation are plotted, and p-values were calculated using the unpaired t test, ratio paired t test, and one-way ANOVA, as noted in each figure legend.

**Figure 2-1: LSB2i differentiation schematic**

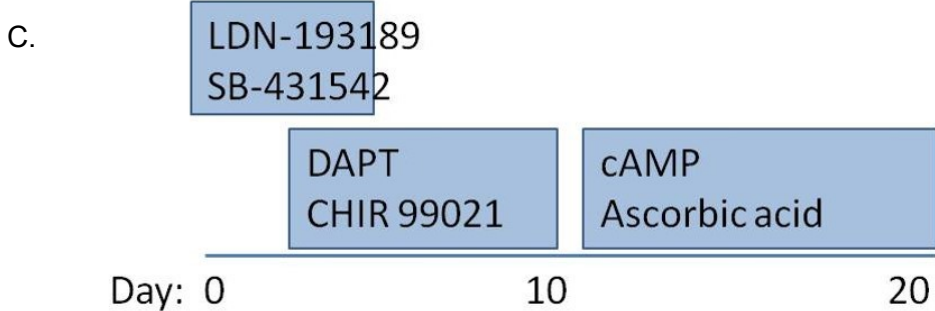
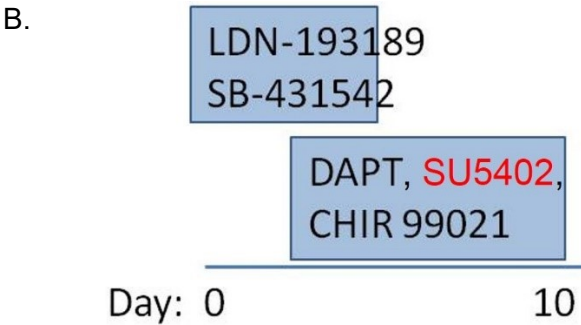
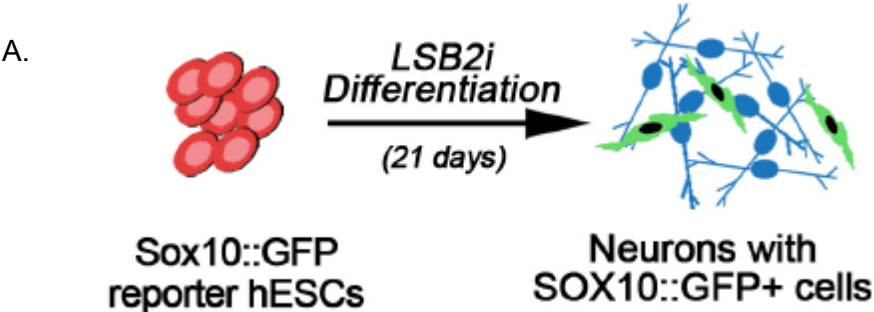


**Figure 2-1. A.** Schematic of LSB2i differentiation. **B.** Previously published LSB3i small molecule treatment timeline for sensory neuron generation. **C.** LSB2i small molecule treatment timeline for Schwann cell generation .

**Figure 2-2: LSB2i treatment yields a mixed population of Schwann cells and neurons**

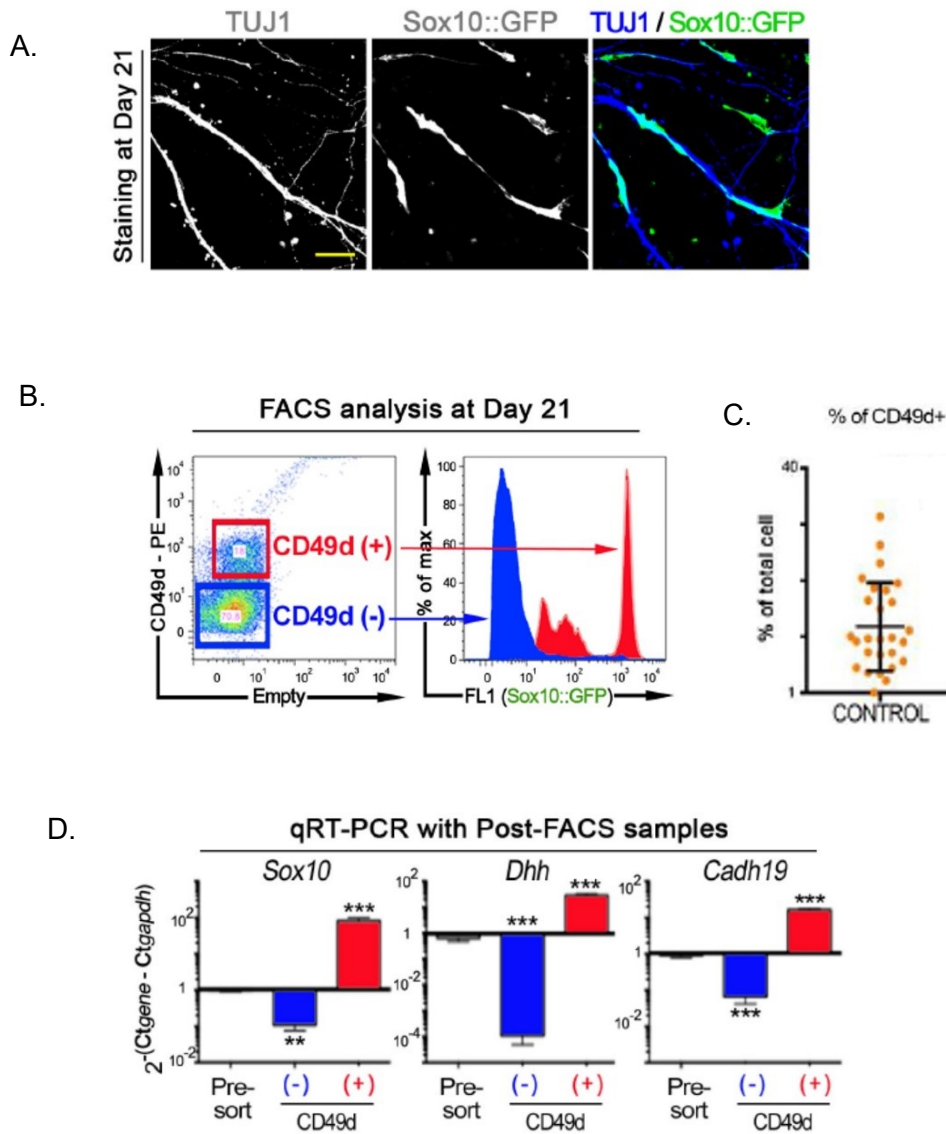
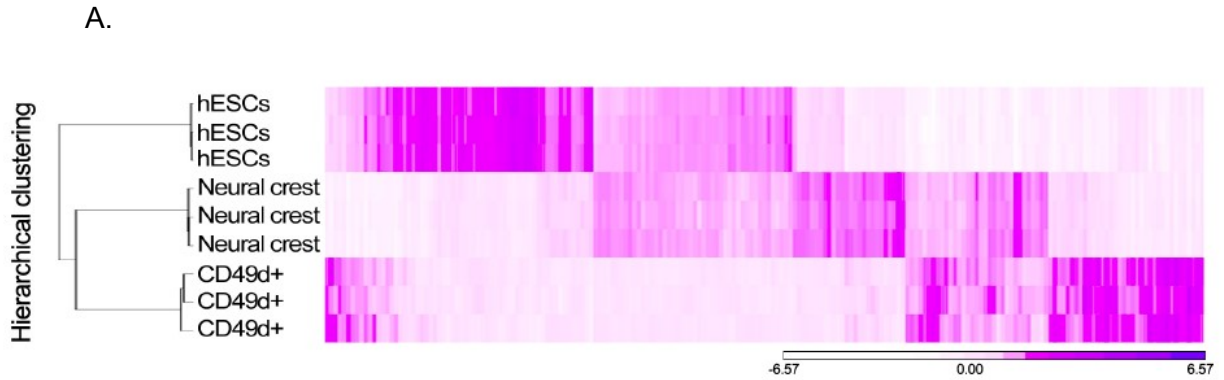


**Figure 2-2. A.** Immunofluorescence for eGFP and TUJ1 demonstrate SOX10+ Schwann cells in association with TUJ1+ neurons (bar = 50  $\mu$ m). **B.** Flow cytometry demonstrates substantial overlap between the CD49d+ population and Sox10::eGFP expression. **C.** FACS purification of LSB2i treated control H9 hESCs. Each dot represents an independent differentiation (n=27). Data expressed as mean +/-SD. **D.** Real time PCR for Schwann cell lineage markers in CD49d+ putative Schwann cells, CD49d- non-Schwann cells, and unsorted cells. Data expressed as mean +/- SD (standard deviation), n = 5 for each cell type, p-values calculated by one-way ANOVA, \*\* p < 0.01, \*\*\* p < 0.001.

**Figure 2-3: Global gene expression profiling of ES, NC, and CD49d+ Schwann cells**



B.

**GO analysis with up-regulated genes  
(CD49d+ over hESCs)**

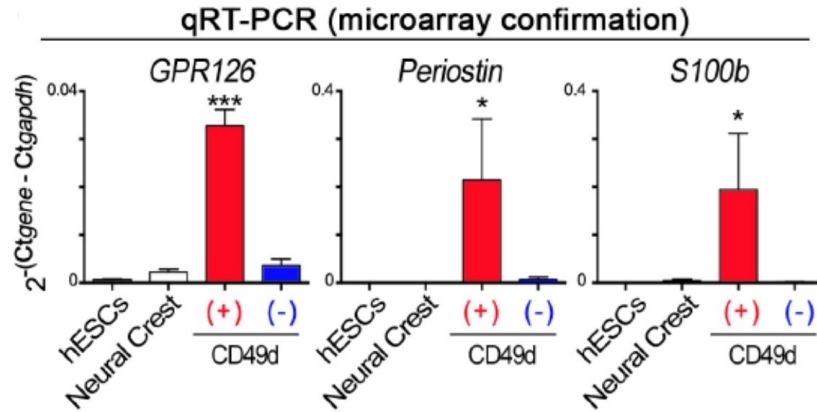
GO terms	p-value
ErbB signaling (Ingenuity IPA)	7.58578E-05
Neuregulin signaling (Ingenuity IPA)	0.000436
Gliogenesis (DAVID)	0.000430
PDGF signaling (Ingenuity IPA)	0.0120
CNTF signaling (Ingenuity IPA)	0.0135
ErbB signaling pathway (DAVID)	0.0370

**Figure 2-3. A.** Heat map representation of supervised hierarchical clustering of Oct4::eGFP+ hESCs, Sox10::eGFP+ neural crest, and CD49d+ putative Schwann cells, based on all differentially expressed genes with  $p < 0.001$ . **B.** Gene ontology and pathway analysis of genes upregulated in CD49d+ population (versus hESCs),  $p < 0.05$ , fold-change  $> 2$ .



**Figure 2-4: Microarray validation and post-FACS purification plating and culturing of CD49d+ Schwann cells**

A.



B.

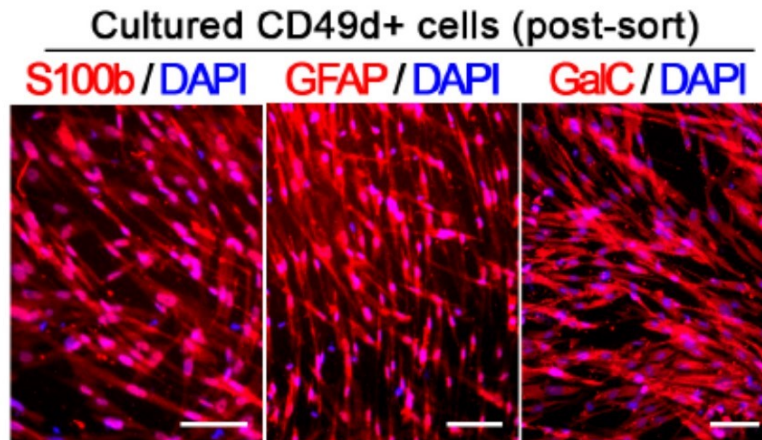


**Figure 2-4. A.** Validation of microarray results with qRTPCR for select Schwann cell genes, normalized to GAPDH.  $n = 3$  differentiations for each cell type. Data expressed as mean  $\pm$  SD; p-values calculated by one-way ANOVA. \*  $p < 0.05$ , \*\*\*  $p < 0.001$ . **B.** Post-FACS purified CD49d+ cells may be replated and cultured up to 80 days. Representative immunofluorescence images for S100B, GFAP, and GalC staining (bar = 50  $\mu$ m).

## Discussion

Here we demonstrate the *in vitro* derivation of human Schwann cells from human embryonic stem cells. In contrast with previously published protocols, this protocol utilizes a monolayer culture method (as opposed to spheres), features defined conditions, and includes a FACS-based purification method, with replating possible. Replating is significant as it enables further study of cell autonomous phenotypes and may also allow for *in vitro* maturation of the Schwann cell precursors along the Schwann cell lineage.

When developing any protocol for human embryonic stem cell differentiation towards a target cell type, several different factors must be taken into consideration to develop an ideal protocol. One major issue is whether the protocol will utilize 3 dimensional (3D) spherical structures (ie embryoid bodies and neurospheres) or a two dimensional (2D) adherent monolayer culture. Whereas the use of 3D structures is well established and perhaps better models the 3D environment in which development occurs *in vivo*, many believe that 2D monolayer cultures provide the operator superior control over the fate of the cells<sup>68,80</sup>. This is because each cell plated in a 2D culture is exposed to the differentiation medium fairly equally, whereas in 3D cultures, each cell is receiving quite varied environmental and differentiation signals based on its location within the embryoid body or neurosphere. Our Schwann cell derivation protocol uses the 2D monolayer method based on the well-adopted dual-SMAD inhibition method of neuronal differentiation, resulting in cleaner, more precise control over their fate specification<sup>68</sup>.

Another determination that needs to be made when designing a stem cell differentiation method is the source of the tissue culture products containing the

molecular cues to pattern the fate of the cells. Generally these sources can fall into two categories: “not defined” and “defined.” “Not defined” tissue culture conditions include animal-derived serums and matrix products that may vary substantially from lot to lot and whose constituent components are poorly understood. They can also include proprietary formulations whose contents are not readily ascertainable. “Defined” tissue culture conditions on the other hand consist of known small molecules, recombinant proteins, and lack animal products. The use of defined conditions in stem cell research is significant for several reasons, and is being increasingly adopted for both hESC maintenance<sup>81-84</sup> and differentiation<sup>85,86</sup>. First of all, particularly in developmental studies, it is valuable to know exactly what molecular cues are patterning the fate of the cells. Second of all, reproducibility is important in stem cell engineering, and batch variation of animal products could result in large variability in stem cell differentiation towards the target cell type. Third of all, exposure to animal products may also induce undesired immunogenic responses in the stem cells<sup>87</sup>, which bodes poorly for their potential transplantation in clinical settings. Finally, using defined conditions also makes the resulting cells readily transferable to a Good Manufacturing Practices facility for future clinical applications. Our protocol uses defined conditions during differentiation until FACS purification. After FACS, the cells are plated in Neurobasal medium + 1% fetal bovine serum, a non-defined condition due to the presence of serum. Much effort was made to find a defined condition for culture of the cells after FACS, and while the cells could survive in Neurobasal + FGF2 + EGF (data not shown), they did not proliferate and often would not survive passaging. Even so, Schwann cells from our

protocol can potentially be adapted to clinical applications if utilized immediately upon FACS purification.

The cells yielded by our defined LSB2i protocol exhibit the morphological, genetic, and protein signatures of Schwann cells, which we interpret to mean they are indeed Schwann cells. However, it should be noted that the ability of these cells to myelinate, perhaps the best known function of Schwann cells, has yet to be demonstrated. Coculture experiments with human ES-derived motor neurons were attempted, without any evidence of myelination. Coculture experiments with rat dorsal root ganglion neurons, in combination with forced overexpression of transcription factors promoting myelination (ie Oct6, Krox20), are in progress. Unfortunately human Schwann cells are extremely difficult to force to myelinate, particularly compared to rodent Schwann cells and oligodendrocytes. First of all, human primary Schwann cells are not nearly as extensively studied *ex vivo* as rodent primary Schwann cells, due to the ethical and technical barriers in obtaining such clinical samples, meaning conditions promoting Schwann cell myelination are also less studied in humans than rodents. During studies of human Schwann cell myelination, species barriers between the human Schwann cells and typically rodent substrate neurons may very well limit myelination efficiency<sup>88</sup>. Additionally, human ESC-derived Schwann cells may also be less developmentally mature than primary Schwann cells, which provides another barrier to myelination. Even though other groups have published Schwann cell differentiation protocols, it is clear that demonstrating their myelination potential has been challenging. In one study on hESC and hiPSC differentiation to Schwann cells the efficiency was low, as demonstrated by a single image of a myelinated segment<sup>6</sup>. In another study on

Schwann cell generation via direct lineage conversion from fibroblasts, they also reported low efficiency, and also did not perform a critical experiment that would rule out myelination from rodent Schwann cells contaminating their rat DRG-human Schwann cell coculture<sup>59</sup>. Our difficulty experienced in human ESC-derived Schwann cell myelination is in line with what has been reported in the literature<sup>88</sup>.

Even in the absence of myelination data, our human ESC-derived Schwann cells still have many potential applications. Because they express all the molecular characteristics of Schwann cells, they are likely useful for modeling the molecular pathology of Schwann cell disorders, particularly hereditary ones. The pathophysiology of most Schwann cell disorders are currently best understood through rodent models, but there can be limitations in extrapolating rodent model data to human patients. As a source of human Schwann cells, they can provide human-specific, and if using hiPS cells, individual patient-specific data that would otherwise be unobtainable using other model systems.

Additionally, these human pluripotent stem cell (hPSC)-derived Schwann cells can also be used for drug screening in a number of different contexts. Control hPSC-derived Schwann cells could be screened for drug doses that minimize toxicity to Schwann cells, which might be useful when developing or dosing potentially neurotoxic drugs. Furthermore, "diseased" hPSCs could be developed that harbor the genetic mutation that causes a Schwann cell disorder. Such disease Schwann cells could also be screened for drugs that alleviate the effects of the genetic mutation; for instance if the mutation results in decreased transcription of a key

gene, high-throughput drug screening could be performed for agents that restore transcription to normal levels.

Given further advances in the clinical and regulatory arenas, our hPSC-derived Schwann cells could potentially be adapted to clinical transplantation studies. Due to the prevalence of hereditary and acquired Schwann cell disorders, hPSC-derived Schwann cell replacement therapy is an exciting possibility. Other potential therapeutic applications of these cells include Schwann cell-mediated spinal cord remyelination in spinal cord injury<sup>89</sup>, central nervous system remyelination in multiple sclerosis<sup>90</sup>, and functional nerve regeneration in limb transplantation surgeries<sup>91-93</sup>.

## **Conclusion**

We have developed a defined protocol for the direct derivation and prospective isolation of Schwann cells from human embryonic and induced pluripotent stem cells. Potential uses of these cells include disease modeling, drug screening, and transplantation therapy, making them an exciting platform for translational research and personalized medicine.

CHAPTER 3: MODELING CHARCOT MARIE TOOTH 1A WITH INDUCED PLURIPOTENT  
STEM CELL-DERIVED SCHWANN CELLS



## Introduction

In chapter 2, we established a protocol for derivation of Schwann cells from human embryonic stem cells. Potential uses of these cells include disease modeling, drug screening, and transplantation therapy. Here we report the use of our Schwann cell derivation protocol from chapter 2 to model the hereditary Schwann cell disorder, Charcot Marie Tooth 1A.

Given the similarities between human embryonic stem cells (hESCs) and human induced pluripotent stem cells (hiPSCs), as human pluripotent stem cells, our hESC-based Schwann cell differentiation protocol should readily be adapted to human iPSCs<sup>94</sup>. While hESCs can be used for disease modeling by introducing the causative genetic mutation into the hESC line, in many regards, hiPSCs provide a superior platform for disease modeling. hiPSCs are generated by epigenetically reprogramming a patient's somatic cells (ie skin fibroblasts) to a pluripotent state and are genomically identical to the patient's cells. Consequently hiPSCs can offer a disease modeling platform that 1) doesn't require any genetic manipulation, 2) is patient-specific, and 3) can better represent the genetic variability present in patients.

As reviewed in Chapter 1, there are many genetic Schwann cell disorders that might potentially benefit from disease modeling with hiPSCs, including numerous CMT1 subtypes, Hereditary Neuropathy with Liability to Pressure Palsies (HNPP), Dejerine-Sottas disease, schwannomatosis, vestibular schwannomas of Neurofibromatosis Type II (NF2), and perhaps Refsum's disease. Several characteristics of CMT1A made it an initial candidate to model with our Schwann

cell differentiation platform. First of all, there is only one major cell type believed to be implicated in CMT1A (the Schwann cell), as opposed to other disorders like NF2 which likely involve multiple cell types and add a layer of complexity to disease modeling. Second of all, the CMT1A duplication appears to vary less from patient to patient compared to mutations causing some of the other Schwann cell disorders. (It should be noted that some cases of CMT1A can be caused by a point mutation in *PMP22*, and those patients were not included in our study.) HNPP, on the other hand, can be caused by either a deletion or a frameshift mutation resulting in premature stop codon, and such genetic heterogeneity would add additional complexity to our analysis. Additionally, the pathophysiology of how the CMT1A duplication results the clinical symptoms is not well understood, resulting in a fair amount of clinical need. Finally, as CMT1A is the most prevalent genetic PNS disorder, any new knowledge generated by CMT1A modeling with hiPSCs may also have the broadest impact.

Here we use skin biopsies from three different clinically affected CMT1A patients (a father, his daughter, and one unrelated individual) to generate CMT1a hiPSCs, differentiate them into Schwann cells, perform gene expression profiling, and validate those expression profiles at the transcriptional and protein levels.

## Methods

### *CMT1a human induced pluripotent stem cell line generation*

Fibroblasts from three CMT1A patients were obtained from the Coriell Biorepository (GM05148, GM05165, GM05167). In accordance with previously published protocols<sup>95</sup>, fibroblasts were reprogrammed into induced pluripotent stem cells using the Cytotune Sendai Reprogramming Kit (LifeTech A1378001). After 2 weeks of reprogramming, hiPSCs were identified by their colony morphology and replated onto mouse embryonic fibroblast (MEF) feeder layers. They were maintained on MEF feeder layers through weekly passaging for up to 50 passages.

### *Schwann cell differentiation from CMT1A hiPSC lines*

CMT1A and control hiPSCs were plated and differentiated into putative Schwann cells, as described extensively in Appendix 1. Briefly, colonies of pluripotent cells were rendered into single cells and plated on Geltrex, an artificial basement membrane-like matrix. They were then treated with a combination of small molecules to induce neuronal and Schwann cell differentiation:

1. To initiate differentiation, aspirate the medium and add KSR medium containing 10  $\mu$ M SB-431542 and 500 nM LDN-193189 (day 0).
2. On day 2 of differentiation, aspirate the medium and add KSR medium containing 10  $\mu$ M SB-431542, 500 nM LDN-193189, 3  $\mu$ M CHIR 99021, 10  $\mu$ M DAPT. (*activates WNT while blocking gamma secretase/Notch*)
3. On day 4 of differentiation, aspirate the medium and add KSR/NB (3:1) medium containing 3  $\mu$ M CHIR 99021 and 10  $\mu$ M DAPT (final

concentrations are for the combined KSR/NB mixture).

4. On day 6 of differentiation, aspirate the medium and add KSR/NB (1:1) medium containing 3  $\mu$ M CHIR 99021 and 10  $\mu$ M DAPT.
5. On day 8 of differentiation, aspirate the medium and add KSR/NB (1:3) medium containing 3  $\mu$ M CHIR 99021 and 10  $\mu$ M DAPT. Some toxicity may be observed that is inversely correlated with efficiency of SOX10 induction.
6. On day 10 of differentiation, aspirate the KSR/NB and add NB medium containing 200  $\mu$ M dibutyrl cAMP and 200  $\mu$ M sodium L-ascorbate.
7. On day 14 of differentiation, aspirate the NB and add NB medium containing 200  $\mu$ M dibutyrl cAMP and 200  $\mu$ M sodium L-ascorbate.
8. On day 18 of differentiation, aspirate the NB and add NB medium containing 200  $\mu$ M dibutyrl cAMP and 200  $\mu$ M sodium L-ascorbate.
9. Maintain in this manner until day 21-23 of differentiation, when the cells are ready for purification.

#### *CMT1A hiPSC-derived Schwann cell purification and culture*

The FACS protocol is described extensively in Appendix 1. Briefly, Schwann cells were purified with Fluorescence Activated Cell Sorting (FACS) after 21-23 days of differentiation using a PE-conjugated antibody to the alpha4 integrin, CD49d (R&D Systems, FAB1354P). After FACS, Schwann cells were replated onto tissue culture plates treated with fibronectin (R&D Systems, 1918-FN-02M) and laminin (Cultrex, R&D Systems, 3400-010-1) coated plates. (Plates were coated with 1ug/mL laminin and 2ug/mL fibronectin in PBS for 24 hours). Cells were maintained in

culture for up to 80 days post-FACS using Neurobasal medium (Life Technologies, 21103-049) supplemented with L-glutamine (Life Technologies, 25030-081), B-27 supplement (Life Technologies, 12587-070), N2 supplement (Life Technologies, cat. no. 17502-048), and 1% fetal bovine serum (Hyclone, cat. no. SH30070.03).

### *Immunofluorescence*

Cells were fixed in 4% Paraformaldehyde for 20 minutes, then blocked and permeabilized in 0.5%BSA and 0.1% Triton X-100 in PBS for 30 minutes. Primary antibodies were diluted 1:100 to 1:500 in 0.5%BSA and 0.1% Triton X-100 in PBS and samples were incubated overnight at 4 degrees. Secondary antibodies were diluted 1:1000 in 0.5%BSA and 0.1% Triton X-100 in PBS, and incubated 2 hours at room temperature. Primary antibodies can be found in Appendix 2. Appropriate 488, 568, and 647-conjugated Alexa fluor secondary antibodies were utilized.

### *RNA extraction, real time PCR, and microarray analysis*

Cells were homogenized in Trizol Reagent (Life Technologies, 15596-026) and manufacturer's protocols were followed to extract total RNA. 0.5 ug total RNA was reverse transcribed into cDNA using the High Capacity cDNA Reverse Transcription Kit (Applied Biosystems, 4387406). Real time PCR was performed on an Eppendorf Realplex Mastercycler Ep gradient S. Cycling conditions are as follows: 95 degrees 2 min, 40 cycles (95 degrees 3 seconds, 60 degrees 30 seconds). Primer probes can be found in Appendix 2. Data from real time PCR for microarray validation probes in were displayed as fold change in CMT1A sample expression versus median gene expression in controls, and analyzed with the ratio paired t-test. Four pairs of CMT1A hiPSC-derived Schwann cells and controls were hybridized to the

Affymetrix Primeview Human Gene Expression Array by the Johns Hopkins Deep Sequencing and Microarray Core. Data was analyzed and visualized using Partek and Spotfire software. Pathway analysis was performed with Ingenuity Pathway Analysis on genes up- and downregulated at least 3 standard deviations from the mean (corresponding to a fold change of 2.9 in CMT1A samples vs controls), and Gene Ontology analysis was performed with DAVID on genes upregulated at least 3 standard deviations from the mean.

#### *Cytokine expression profiling*

Upon FACS purification, matched pairs of CMT1A and control hiPSC-Schwann cells with at least 1.5-fold upregulation of *PMP22* transcript were identified. FACS purified CD49d+ Schwann cells were maintained in culture for 10 days post-FACS. Cell conditioned medium was profiled with the Human Cytokine Array Kit (R&D Systems, ARY005) according to manufacturer's instructions, and fold change in expression of a given protein in CMT1A hiPSC-Schwann cells versus control hiPSC-Schwann cells were reported.

#### *Statistical analyses*

Data was analyzed using Graphpad Prism 6. Means +/- standard deviation are plotted, and p-values were calculated using the unpaired t test, ratio paired t test, and one-way ANOVA, as noted in each figure legend.

## Results

*CMT1A patient fibroblasts may be successfully reprogrammed into induced pluripotent stem cells*

Here we report the successful generation of CMT1A hiPSCs and their subsequent differentiation into Schwann cells (**Fig. 3-1A**). We obtained skin fibroblasts from three different CMT1a patients from the Coriell biorepository: a father (51 year old Caucasian male), his daughter (a 28 year old Caucasian female), and an unrelated CMT1A patient (17 year old Caucasian male). Using multiplex ligation dependent probe amplification (MLPA), Coriell had confirmed the presence of the *PMP22* duplication in the CMT1A patients. Skin fibroblasts were also obtained from two unrelated healthy controls for hiPSC generation, and hESC line H9 was used as an additional control (**Table 1**). CMT1A and control fibroblasts were reprogrammed into hiPSCs using non-integrating Sendai virus delivery of the four Yamanaka factors (*OCT4*, *SOX2*, *KLF4*, and *c-MYC*). The resulting hiPSC colonies are positive for several classical pluripotency markers, including NANOG, TRA1-60, TRA1-81, SSEA3, and SSEA4 (**Fig. 3-2**). Because the epigenetic reprogramming process can introduce chromosomal rearrangements and the cell culture process can select for genomic rearrangements conferring a growth advantage, it is also important to verify that all the hiPSC lines have normal karyotypes<sup>96</sup> (**Fig. 3-3A**). In addition, because of the use of Sendai virus to deliver the four reprogramming transcription factors, it is important to make sure that the Sendai virus is no longer present in the hiPSC culture after several passages; long-term presence of Sendai virus would likely alter the differentiation propensity of the hiPSC line. PCR amplification of Sendai virus-specific genes demonstrated that

there is no residual Sendai virus contaminating our hiPSC cultures (**Fig. 3-3B**). From three starting fibroblasts, a total of 18 hiPSC clones were ultimately created. It is well established that different hiPSC clones have varying propensity to differentiate towards different lineages<sup>94</sup>, and that expression of certain RNAs and microRNAs can predict whether an hiPSC clone will differentiate more readily towards neuronal lineages<sup>97,98</sup> (as opposed to remaining undifferentiated or tending towards mesodermal and endodermal lineages). We screened our 18 clones for expression of the genes *HHLA1* and *LincROR*, which were shown by Shinya Yamanaka's group to predict clones would be differentiation-defective versus differentiation competent<sup>98</sup>. In addition, we also screened all our clones for *microRNA 371* cluster expression, which was shown by Kim, et al to predict differentiation towards neuronal lineages<sup>99</sup>. Based on the results of our screens (data not shown), five CMT1A hiPSC clones representing three patients were chosen for Schwann cell differentiation.

*CMT1A and control hiPSCs can generate Schwann cells with comparable yield and Schwann cell marker gene expression levels*

These CMT1A hiPSCs (and control hiPSCs) were then differentiated into Schwann cells using the LSB2i protocol developed in chapter 2 of this dissertation. After following the LSB2i differentiation scheme for 21-23 days, the Schwann cells were FACS purified using an antibody against Schwann cell alpha4 integrin, CD49d. Over the course of dozens of control (n=28) and CMT1A (n=95) hiPSC differentiation batches, it was found that both populations give rise to similar percentages of CD49d+ Schwann cells (**Fig. 3-4A**). Additionally, we used real time



PCR to examine the enrichment of Schwann cell genes cadherin 19 (*CDH19*) and myelin protein zero (*MPZ*) between the CD49d+ Schwann cell fraction and the CD49d- non-Schwann cell fraction, providing a quality control metric for FACS purification efficacy. In both the control and CMT1A Schwann cell purifications, no significant differences were found between *CDH19* and *MPZ* enrichment in control hiPSC-derived Schwann cells and CMT1A hiPSC-derived Schwann cells (**Fig.3-4B**). These experiments demonstrate that the CMT1A and control hiPSC lines all yield similar percentages of Schwann cells with similar Schwann cell lineage gene enrichment levels, making them a fair platform for further molecular studies.

*CMT1A hiPSC-derived Schwann cells upregulate PMP22 gene expression relative to controls*

Next we looked at the *PMP22* gene expression levels of the CMT1A Schwann cells versus controls (**Fig. 3-4C**). We found that while *PMP22* expression had quite a broad range in both CMT1A- and control hiPSC-derived Schwann cells, overall, the CMT1A Schwann cells did indeed express more *PMP22* ( $p = 0.0039$ ). Because CMT1A patients have a total of three copies of *PMP22* and healthy controls have two copies of *PMP22*, 1.5x more *PMP22* expression in the CMT1A hiPSC-derived samples might theoretically be expected. Yet, the variability in *PMP22* gene expression that we see is in line with what is seen in clinical samples as well<sup>13-15</sup>.

*Microarray profiling of CMT1A hiPSC-derived Schwann cells and controls reveals upregulation of a non-PMP22 CMT1A duplicated region gene, as well as upregulation of inflammatory signaling pathways*

To find global gene expression differences between CMT1A hiPSC-Schwann cells and controls, four independently differentiated samples from CMT1A hiPSCs (three samples from one clone from patient 5148, one sample from one hiPSC clone from unrelated patient 5165) and controls (two samples from one clone from control patient 2623, two samples from hESC line H9) were submitted for microarray analysis. Samples were collected immediately after FACS purification, and were selected for a minimum of 1.5-fold *PMP22* upregulation by qRT-PCR. The Affymetrix Human Primeview array was chosen as it profiles expression of 49,000 probes for well characterized genes. In **Fig. 3-5**, a volcano plot of microarray results can be viewed, with  $\text{Log}_2(\text{fold change in gene expression})$  on the x-axis, and the significance of that fold change,  $-\text{Log}(\text{p-value})$ , on the y-axis. Overall, it is apparent that several genes are upregulated in the CMT1A hiPSC-Schwann cells relative to controls. Notably, *PMP22* is 1.74-3.14 fold upregulated in the profiled CMT1A samples, and *HS3ST3B1*, another gene from the CMT1A duplicated region, is upregulated 3.07-5.35 fold. The upregulation of *HS3ST3B1* is very interesting as it is located in the CMT1A duplicated region, but previously has not been studied in CMT1A pathogenesis (**Fig. 3-1B**). The Primeview array also contains probes for a handful of other genes from the CMT1A duplicated region, and while none of those appear to be differentially expressed (**Fig. 3-8**), it is indeed possible that other non-coding RNAs and predicted genes that were not evaluated by the microarray

may be found to be differentially expressed by RNA-sequencing analysis in a future study.

To better understand the broader patterns characterizing the differentially expressed genes, all the genes that were differentially expressed at least 3 standard deviations from the mean (corresponding to a fold change of 2.9x higher expression in CMT1A samples) were analyzed with Ingenuity Pathway Analysis (IPA; Canonical Pathways function) and DAVID (Biological Process, Cellular Components, and Biocarta functions). One clear theme was that several inflammatory pathways appeared to be implicated in several types of gene ontology analysis: the complement cascade, humoral immunity, granulocytes and agranulocytes, chemotaxis and cytokine response pathways all received statistically significant scores (**Fig. 3-6**). To validate these results, several genes of interest were selected based on the IPA and DAVID results (**Fig. 3-5**, marked genes) and evaluated with qRTPCR on biologically independent samples from additional CMT1A hiPSC clones and genotypes (**Fig. 3-7A**). hiPSC-Schwann cells from five hiPSC clones representing three CMT1A patients were represented. Although it is apparent that there is quite a bit of variability in expression levels of these genes, there appears to be a pattern of increased inflammatory gene expression (specifically, *TGFBi*,  $p < 0.0001$ ; *CXCL14*,  $p < 0.001$ ; *CXCL12*,  $p < 0.01$ ; *IL1R1*,  $p < 0.01$ , *IL8*,  $p < 0.05$ ) in CMT1A hiPSC-Schwann cells relative to controls.

*CMT1A hiPSC-derived Schwann cells upregulate protein expression of multiple pro-inflammatory cytokines*

This implores the question of whether the upregulated inflammatory gene expression translates into increased inflammatory protein expression. To investigate inflammatory protein expression, commercially available cytokine array panels were purchased from R&D systems. These panels consist of a membrane spotted with antibodies to 36 different cytokines, chemokines, complements, and acute phase proteins, and using method similar to a sandwich ELISA, inflammatory proteins secreted by Schwann cells into their tissue culture media can be assessed. The results of our study (**Fig. 3-7b**) demonstrate statistically significant upregulation of 14 of the 36 proinflammatory proteins profiled, including CXCL1<sup>100-104</sup> ( $p < 0.05$ ), IL-6<sup>105-108</sup> ( $p < 0.01$ ), IL-8<sup>109,110</sup> ( $p < 0.01$ ), MCP-1<sup>110-115</sup> ( $p < 0.01$ ), and sTREM-1 ( $p < 0.001$ )<sup>116</sup>. Most pro-inflammatory cytokines have multiple functions in different contexts, but two common themes among all these particular proteins are that they can either recruit monocytes/macrophages or neutrophils to areas of tissue damage. These observations indicate that CMT1A hiPSC-Schwann cells secrete increased levels of monocyte and neutrophil chemotactic agents, which in turn suggests that endogenous Schwann cells of CMT1A patients may also secrete increased levels of pro-inflammatory mediators.

**Figure 3-1: CMT1A hiPSC generation and Schwann cell differentiation overview**

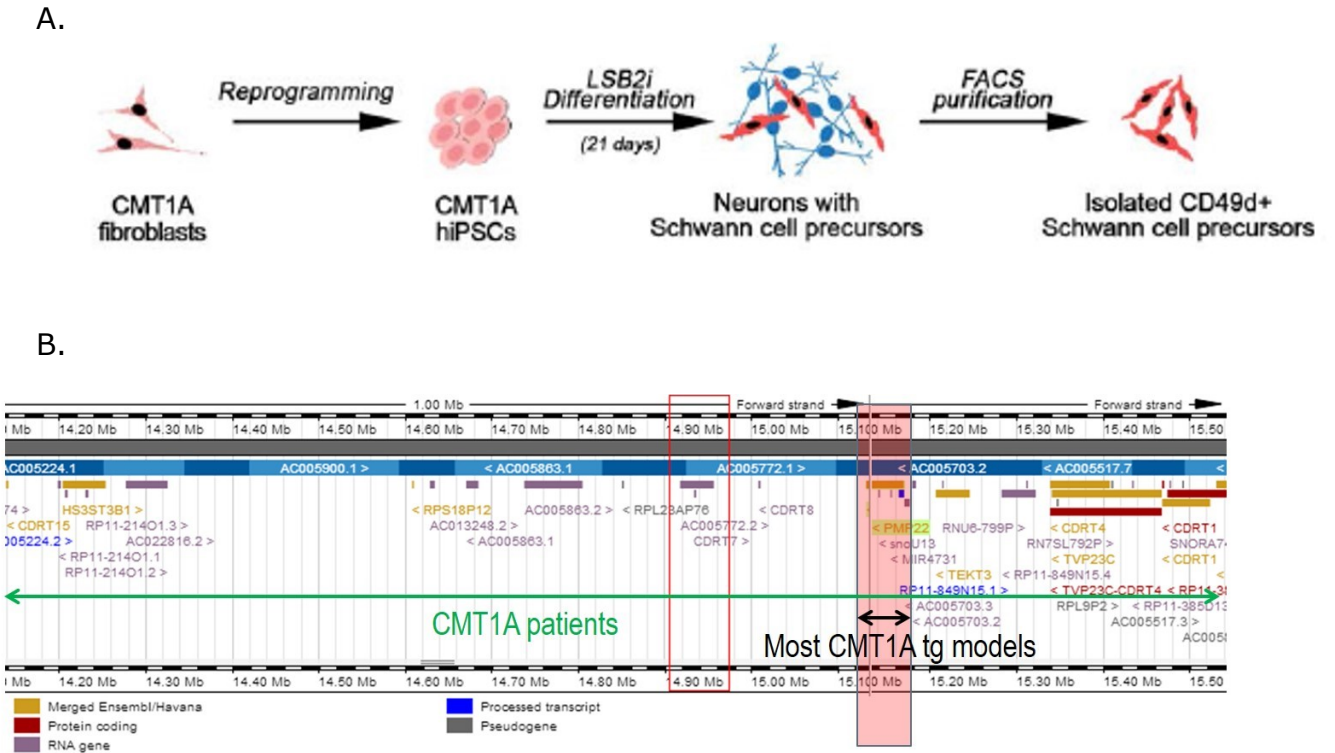


**Figure 3-1. A.** Schematic of the reprogramming methods used to generate CMT1A patient hiPSC derived Schwann cells from CMT1A patient fibroblasts. **B.** The 1.4MB CMT1A duplicated region on chromosome 17 present in CMT1A patients, with the region overexpressed in most rodent models highlighted.

**Table 3-1: Control and CMT1A lines included in this study**

<b>Type</b>	<b>Age (years)</b>	<b>Sex</b>	<b># clones</b>
CMT1A (5148)	17	M	3
CMT1A (5165)	51	M	7
CMT1A (5167)	28	F	8
Healthy control (2623)	61	F	4
Healthy control (01582)	11	F	8
Embryonic stem cell (H9)	n/a	F	n/a

**Figure 3-2: CMT1A patient-derived hiPSCs exhibit clonal morphology and express pluripotency markers**

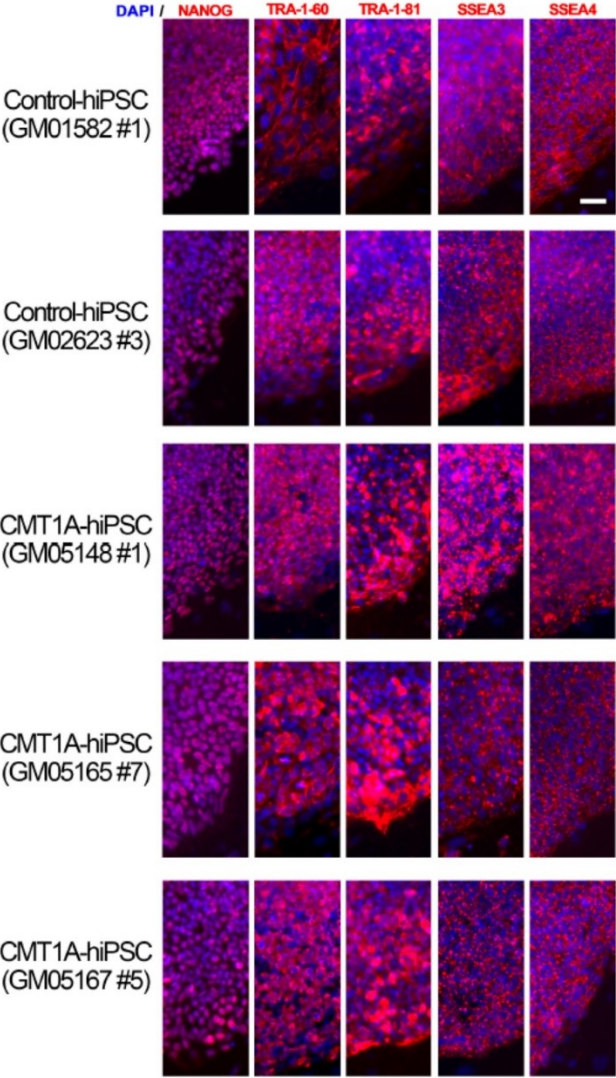


**Figure 3-2.** CMT1A and control hiPSCs acquire clonal morphology and express human stem cell pluripotency markers. Representative immunofluorescence for Nanog, TRA1-60, TRA1-81, SSEA3, and SSEA4 staining.

**Figure 3-3: CMT1A hiPSC quality control**

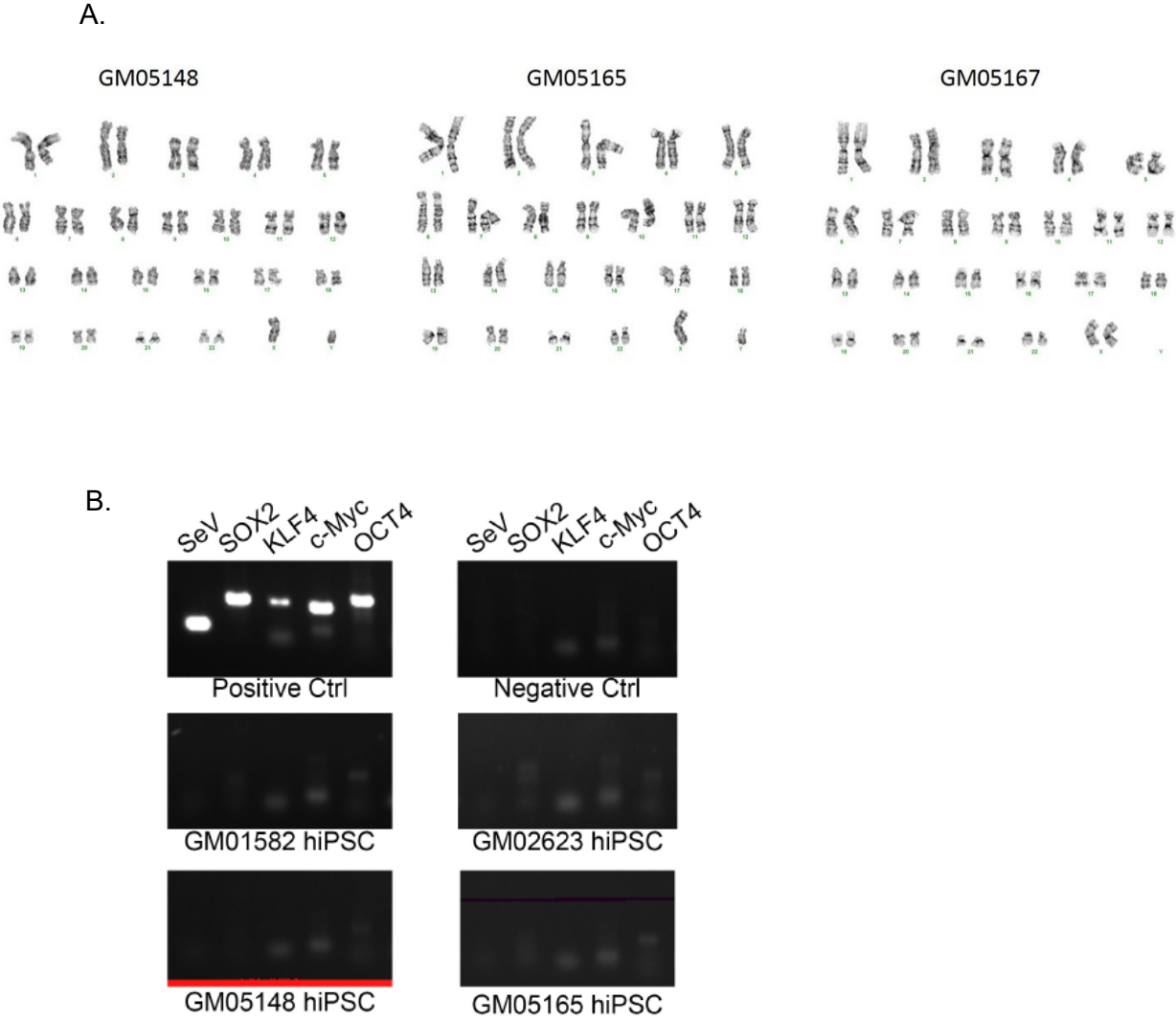


**Figure 3-3. A.** CMT1A hiPSC lines from three different patients exhibit normal karyotypes, as demonstrated by representative images from cytogenetic analysis. **B.** PCR for Sendai virus transgenes demonstrate that CMT1A hiPSCs and control lines do not express Sendai virus transgenes after 10 passages.



### Figure 3-4: CMT1A hiPSC differentiation into Schwann cells

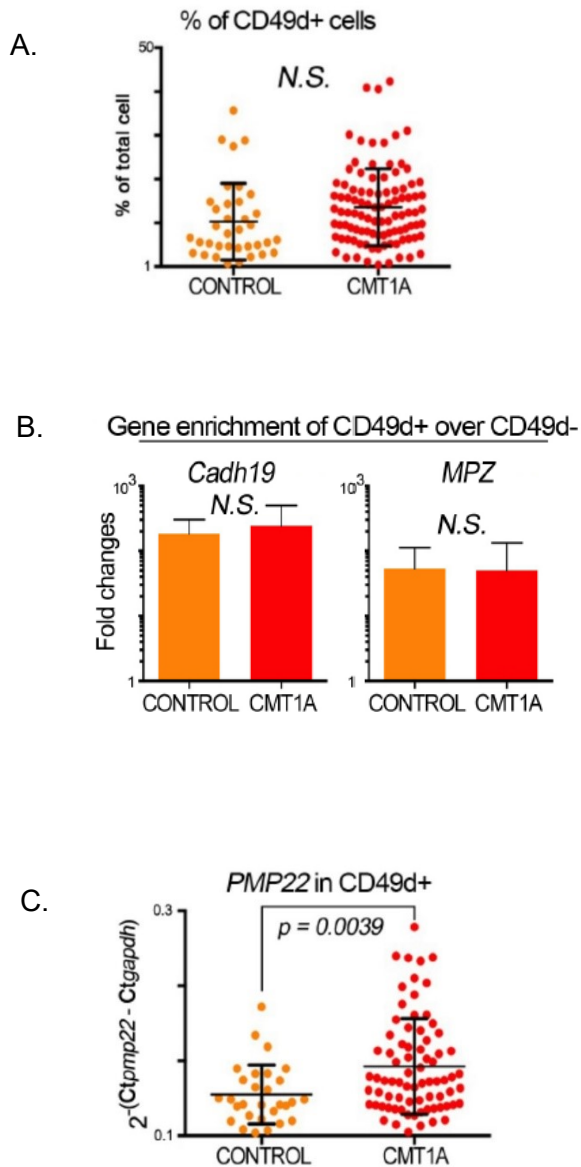


**Figure 3-4. A.** FACS purification of LSB2i treated CMT1A and control hiPSCs reveals similar yields of CD49d+ Schwann cells. Control n=36, CMT1A n=99, p-value=ns, unpaired t test. Data expressed as mean +/- SD. **B.** Post-FACS evaluation of Schwann cell gene enrichment in CD49d+ Schwann cells versus matched CD49d- non-Schwann cells, by real time PCR. Control n=11 for *CDH19*, n =15 for *MPZ*. CMT1A n=28 for *CDH19* and n = 37 for *MPZ*. p =ns by unpaired t test. **C.** Real time PCR for *PMP22* in CMT1A and control CD49d+ Schwann cells. Data expressed as mean +/- SD. Control n=29, CMT1A n=76, p<0.0039, unpaired t-test.

**Figure 3-5: Global gene expression profiling of CMT1A hiPSC-Schwann cells**

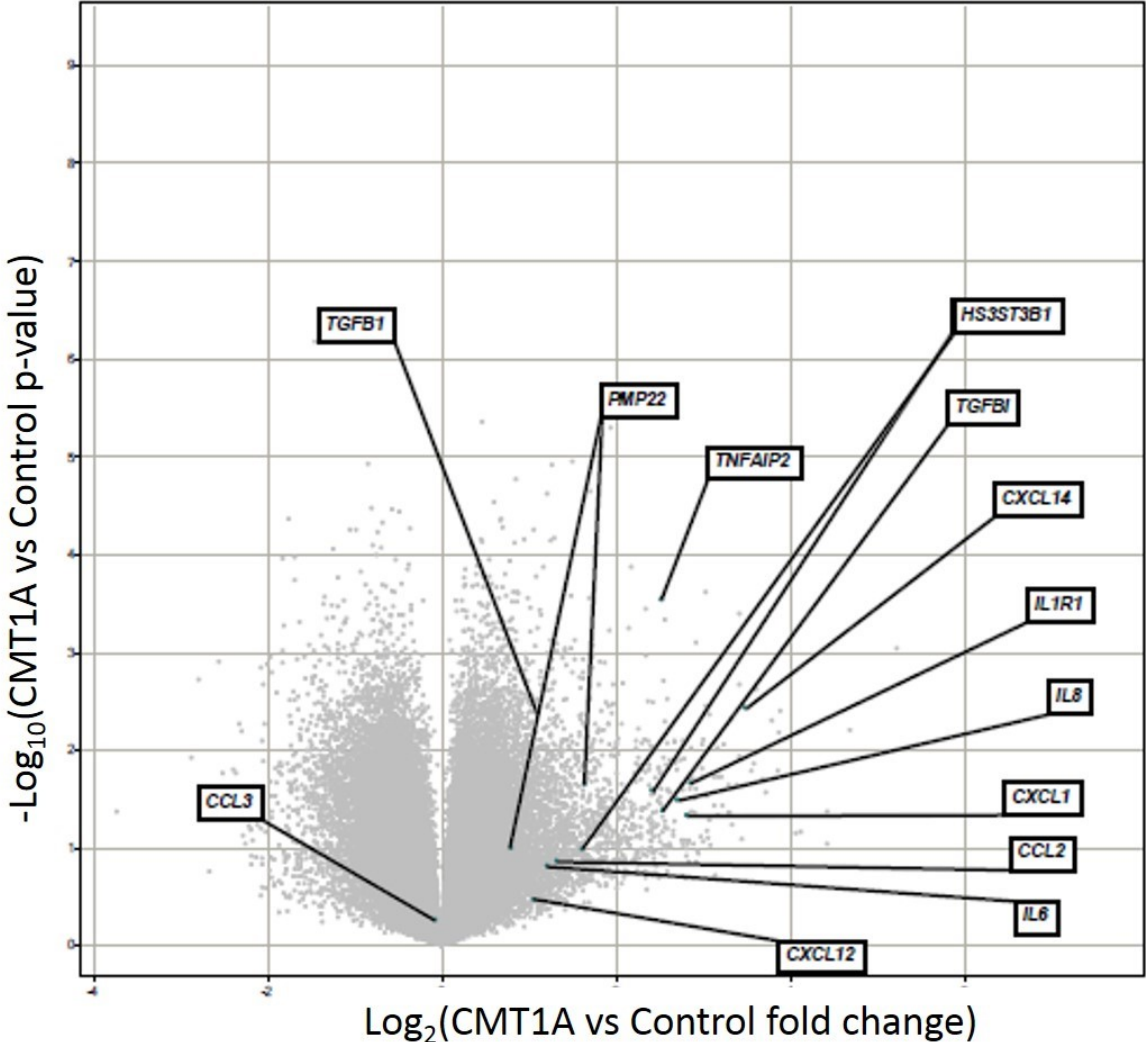


**Figure 3-5.** Volcano plot representation of microarray array expression profiling of four biologically independent CMT1A hiPSC-Schwann cells samples and four biologically independent control hPSC-Schwann cell samples with *PMP22* fold change greater than 1.5. Select genes of interest highlighted and designated for validation with qRT-PCR.

**Figure 3-6: Gene ontology and pathway analysis of CMT1A hiPSC-Schwann cell expression profiling results**

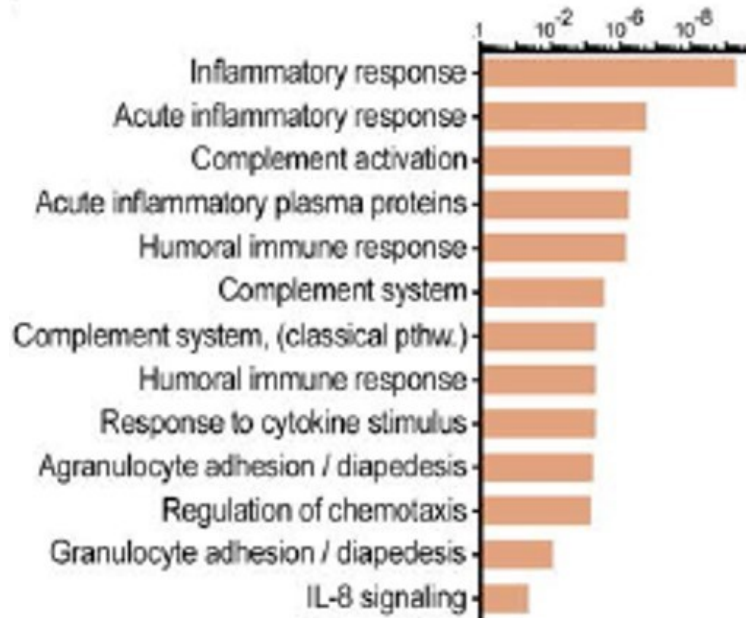


**Figure 3-6.** Results from DAVID gene ontology and Ingenuity Pathway Analysis of differentially expressed genes. Data expressed as p-value of each pathway.

**Figure 3-7: Validation of CMT1A hiPSC-Schwann cell microarray results**

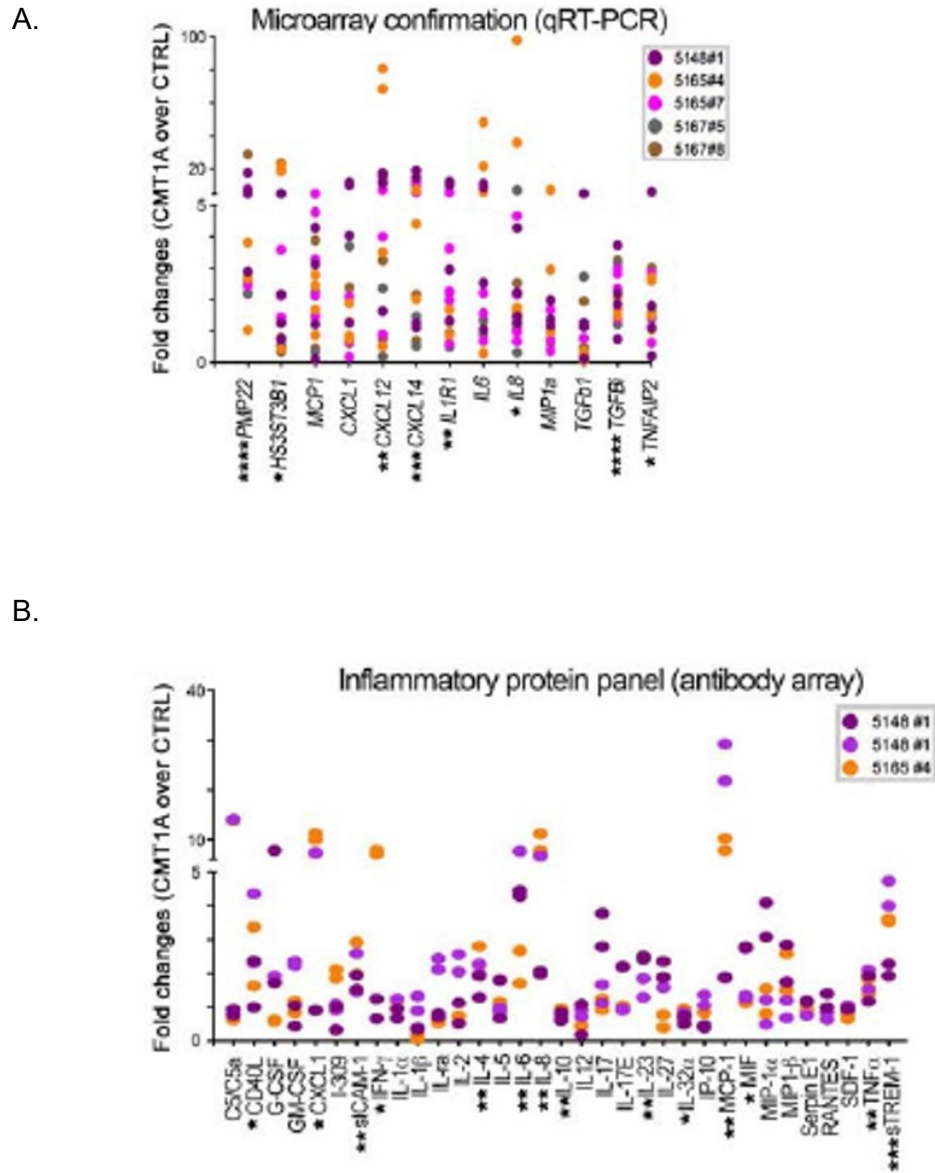


**Figure 3-7. A.** Real time PCR validation of microarray results in biologically independent samples from 5 hiPSC clones representing 3 CMT1A patients. Data expressed as fold change versus gene expression in control hiPSC-derived Schwann cells. \*  $p < 0.05$ , \*\*  $p < 0.01$ , \*\*\*  $p < 0.001$ , \*\*\*\*  $p < 0.0001$ , ratio paired t test. **B.** Cytokine array profiling of cell conditioned medium from Day 10 post-FACS CD49d+ Schwann cells. Data expressed as fold change in protein expression between CMT1A Schwann cells versus matched control. Data from independent differentiations are displayed as different colors. \*  $p < 0.05$ , \*\*  $p < 0.01$ , \*\*\*  $p < 0.001$ , \*\*\*\*  $p < 0.0001$ , ratio paired t-test.

**Figure 3-8: Microarray expression of CMT1A duplicated region genes**

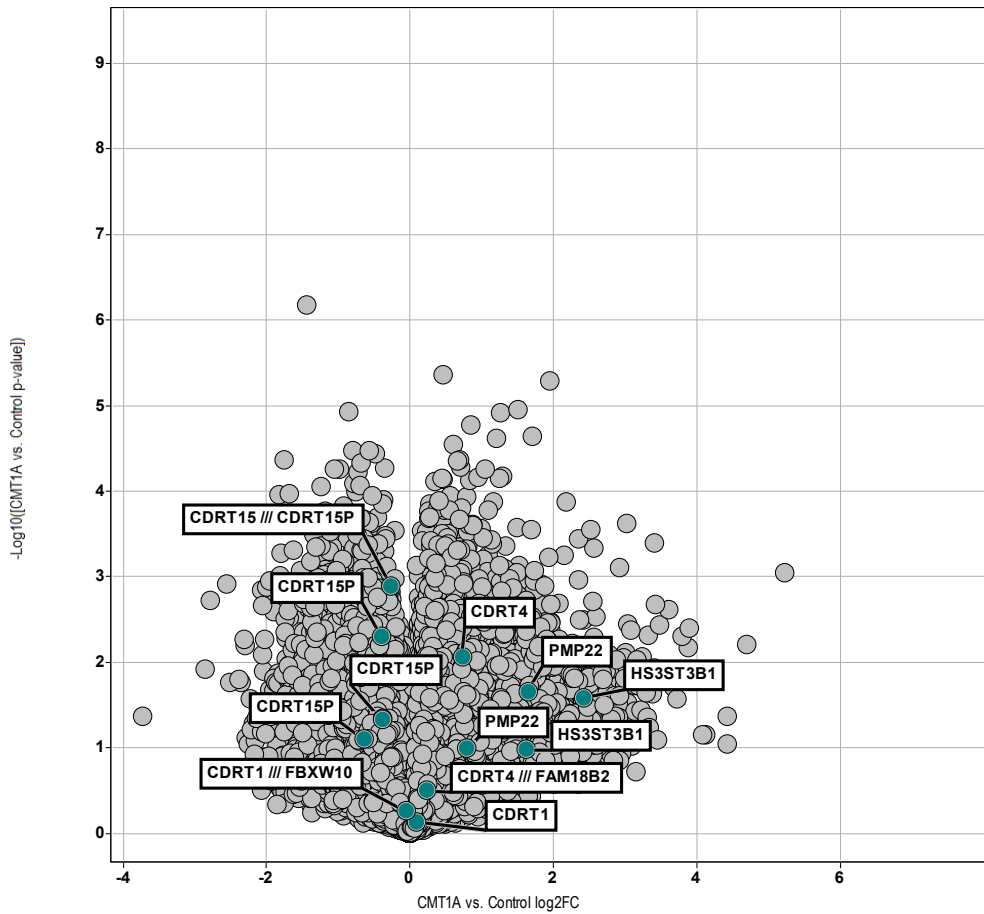


**Figure 3-8.** Volcano plot visualization of CMT1A duplicated region probes included on the Affymetrix human primeview array. X-axis displays the  $\log_2$ (fold change) in expression of a given gene in CMT1A vs control samples. Y-axis displays the  $-\log(p \text{ value})$ .

## Discussion

CMT1A is not clinically thought of as inflammatory disorder, although there is increasing laboratory evidence to support this idea<sup>23,117-119</sup>. Our study found statistically significant upregulation of several cytokines, and of those cytokines, CXCL1, IL-6, IL-8, MCP-1, and STREM-1 have particularly large magnitudes of upregulation.

MCP-1, which has the most dramatic magnitude of upregulation, is known to be expressed by Schwann cells in other pathological contexts, such as Wallerian degeneration<sup>120-122</sup>. It is a potent monocyte/macrophage chemoattractant<sup>114,115</sup>, and has been implicated in CNS neurodegenerative diseases as well<sup>120</sup>. CXCL1, in contrast, appears largely to mediate neutrophil recruitment<sup>100-103</sup>, with only one report of its role in monocyte recruitment<sup>104</sup>. IL-6 has previously been reported as being produced by injured Schwann cells<sup>50</sup>, and is involved in both neutrophil<sup>108</sup> and monocyte<sup>105,106,121</sup> chemotaxis. One study even suggests that it acts as a switch between neutrophil and monocyte recruitment<sup>107</sup>. Similarly, IL-8 also seems to mediate both neutrophil and monocyte chemotaxis<sup>109,110</sup>. STREM-1, is the soluble form of TREM-1, which is an Ig superfamily receptor whose binding induces secretion of IL-8, MCP-1, and other cytokines as well as the activation of neutrophils and monocytes during acute inflammation<sup>116</sup>.

As these cytokines largely function as either neutrophil or monocyte chemoattractants, it implies that those cell types might be pathologically recruited to CMT1A patient myelin and contribute to nerve damage. This idea is corroborated by rodent studies from Rudolf Martini and Lucia Notterpek's groups, which have

found that two different CMT1A mouse models overexpressing *PMP22* (the C22 and C61 models) and one model with a *PMP22* point mutation (the Trembler-J model) all exhibit increased macrophage infiltration in their nerves<sup>23,118,119</sup>. Furthermore, the Martini group found that they found that macrophage infiltration in the C22 mouse is largely mediated by increased MCP-1<sup>22</sup>, one of the very proteins upregulated in our cytokine array panel. The Martini group's results largely corroborate our own, demonstrating that our hiPSC-based studies can indeed yield relevant and reproducible findings.

Our study may also help illuminate two questions that currently remain unaddressed by *in vivo* rodent or clinical studies. One such question regards the role of the leukocytes recruited to CMT1A nerve lesions. Are these leukocytes a secondary source of pathology, responding to phagocytose myelin debris from chronic myelin damage? Or are they a source of primary pathology, being recruited to undamaged nerves and actively mediating their destruction. Our data, taken from Schwann cell precursors that have been differentiated for only 31-33 days (21-23 days pre-FACS, 10 days post-FACS), suggests that the latter *is* the case. Schwann cell precursors, the earliest member of the Schwann cell lineage, likely best mimic the status of human fetal Schwann cells. If a patient's endogenous Schwann cells precursors are secreting such high levels of pro-inflammatory cytokines, it implies that leukocytes might be recruited early to the patient's nerves and actively contribute to pathology even before symptoms become clinically apparent. Alternatively, it is also quite likely that these cytokines are not acting as leukocyte chemoattractants in the context of CMT1A, but rather as more general mediators of immune signaling.

Another question raised by rodent models of CMT1A is what cell type is responsible for the observed increase in macrophage recruitment to CMT1A rodent nerve lesions? This question is technically difficult to address through rodent and clinical studies, as it would be challenging to determine which cell type within a nerve biopsy—a mixture of neurons, Schwann cells, fibroblasts, and others—is actually secreting the chemokines. Our study though, through its use of a FACS-purified population of Schwann cells, is well positioned to address this question, and our findings imply that the Schwann cells are specifically responsible for the secretion of the pro-inflammatory cytokines.

Aside from the inflammatory phenotype, our CMT1A hiPSC-Schwann cells exhibit another novel genetic phenotype. They overexpress the gene Heparan sulfate glucosamine 3-O-sulfotransferase 3B1 (*HS3ST3B1* or 3-OST-3b), one of the genes from the CMT1A duplicated region that has not previously been reported as upregulated in CMT1A Schwann cells. Heparan sulfates are linear disaccharide glycosaminoglycans that are found tethered to a protein core to form proteoglycans. These proteoglycans are ubiquitously found as cell surface integral membrane proteins and also in the extracellular matrix, where they play a myriad of roles regulating cell-cell interactions, cell signaling, migration, adhesion, growth, differentiation, and more<sup>123,124</sup>. Heparan sulfates can also bind antithrombin, fibroblast growth factors, vascular endothelial growth factor, interleukin-3, interferon-gamma, granulocyte macrophage colony stimulating factor, and many additional growth factors, thereby regulating coagulation, angiogenesis, and many other biological processes<sup>125</sup>. The fine structures of heparan sulfate determines



their affinity for a given ligand, and these fine structures are created through the action of sulfotransferases (ie 3-O-sulfotransferase1, 3-O-sulfotransferase 2, etc).

The *HS3ST3B1* gene in the CMT1A duplicated region encodes one such sulfotransferase, specifically a type II integral membrane protein. *HS3ST3B1* is one of seven isoforms belonging to the 3-O-sulfotransferase family, which catalyzes the addition of sulfate groups to the 3-OH position of glucosamine in heparan sulfate<sup>126</sup>. Sulfation at the C3-OH moiety of heparan sulfate is one of the rarest heparan sulfate modifications, occurs late in heparan sulfate biosynthesis, and can be regulated in a tissue specific manner (due to the availability of a multitude of isoforms), making 3-O-sulfonation a rate limiting step that is likely an important regulator of numerous biological processes<sup>127,128</sup>.

The *HS3ST3B1* enzyme is expressed in a broad range of tissues and is particularly enriched in liver and placenta<sup>129</sup>. Whereas two other isoforms (HS3ST2 and HS3ST4) appear to be the predominant isoforms expressed in the nervous system, one study found low, yet certainly detectable, *HS3ST3B1* expression in the trigeminal ganglia<sup>128</sup>. Interestingly, that study did not detect any *HS3ST3B1* gene expression in axonal/Schwann cell biopsies, yet our study does find it expressed in Schwann cells.

Various functions have already been ascribed to *HS3ST3B1* in pathological contexts. It can mediate viral entry of Herpes Simplex Virus-1 (HSV-1) into cells, as its overexpression has been found to convert HSV-1 resistant cells to HSV-1 susceptible cells<sup>124,130</sup>. *HS3ST3B1* can also induce the epithelial mesenchymal transition in cancer, as was demonstrated in a study of a pancreatic cancer cell

line<sup>131</sup>. Linkage analysis of a family with autosomal dominant idiopathic sclerosis mapped the likely genetic cause to either *HS3STB1* or the nearby *HS3STA1*, suggesting the gene may play a role in musculoskeletal development<sup>132</sup>, though it should be noted that no specific mutations in *HS3STB1* could actually be identified in that study. More generally, the broader family of 3-O-sulfotransferases (which includes HS3ST1, HS3ST2, HS3ST3, etc) has been found to be a key regulator between production of an anticoagulant form of heparan sulfate, versus a non-anticoagulant form of heparan sulfate, though HS3ST1 appears to be the major isoform mediating this role<sup>127</sup>.

As to the specific function of HS3ST3B1 in Schwann cells, further investigation is warranted. A literature search didn't produce any previous publications on HS3ST3B1 action in Schwann cells or myelin. A search on HS3STB1 roles in the central nervous system produced one marginally relevant paper on HIV neuroimmunology<sup>133</sup>. A group cloned the Tat gene from patients with HIV and HIV-dementia and overexpressed it in monocytoid lines; they found a specific induction of the *HS3ST3B1* gene when using the HIV-dementia Tat clone, and an induction of the *MCP-1* gene when overexpressing either Tat clone. Their results have some commonalities with our results (CMT1A Schwann cells upregulate *HS3STB1* gene and MCP-1 protein), but it is unclear whether any broader meaning can be ascertained from these parallels. Perhaps HS3STB1 plays a role in neuroimmune regulation – the best way to determine its specific role in the context of our study would be to overexpress it in control hESC or hiPSC-Schwann cells and perform microarray analysis.

In summary, in this profiling of CMT1A patient hiPSC-derived Schwann cells, we found upregulation of several pro-inflammatory cytokines and upregulation of *HS3ST3B1*, a gene from the CMT1A duplicated region. As exciting as our results may be, there are some limitations that should be kept in mind. First of all, individual hiPSC lines vary quite dramatically in their *in vitro* behavior, meaning their differentiation capacity and gene expression profiles. For instance, it has been found that two different hiPSC lines derived from the same patient can vary as much as hiPSC lines from two different patients<sup>94</sup>. Consequently, it is prudent to validate all hiPSC results using a second method. In the stem cell field, most hiPSC studies are validated through use of genetically manipulated congenic lines. That is, genome editing is used to either correct a genetic mutation in a disease hiPSC line or introduce a genetic mutation to a control hiPSC line. By maintaining a constant genomic background, such studies can control for the variable “personalities” of hiPSC lines and demonstrate that a given phenotype is specific to the mutation of interest. The large 1.4MB size of the CMT1A duplicated region makes genetic correction challenging, so our validation studies will be performed using an alternative method in Chapter 4.

Another caveat of our results is that these studies were performed under *in vitro* settings, using serum containing tissue culture media to presumably induce cytokine release. In an *in vivo* setting, under different environmental conditions, the same combination of cytokines may not be released from the Schwann cells, though the Martini group’s *in vivo* corroboration of our *in vitro* MCP-1 upregulation suggests this concern may not be merited.

## Conclusion

CMT1A patient hiPSC-derived Schwann cells express higher levels of *PMP22* and heparan sulfate sulfotransferase *HS3ST3B1* transcripts, as well as higher levels of several inflammatory gene transcripts and proteins. It implies that immune signaling dysregulation may be a pathologic feature of CMT1A, that this dysregulation is a Schwann cell intrinsic phenomenon, and suggests that leukocyte recruitment to early nerves may be a primary contributor to CMT1A pathogenesis, rather than a late reaction to myelin damage. If these results can be validated by a second model, it may compel us to reexamine our current understanding of CMT1A pathogenesis and treatment to better incorporate this new model of inflammatory pathology.

CHAPTER 4: VALIDATION OF THE CMT1A HIPSC PHENOTYPE WITH TWO  
ADDITIONAL PATIENT DERIVED CMT1A MODELS

## Introduction

Most disease modeling studies in the stem cell field are currently performed using human induced pluripotent stem cells (hiPSCs), yet there also exist two other methods for generating patient-derived cells that can be harnessed to model disease. One such method is direct lineage reprogramming, also known as transdifferentiation, in which one somatic cell type, typically a fibroblast, is epigenetically reprogrammed into a another somatic cell type. The resulting cell is generally referred to as a “directly converted” or “induced” cell. Methods have already been generated for direct lineage reprogramming into myoblasts<sup>134</sup>, pancreatic B-islet cells<sup>135</sup>, neurons<sup>136</sup>, neural progenitors<sup>137</sup>, motor neurons<sup>138</sup>, oligodendrocytes<sup>139,140</sup>, neural crest<sup>141</sup>, hematopoietic cells<sup>142</sup>, and many more cell types, and their ability to model human diseases *in vitro* has been established as well<sup>141,143,144</sup>.

Another source of patient-derived cells for disease modeling are embryonic stem cell lines from blastocysts with a preimplantation genetic diagnosis (PGD) of a disease of interest. PGD is a technique that allows for genotyping of IVF-generated embryos in couples carrying<sup>145</sup> a serious genetic defect. A representative cell is biopsied three to four days post-fertilization and tested for the genetic defect, and unaffected embryos can be transplanted into the carrier. The inner cell mass of affected embryos may be cultured to establish an embryonic stem cell line (PGD-hESC) that can be used to further study the disorder caused by the genetic variant. The NIH Stem Cell Repository has a limited yet growing collection of PGD-hESC lines that can be studied with federal funding, including lines carrying the genetic

mutations causing Duchenne muscular dystrophy, spinal muscular atrophy, Huntington's disease, hemophilia B, hypertrophic cardiomyopathy, hydroxysteroid dehydrogenase deficiency, cystic fibrosis, fascioscapulohumoral muscular dystrophy, multiple endocrine neoplasia 2A, and many more. It may be argued that using a PGD-hESC line is preferable to using a control hESC line with an engineered mutation, as it eliminates possibility of off-target effects also allows for expression of the genetic variant with the most physiologically relevant timeline and tissue expression pattern. If CMT1A were modeled through genetic manipulation of control hESC lines, *a priori* assumptions would also need to be made about which genes from the 1.4 MB CMT1A duplicated region should be overexpressed, what dosage of overexpression should be used, where those genes should be inserted in the genome, and under which promoter, and use of PGD-hESC lines the need to make such assumptions. Thus far, Huntington's disease<sup>146</sup> and Fragile X-Syndrome<sup>147</sup> have been successfully modeled using PGD-hESC lines, though hiPSC-based disease modeling has largely overshadowed use of PGD-hESC lines. Presumably, as additional PGD-hESC lines are deposited into the NIH repository this disparity may narrow.

In chapter 3, we modeled the CMT1A using patient-hiPSC derived Schwann cells. However, as previously discussed, hiPSC based data can be quite variable and should ideally be validated using alternative methods. Generally, genome editing is used to introduce a mutation into control hiPSCs or to correct a mutation in disease hiPSCs, to control for genomic background and demonstrate that an observed phenotype is specific to that particular genotype.

In contrast, here we propose to validate our CMT1A hiPSC data using two other sources of reprogrammed CMT1A Schwann cells. We have obtained two embryonic stem cell lines derived from blastocytes that have a pre-implantation genetic diagnosis of CMT1A (referred to as CMT1A PGD-hESC lines). Schwann cells can be obtained from these CMT1A PGD-hESC lines through the same LSB2i protocol developed in Chapter 2 and used for CMT1A hiPSC disease modeling in Chapter 3. In addition, our lab has recently published a method for the direct conversion of fibroblasts into neural crest (termed iNC, or induced neural crest)<sup>141</sup>, which can be further differentiated into Schwann cells (termed iNC-SC). The same CMT1A patient fibroblasts that were used to generate CMT1A hiPSCs can also be directly converted into CMT1A iNC-SC, therefore controlling for genotypic differences between the cell lines.

In **Figure 4-1** we can see a diagram of Waddington's epigenetic landscape and how hiPSC-Schwann cells, PGD-hESC-Schwann cells, and iNC-Schwann cells all fit within that paradigm. Use of all three methods of generating patient-derived reprogrammed cells has never been previously implemented, and utilizing three congruent models (**Figure 4-2**) to find a converged phenotype offers a novel paradigmatic contribution to the field of stem cells and regenerative medicine.



## **Methods**

### *CMT1a Preimplantation Genetic Diagnosis embryonic stem (PGD-hESC) cell line generation*

Two embryonic stem cell lines with a preimplantation genetic diagnosis of CMT1A were obtained from the NIH Human Embryonic Stem Cell Repository (HUES PGD11 and 12; NIH registration numbers 94 and 95; NIH approval numbers NIHhESC-11-0094 and NIHhESC-11-0095). Embryonic stem cell lines were generated from blastocysts that were determined to have the CMT1A duplication through pre-implantation genetic diagnosis, and genomic DNA real time PCR was used to verify the presence of the PMP22 duplication in the resulting hESC lines. A Materials Transfer Agreement was performed with Harvard University, and all work performed at Johns Hopkins University was under guidance of the JHU Institutional Stem Cell Research Oversight Committee (ISCRO).

CMT1A PGD-hESC line generation was performed by Benjamin Lannon, a clinical fellow in the laboratory of Kevin Eggan, Harvard Stem Cell Institute.

### *Schwann cell differentiation from CMT1A PGD-hESC cells*

CMT1A and control hiPSCs were plated and differentiated into putative Schwann cells, as described extensively in Appendix 1. Briefly, colonies of pluripotent cells were rendered into single cells and plated on Geltrex, an artificial basement membrane-like matrix. They were then treated with a combination of small molecules to induce neuronal and Schwann cell differentiation:

1. To initiate differentiation, aspirate the medium and add KSR medium

- containing 10  $\mu$ M SB-431542 and 500 nM LDN-193189 (day 0).
2. On day 2 of differentiation, aspirate the medium and add KSR medium containing 10  $\mu$ M SB-431542, 500 nM LDN-193189, 3  $\mu$ M CHIR 99021, 10  $\mu$ M DAPT. (*activates WNT while blocking gamma secretase/Notch*)
  3. On day 4 of differentiation, aspirate the medium and add KSR/NB (3:1) medium containing 3  $\mu$ M CHIR 99021 and 10  $\mu$ M DAPT (final concentrations are for the combined KSR/NB mixture).
  4. On day 6 of differentiation, aspirate the medium and add KSR/NB (1:1) medium containing 3  $\mu$ M CHIR 99021 and 10  $\mu$ M DAPT.
  5. On day 8 of differentiation, aspirate the medium and add KSR/NB (1:3) medium containing 3  $\mu$ M CHIR 99021 and 10  $\mu$ M DAPT. Some toxicity may be observed that is inversely correlated with efficiency of SOX10 induction.
  6. On day 10 of differentiation, aspirate the KSR/NB and add NB medium containing 200  $\mu$ M dibutyrl cAMP and 200  $\mu$ M sodium L-ascorbate.
  7. On day 14 of differentiation, aspirate the NB and add NB medium containing 200  $\mu$ M dibutyrl cAMP and 200  $\mu$ M sodium L-ascorbate.
  8. On day 18 of differentiation, aspirate the NB and add NB medium containing 200  $\mu$ M dibutyrl cAMP and 200  $\mu$ M sodium L-ascorbate.
  9. Maintain in this manner until day 21-23 of differentiation, when the cells are ready for purification.

*CMT1A PGD-hESC-derived Schwann cell purification and culture*

The FACS protocol is described extensively in Appendix 1. Briefly, Schwann cells were purified with Fluorescence Activated Cell Sorting (FACS) after 21-23 days of differentiation using a PE-conjugated antibody to the alpha4 integrin, CD49d (R&D Systems, FAB1354P). After FACS, Schwann cells were replated onto tissue culture plates treated with fibronectin (R&D Systems, 1918-FN-02M) and laminin (Cultrex, R&D Systems, 3400-010-1) coated plates. (Plates were coated with 1ug/mL laminin and 2ug/mL fibronectin in PBS for 24 hours). Cells were maintained in culture for up to 80 days post-FACS using Neurobasal medium (Life Technologies, 21103-049) supplemented with L-glutamine (Life Technologies, 25030-081), B-27 supplement (Life Technologies, 12587-070), N2 supplement (Life Technologies, cat. no. 17502-048), and 1% fetal bovine serum (Hyclone, cat. no. SH30070.03).

#### *CMT1a Induced Neural Crest-derived Schwann cell generation*

Three CMT1A patient fibroblasts and two matching controls were reprogrammed into induced neural crest (iNC) and FACS purified using methods previously published by the Lee Lab<sup>141</sup>. FACS purified iNC were maintained in Neurobasal medium containing 1 ug/ml of doxycycline for 3 days, followed by one more week of incubation with hESC-derived Schwann cell conditioned medium supplemented with CNTF (10 ng/ml) and NRG1 (20 ng/ml), without doxycycline. To stimulate cytokine release, medium was changed to Neurobasal + 1% fetal bovine serum for the last 3 days. Cells were maintained in culture for 2-5 weeks post-FACS.

This work was performed in collaboration with Yong Jun Kim, a postdoctoral fellow in the Lee Lab.

#### *Immunofluorescence*

Cells were fixed in 4% Paraformaldehyde for 20 minutes, then blocked and permeablized in 0.5%BSA and 0.1% Triton X-100 in PBS for 30 minutes. Primary antibodies were diluted 1:100 to 1:500 in 0.5%BSA and 0.1% Triton X-100 in PBS and samples were incubated overnight at 4 degrees. Secondary antibodies were diluted 1:1000 in 0.5%BSA and 0.1% Triton X-100 in PBS, and incubated 2 hours at room temperature. Primary antibodies can be found in Appendix 2. Appropriate 488, 568, and 647-conjugated Alexa fluor secondary antibodies were utilized.

#### *RNA extraction and real time PCR*

Cells were homogenized in Trizol Reagent (Life Technologies, 15596-026) and manufacturer's protocols were followed to extract total RNA. 0.5 ug total RNA was reverse transcribed into cDNA using the High Capacity cDNA Reverse Transcription Kit (Applied Biosystems, 4387406). Real time PCR was performed on an Eppendorf Realplex Mastercycler Ep gradient S. Cycling conditions are as follows: 95 degrees 2 min, 40 cycles (95 degrees 3 seconds, 60 degrees 30 seconds). Primer probes can be found in Appendix 2. Data from real time PCR for microarray validation probes in were displayed as fold change in CMT1A sample expression versus median gene expression in controls, and analyzed with the ratio paired t-test.

#### *Cytokine expression profiling of CMT1A PGD-hESC- and iNC-Schwann cells*

For secreted protein profiling in PGD-hESC-Schwann cells, upon FACS purification, matched pairs of CMT1A and control PGD-hESC-Schwann cells with at least 1.5-fold upregulation of *PMP22* were identified. FACS purified CD49d+ Schwann cells were maintained in culture for 10 days post-FACS. For secreted protein profiling in iNC-Schwann cells, upon FACS purification, matched pairs of CMT1A and control hiPSC-

Schwann cells with at least 1.5-fold upregulation of *PMP22* were identified. Cells were maintained in culture for 2-5 weeks, and to stimulate cytokine release medium was changed to Neurobasal + 1% fetal bovine serum for the last 3 days. Cell conditioned medium was profiled with the Human Cytokine Array Kit (R&D Systems, ARY005) according to manufacturer's instructions, and fold change in expression of a given protein in CMT1A Schwann cells versus control Schwann cells were reported.

#### *Cytokine expression profiling of CMT1A and control patient samples*

De-identified sural nerve biopsies from two patients with genetically proven CMT1A and two histologically normal samples from non-CMT1A patients were obtained from the Johns Hopkins Neuromuscular Histopathology Laboratory under an appropriate Institutional Review Board protocol. Lysates were obtained by sonicating nerve biopsies in RIPA buffer, and equal amounts of protein were then used for secreted protein expression profiling.

#### *Transwell migration assay*

THP-1 human monocyte chemotaxis assays were performed by using the HTS transwell plate system (5 $\mu$ m pore size, Corning). Schwann cell conditioned medium was collected from Day 10 post-FACS hiPSC- and PGD-hESC-Schwann cells, and 2-5 week post FACS iNC-Schwann cells. 100 $\mu$ L of Schwann cell conditioned medium was placed in bottom well with or without anti-MCP1 (R&D). THP-1 monocytes were resuspended in Neurobasal medium (Gibco) + 1% FBS to a concentration of 2.5 million cells/mL, and 100 $\mu$ L was placed in upper wells. After 3 hrs incubation in 37 °C with 5% CO<sub>2</sub>, migrated cells were counted.

### *Compound testing*

CMT1A hiPSC-Schwann cells were incubated with 10 uM each of bortezomib, fenretinide, and olvanil for 24 hours. Total RNA was utilized for PMP22 real time PCR, and cell conditioned medium was used for secreted protein expression profiling.

### *Statistical analyses*

Data was analyzed using Graphpad Prism 6. Means +/- standard deviation are plotted, and p-values were calculated using the unpaired t test, ratio paired t test, and one-way ANOVA, as noted in each figure legend.

## Results

*CMT1A PGD-hESCs exhibit colony morphology, express classical pluripotency markers, are karyotypically normal, and harbor the CMT1A duplication*

Two independent embryonic stem cell lines with a preimplantation genetic diagnosis (PGD-hESC) of CMT1A were obtained, and we verified their pluripotency marker expression by immunofluorescence, normal chromosomal architecture by karyotype analysis, and presence of the CMT1A duplication by fluorescence in situ hybridization (FISH) (**Fig. 4-3B-D**).

*CMT1A PGD-hESC-derived Schwann cells exhibit comparable Schwann cell yields, Schwann cell gene enrichment levels, and increased PMP22 gene expression relative to controls*

These CMT1A PGD-hESC lines were then differentiated into Schwann cells using the LSB2i protocol developed in Chapter 2 (**Fig. 4-3A**), and the human embryonic stem cell line H9 was used as a control. After 21-23 days of differentiation, the Schwann cell populations were FACS-purified by staining for CD49d, an antibody we identified in Chapter 2 as being selective for the Schwann cell population. From **Fig. 4-4A** it can be seen that both the control and CMT1A PGD-hESC lines yield similar percentages of CD49d+ Schwann cells. As a quality control measure, with each differentiation and FACS purification, we harvested both the CD49d+ (Schwann cell) fraction and the CD49d- (non-Schwann cell) fraction, and used real time PCR to validate that Schwann cell marker genes are indeed enriched in the CD49d+ (Schwann cell) population relative to the CD49d- (non-Schwann cell) population. We found that the CD49d+ Schwann cell fraction was substantially

enriched for the Schwann cell lineage markers Cadherin 19 and Myelin Protein Zero, verifying that our FACS purification system is indeed selecting for Schwann cells. We also found no significant differences between Schwann cell marker enrichment in control and CMT1A PGD-hESC-derived Schwann cells (**Fig. 4-4B**). Next, we assessed their *PMP22* expression levels (**Fig. 4-4C**), and found that while the *PMP22* expression levels are quite variable, on average the CMT1A PGD-hESC Schwann cells express more *PMP22* than the controls, reflecting the *PMP22* enrichment seen in the CMT1A patient biopsies<sup>15</sup> and our CMT1A hiPSC-derived Schwann cells of chapter 3.

*CMT1A PGD-hESC-derived Schwann cells upregulate gene and protein expression of multiple pro-inflammatory cytokines*

The real time PCR probes used to validate the CMT1A microarray data from Chapter 3 (**Fig. 3-7A**) were also evaluated in CMT1A PGD-hESC Schwann cells (**Fig. 4-5A**). The rationale was to determine whether these particular inflammatory genes overexpressed in CMT1 hiPSC-Schwann cells were also overexpressed in the CMT1A PGD-hESC-Schwann cells. Upregulation of these genes in the CMT1A PGD-hESC lines is more modest than their upregulation in CMT1A hiPSC lines (with *MCP1*, *CXCL14*, *IL1R1*, and *TGFB1* upregulation reaching statistical significance), which is not necessarily surprising given that these lines were never included in the initial microarray experiment used to select the real time PCR probes (**Fig. 3-5**). Subsequent to looking at expression levels of inflammatory genes, we also examined inflammatory protein expression levels through the same cytokine array panel used in Chapter 3 (**Fig. 4-5B**). We found statistically significant upregulation



of several proteins (CXCL1, sICAM-1, IFN- $\gamma$ , MCP-1, MIF, TNF- $\alpha$ , and STREM-1), mirroring the results seen in CMT1A hiPSC-Schwann cells in Chapter 3. In particular, of the 36 cytokines profiled, MCP-1, CXCL1, and sTREM-1 are commonly upregulated in both CMT1A hiPSC-Schwann cells and PGD-hESC-Schwann cells, strengthening the idea that they may play a role in CMT1A pathogenesis. The fact that multiple inflammatory proteins were commonly upregulated in both the CMT1A hiPSC-Schwann cells and PGD-hESC-Schwann cells increases confidence in our hypothesis that pro-inflammatory cytokine release may be an early pathological feature of CMT1A and an intrinsic property of human CMT1A Schwann cells.

*CMT1A iNC-Schwann cells and controls exhibit classical Schwann cell bipolar morphology, are immunoreactive for Schwann cell markers, and upregulate PMP22 gene expression*

To further validate this result, we also utilized a third CMT1A model available to our lab, fibroblasts that have been directly converted into Schwann cells (termed induced neural crest-derived Schwann cells or iNC-Schwann cells). Whereas hiPSC-derived Schwann cells are made by de-differentiating fibroblasts into induced pluripotent stem cells and subsequently re-differentiating them into Schwann cells, in this experiment we directly convert fibroblasts into multipotent neural crest and subsequently differentiate them into Schwann cells (**Fig. 4-6A**). This technique bypasses the pluripotent stem cell stage, and may yield a Schwann cell population with a different epigenetic footprint than the hiPSC- and PGD-hESC-derived Schwann cells. Interestingly, because reprogrammed cells often retain some epigenetic memory of the starting cell type, in bypassing the pluripotent stem cell

stage, it is possible that the iNC-Schwann cells maintain a more mature epigenetic footprint than the other two Schwann cell models utilized, though this needs to be further investigated in future experiments.

CMT1A iNC-Schwann cells were generated using fibroblasts from three CMT1A patients, two of which were included in our earlier hiPSC study in Chapter 3 (**Table 4-1**). These fibroblasts were directly converted into induced neural crest (iNC) using Sox10 overexpression and Wnt pathway activation for 14 days. On day 14, they were then FACS purified using an antibody to CD34, a cell surface marker which is specifically expressed on our induced Neural Crest. After FACS, the induced neural crest were replated in Schwann cell differentiation media for 2-5 weeks. The result is a pure Schwann cell population, as evidenced by all of the DAPI-positive nuclei also staining robustly for Schwann cell markers S100b and GFAP and exhibiting an elongated morphology stereotypical of Schwann cells (**Fig. 4-6B**). Real time PCR was used to evaluate *PMP22* expression levels in both CMT1A and control iNC-Schwann cells, and again expression levels were variable with generally higher *PMP22* expression in CMT1A iNC-Schwann cells versus controls (**Fig. 4-6C**,  $p=0.0025$ ), mirroring what was found in our CMT1A hiPSC-Schwann cells, CMT1A PGD-hESC-Schwann cells, and patient biopsies<sup>15</sup>.

*CMT1A iNC-Schwann cells upregulate gene and protein expression of multiple pro-inflammatory cytokines*

Again, expression of a panel of inflammatory genes was evaluated, and those genes were chosen based on microarray profiling of CMT1A hiPSC-Schwann cells in Chapter 2 (**Fig. 3-7A**). Relative expression levels of these inflammatory genes

were quite variable, yet many do appear to be upregulated, including *MCP-1* ( $p < 0.001$ ), *CXCL1* ( $p < 0.01$ ), *CXCL14*, ( $p < 0.01$ ), and *IL1R1* ( $p < 0.01$ ) (**Fig. 4-7A**). In parallel, cell conditioned medium from CMT1A iNC-Schwann cells were profiled using an inflammatory protein panel, and it was found that several immune mediators are upregulated in the CMT1A iNC-Schwann cells relative to controls, most robustly *CXCL1* ( $p < 0.0001$ ), *MCP-1* ( $p < 0.001$ ), and *RANTES* ( $p < 0.01$ ) (**Fig. 4-7B**).

*Comparison across three congruent models yields a converged phenotype of CXCL1 and MCP-1 protein upregulation that can be validated in CMT1A patient nerve biopsies*

By comparing across the hiPSC, PGD-hESC, and iNC systems, ultimately two proteins, *CXCL1* and *MCP-1*, were found to be upregulated among all three congruent models, resulting in a converged phenotype (**Fig. 4-8A**). To verify the increased levels of *CXCL1* and *MCP-1* expression in CMT1A patients, sural nerve biopsies were obtained. As shown in **Fig. 4-8B**, nerve biopsies from two genetically diagnosed CMT1A patients show significantly enriched levels of *CXCL1* and *MCP-1* proteins over control samples.

*Three congruent models of CMT1A Schwann cells induce increased monocyte chemotaxis, in an MCP-1 dependent manner*

Furthermore, to determine whether this increased cytokine expression is sufficient to induce monocyte chemoattraction, a transwell migration assay was used to evaluate THP-1 human monocyte migration towards CMT1A and control Schwann cell conditioned medium. In all three congruent models, significantly

increased numbers of THP-1 monocytes migrate towards CMT1A Schwann cell conditioned medium than controls ( $p < 0.05$  to  $p < 0.0001$  in hiPSC-SCs (**Fig. 4-9A**),  $p < 0.0001$  in PGD-hESC SCs,  $p < 0.0001$  in iNC-SCs (**Fig. 4-9B**)), and inhibition of MCP-1 signaling through a neutralizing antibody diminishes this effect ( $p < 0.01$  in hiPSC-SCs,  $p < 0.0001$  in PGD-hESC-SCs,  $p < 0.0001$  in iNC-SCs). This demonstrates that monocytes are indeed more readily attracted to CMT1A Schwann cells in our *in vitro* model, in an MCP-1 dependent manner.

*CMT1A patient-derived Schwann cells can be used for in vitro drug testing to modulate PMP22 gene expression as well as CXCL1 and MCP-1 protein expression*

Another key promise of human iPSC research is the use of patient-specific cells in drug testing. Thus far, our data has demonstrated the feasible generation of disease-specific Schwann cells from multiple patient samples, and these CMT1A patient-derived Schwann cells display increased levels of *PMP22*, as well as upregulated protein expression of immune mediators CXCL1 and MCP-1. We next tested whether exposure to candidate drugs could affect any of these three parameters. Three candidate chemical compounds (bortezomib, fenretinide, and olvanil) had previously been identified through a large-scale drug screening using rat Schwann cell line carrying luciferase construct to monitor *PMP22* expression<sup>148</sup>. Exposure of CMT1A hiPSC-Schwann cells to two of the three candidates drugs (bortezomib and olvanil) resulted in a marked reduction of the *PMP22* expression, in only one of our CMT1A genotypes (5167 hiPSC line) (**Fig. 4-10A**, left, and **Fig. 4-10B**). In contrast, no significant changes of *PMP22* expression were observed in another genotype (5165 hiPSC line). In addition, we examined the effect of

bortezomib treatment (which showed a statistically stronger effect on *PMP22* expression) on inflammatory cytokine release in the bortezomib-responsive CMT1A hiPSC line, and notably bortezomib treatment induced a significant decrease in the protein level of MCP-1, but not CXCL1 (**Fig. 4-10A**, right), suggesting a partial rescue of our novel CMT1A phenotype.

**Figure 4-1: Comparison of hiPSCs, hESCs, and directly converted cells**

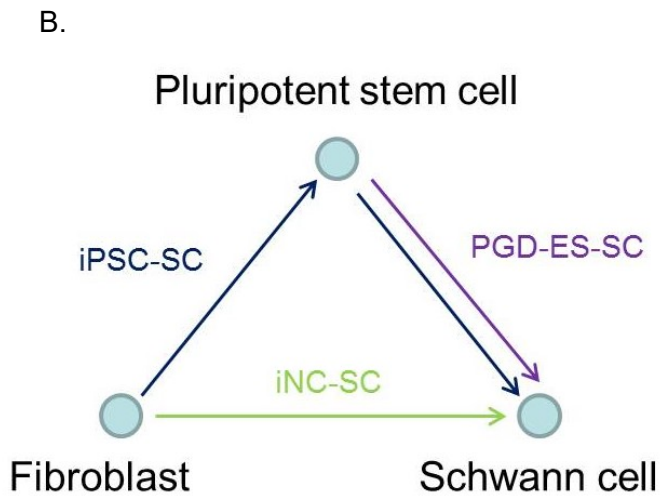
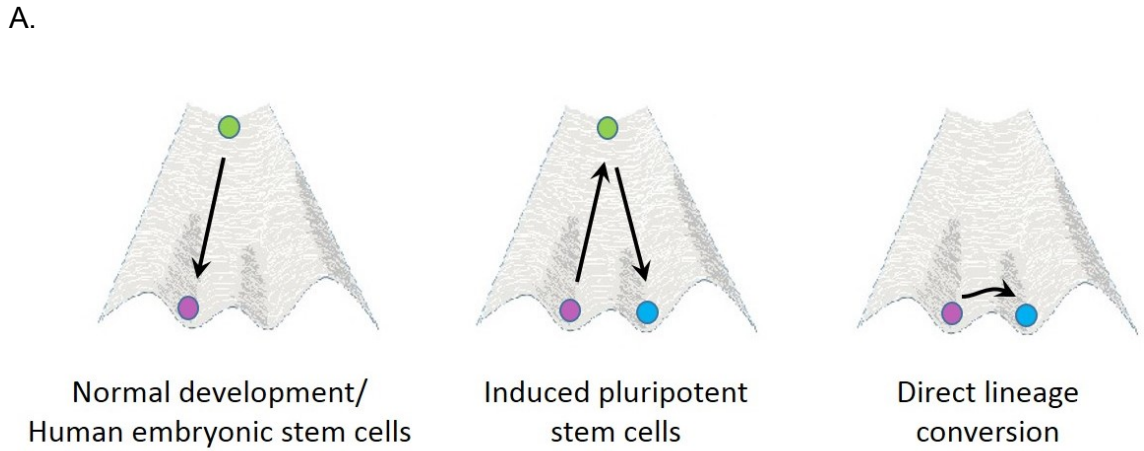


**Figure 4-1. A.** Waddington's epigenetic landscape and the relationship between three major cellular reprogramming technologies. **B.** Epigenetic relationship between hiPSC-Schwann cells, PGD-hESC-Schwann cells, and iNC-Schwann cells.

**Figure 4-2: Use of three congruent Schwann cell models to find a converged phenotype**

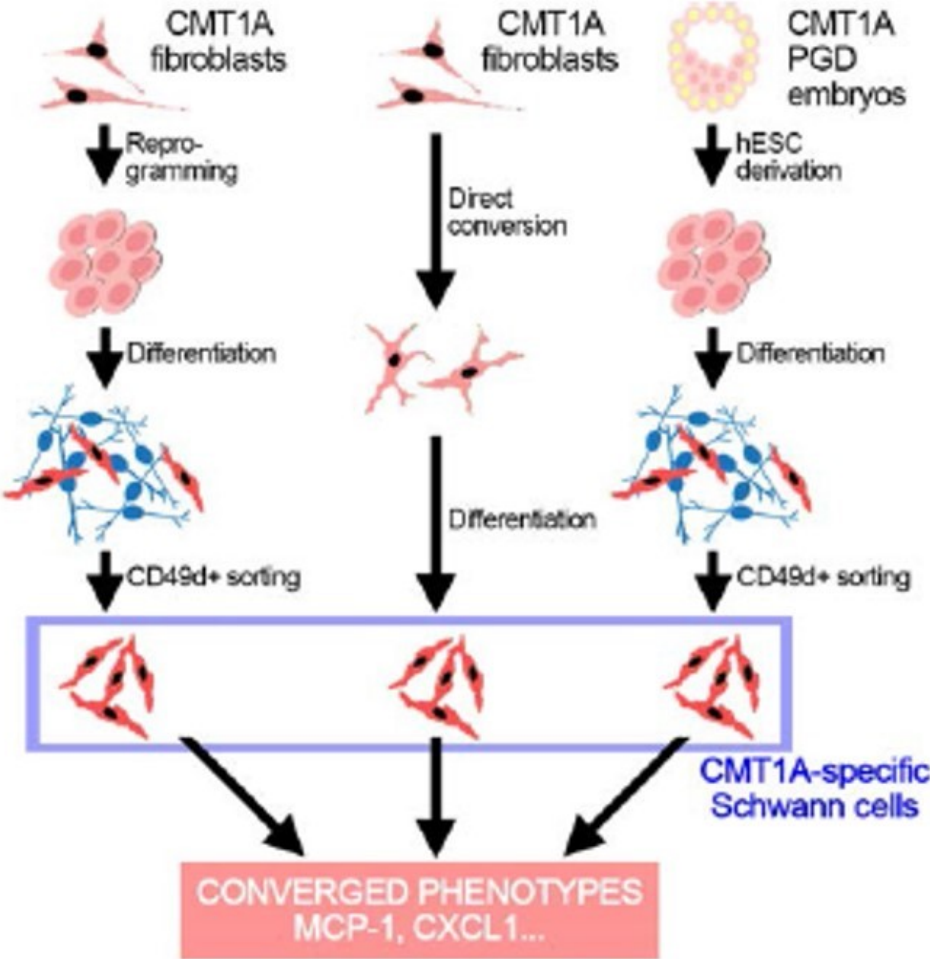
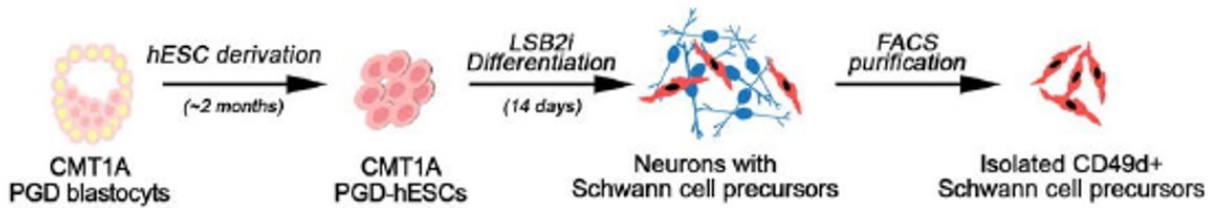


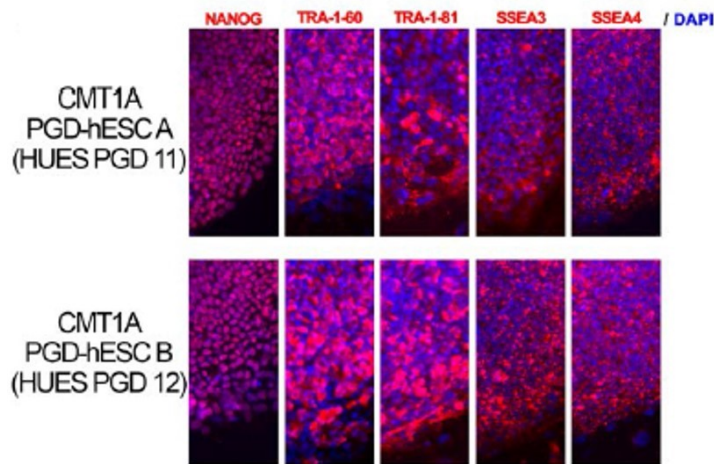
**Figure 4-2.** Experimental schematic outlining use of three congruent CMT1A Schwann cell models to identify a novel converged phenotype.

**Figure 4-3: CMT1A PGD-hESC-Schwann cell generation and characterization**

A.



B.



C.

PGD-hESC Line	2n	X	Y	Sex	Abn.
HUES PGD 11	46	XX	XY	Female	None
HUES PGD 12	46	XX	XY	Female	None
HUES PGD 13	46	XX	XY	Female	None
HUES PGD 14	46	XX	XY	Female	None
HUES PGD 15	46	XX	XY	Female	None
HUES PGD 16	46	XX	XY	Female	None
HUES PGD 17	46	XX	XY	Female	None
HUES PGD 18	46	XX	XY	Female	None
HUES PGD 19	46	XX	XY	Female	None
HUES PGD 20	46	XX	XY	Female	None
HUES PGD 21	46	XX	XY	Female	None
HUES PGD 22	46	XX	XY	Female	None
HUES PGD 23	46	XX	XY	Female	None
HUES PGD 24	46	XX	XY	Female	None
HUES PGD 25	46	XX	XY	Female	None
HUES PGD 26	46	XX	XY	Female	None
HUES PGD 27	46	XX	XY	Female	None
HUES PGD 28	46	XX	XY	Female	None
HUES PGD 29	46	XX	XY	Female	None
HUES PGD 30	46	XX	XY	Female	None
HUES PGD 31	46	XX	XY	Female	None
HUES PGD 32	46	XX	XY	Female	None
HUES PGD 33	46	XX	XY	Female	None
HUES PGD 34	46	XX	XY	Female	None
HUES PGD 35	46	XX	XY	Female	None
HUES PGD 36	46	XX	XY	Female	None
HUES PGD 37	46	XX	XY	Female	None
HUES PGD 38	46	XX	XY	Female	None
HUES PGD 39	46	XX	XY	Female	None
HUES PGD 40	46	XX	XY	Female	None
HUES PGD 41	46	XX	XY	Female	None
HUES PGD 42	46	XX	XY	Female	None
HUES PGD 43	46	XX	XY	Female	None
HUES PGD 44	46	XX	XY	Female	None
HUES PGD 45	46	XX	XY	Female	None
HUES PGD 46	46	XX	XY	Female	None
HUES PGD 47	46	XX	XY	Female	None
HUES PGD 48	46	XX	XY	Female	None
HUES PGD 49	46	XX	XY	Female	None
HUES PGD 50	46	XX	XY	Female	None

D.

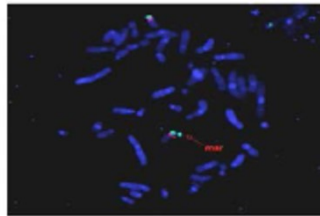


**Figure 4-3 A.** Overview of CMT1A PGD-hESC generation from CMT1A PGD blastocysts, and subsequent differentiation into Schwann cells precursors. **B.** Pluripotent stem cell marker expression including NANOG, TRA-1-60, TRA-1-81, SSEA4 and SSEA4. **C.** Representative karyotype images of the PGD-hESC lines. **D.** Fluorescence in situ hybridization revealing a genomic duplication corresponding to the CMT1A duplicated region.



**Figure 4-4: CMT1A PGD-hESC differentiation into Schwann cells**

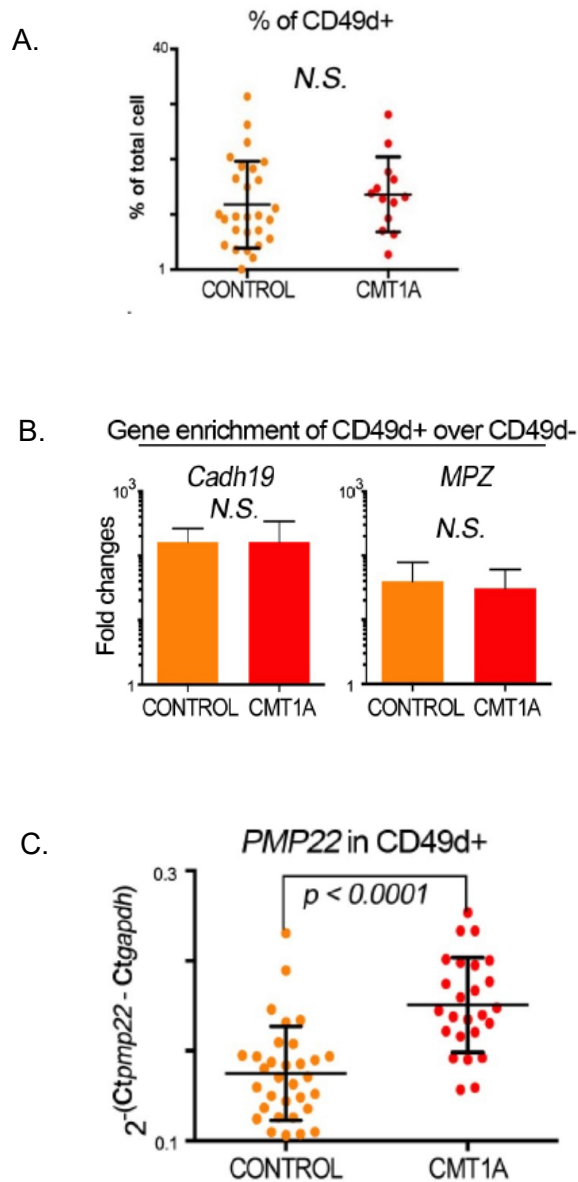


**Figure 4-4. A.** FACS purification of LSB2i treated CMT1A and control PGD-hESCs reveals similar yields of CD49d+ Schwann cells. Control n=27, CMT1A n=13. p=ns, unpaired t test. Data expressed as mean +/- SD. **B.** Post-FACS evaluation of Schwann cell gene enrichment in CD49d+ Schwann cells versus matched CD49d- non-Schwann cells, by real time PCR. Control n=9 for *CDH19*, n=9 for *MPZ*; CMT1A n=7 for *CDH19*, n=9 for *MPZ*. p=ns, unpaired t test. Data expressed as mean +/- SD. **C.** Real time PCR for *PMP22* in CMT1A and control CD49d+ Schwann cells. Control n=32, CMT1A n = 25. p<0.0001, unpaired t-test. Data expressed as mean +/- SD.

**Figure 4-5: Validation of CMT1A hiPSC-Schwann cell microarray results with CMT1A PGD-hESC-Schwann cells**

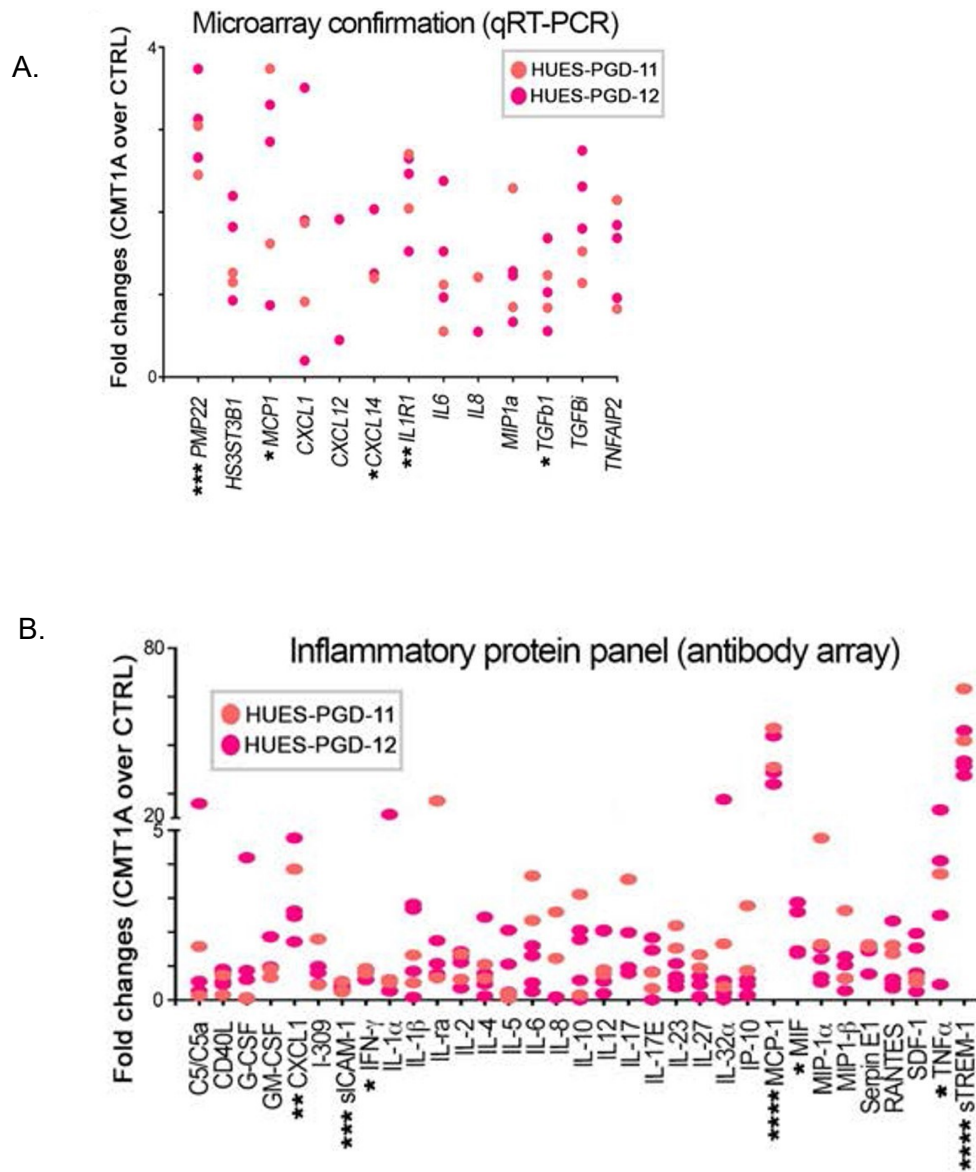
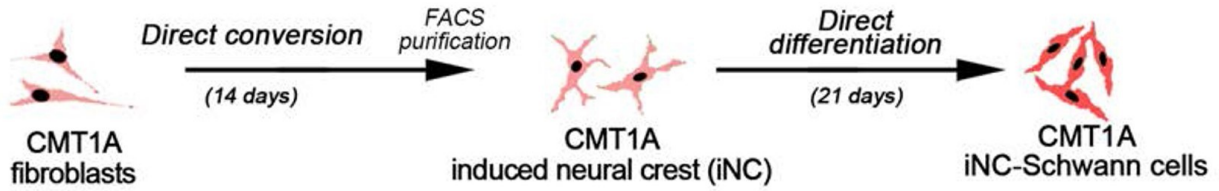


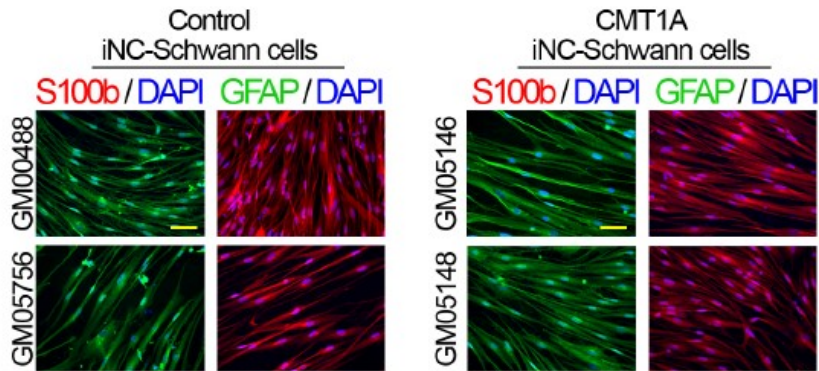
**Figure 4-5. A.** Real time PCR validation of CMT1A hiPSC microarray results in two independent CMT1A PGD-hESC lines representing two different CMT1A blastocysts. Data expressed as fold change versus gene expression in control hESC-derived Schwann cells. \*  $p < 0.05$ , \*\*  $p < 0.01$ , \*\*\*  $p < 0.001$ , \*\*\*\*  $p < 0.0001$ , ratio paired t-test. **B.** Cytokine array profiling of cell conditioned medium from Day 10 post-FACS CD49d+ Schwann cells. Data expressed as fold change in protein expression between CMT1A Schwann cells versus matched control. Data from independent differentiations are displayed as different colors. \*  $p < 0.05$ , \*\*  $p < 0.01$ , \*\*\*  $p < 0.001$ , \*\*\*\*  $p < 0.0001$ , ratio paired t-test.

**Figure 4-6: Overview of CMT1A iNC-Schwann cell generation and characterization**

A.



B.



C.

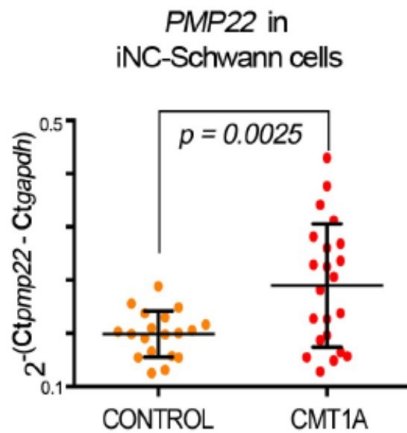


**Figure 4-6. A.** Schematic of the method to directly convert CMT1A patient fibroblasts into CMT1A iNC-Schwann cells. **B.** Representative immunofluorescence for GFAP and S100b in iNC-Schwann cells from two control fibroblasts and two CMT1A fibroblasts. **C.** Real time PCR for *PMP22* in CMT1A and control CD49d+ Schwann cells. Control n=19, CMT1A n=22. p<0.0025, unpaired t-test. Data expressed as mean +/- SD.

**Figure 4-7: Validation of CMT1A hiPSC-Schwann cell microarray results with CMT1A iNC-Schwann cells**

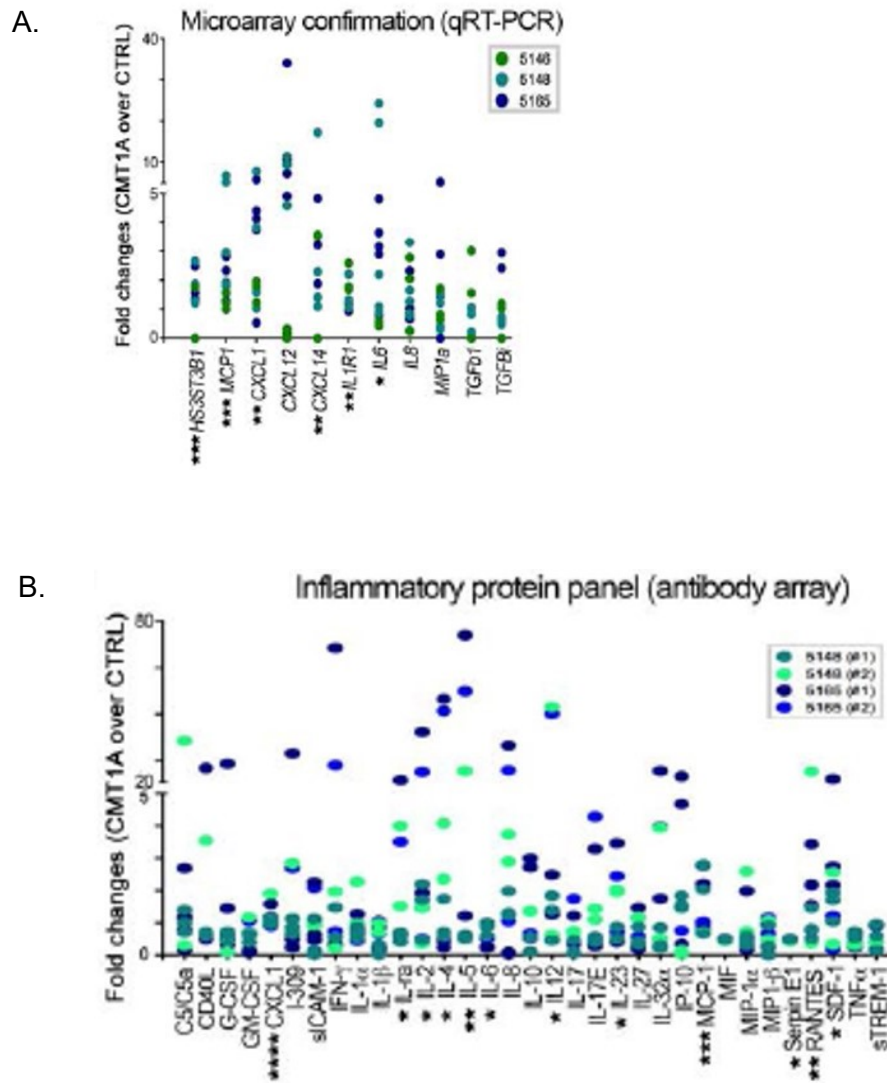


**Figure 4-7. A.** Real time PCR validation of CMT1A hiPSC microarray results in two independent CMT1A iNC-Schwann cell lines representing two different CMT1A patients. Data from independent differentiations represented as different colors. Data expressed as fold change versus gene expression in control iNC Schwann cells. \*  $p < 0.05$ , \*\*  $p < 0.01$ , \*\*\*  $p < 0.001$ , \*\*\*\*  $p < 0.0001$ , ratio paired t-test. **B.** Cytokine array profiling of cell conditioned medium from 2 weeks post-FACS iNC-Schwann cells derived from two different patients. Data expressed as fold change in protein expression between CMT1A Schwann cells versus matched control. Data from independent differentiations are displayed as different colors. \*  $p < 0.05$ , \*\*  $p < 0.01$ , \*\*\*  $p < 0.001$ , \*\*\*\*  $p < 0.0001$ , ratio paired t-test.

**Figure 4-8: Three congruent CMT1A models reveal a converged phenotype that is consistent with patient nerve biopsies**

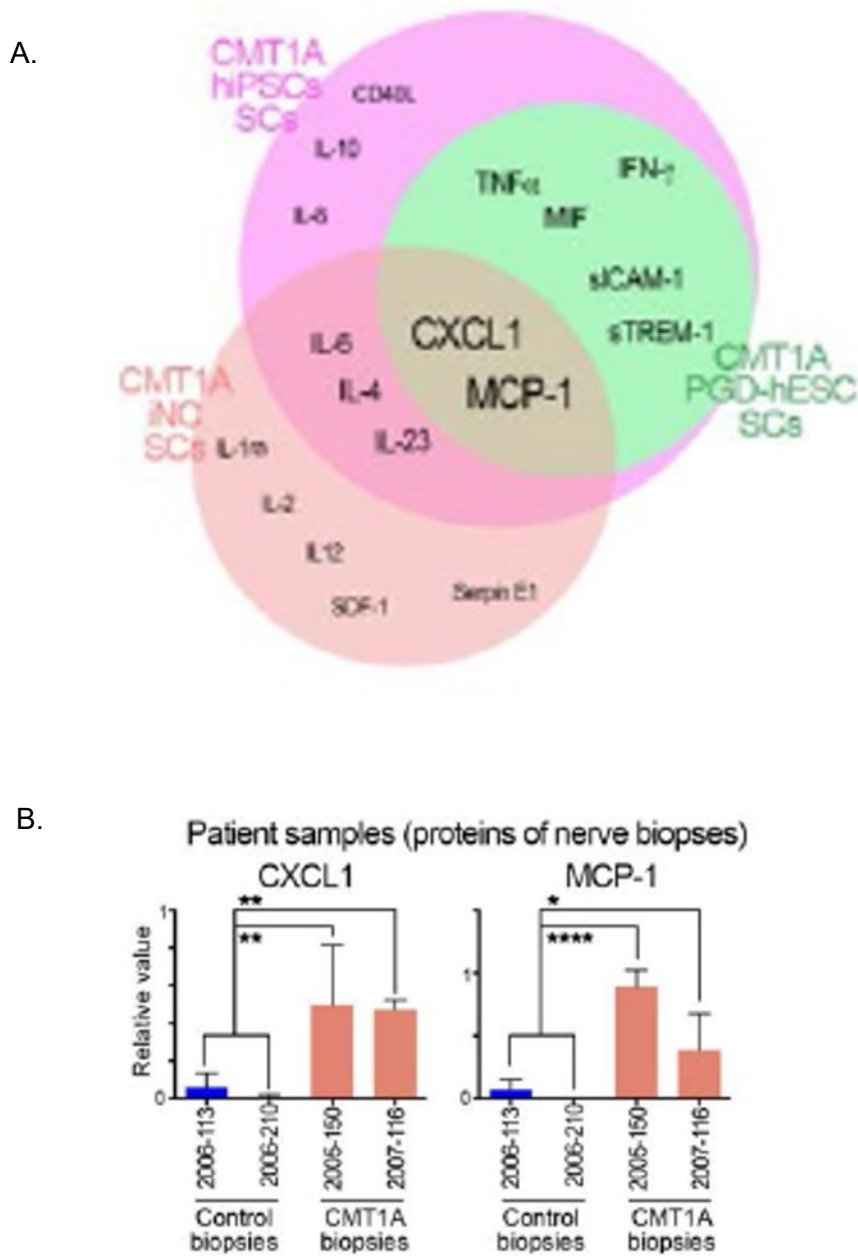


**Figure 4-8. A.** Venn diagram of upregulated secreted proteins in each model, with a converged phenotype of CXCL1 and MCP-1 upregulation. **B.** Protein expression level of CXCL1 and MCP-1 in nerve biopsies from two CMT1A and two control patients. Data expressed as mean  $\pm$  SD of cytokine dot array intensity.  $n=4$  technical repeats per condition. \*  $p<0.05$ , \*\*  $p<0.01$ , \*\*\*\*  $p<0.0001$ , one-way ANOVA.

**Figure 4-9: THP-1 human monocytes are more readily recruited to CMT1A Schwann cells, in an MCP-1 dependent manner**

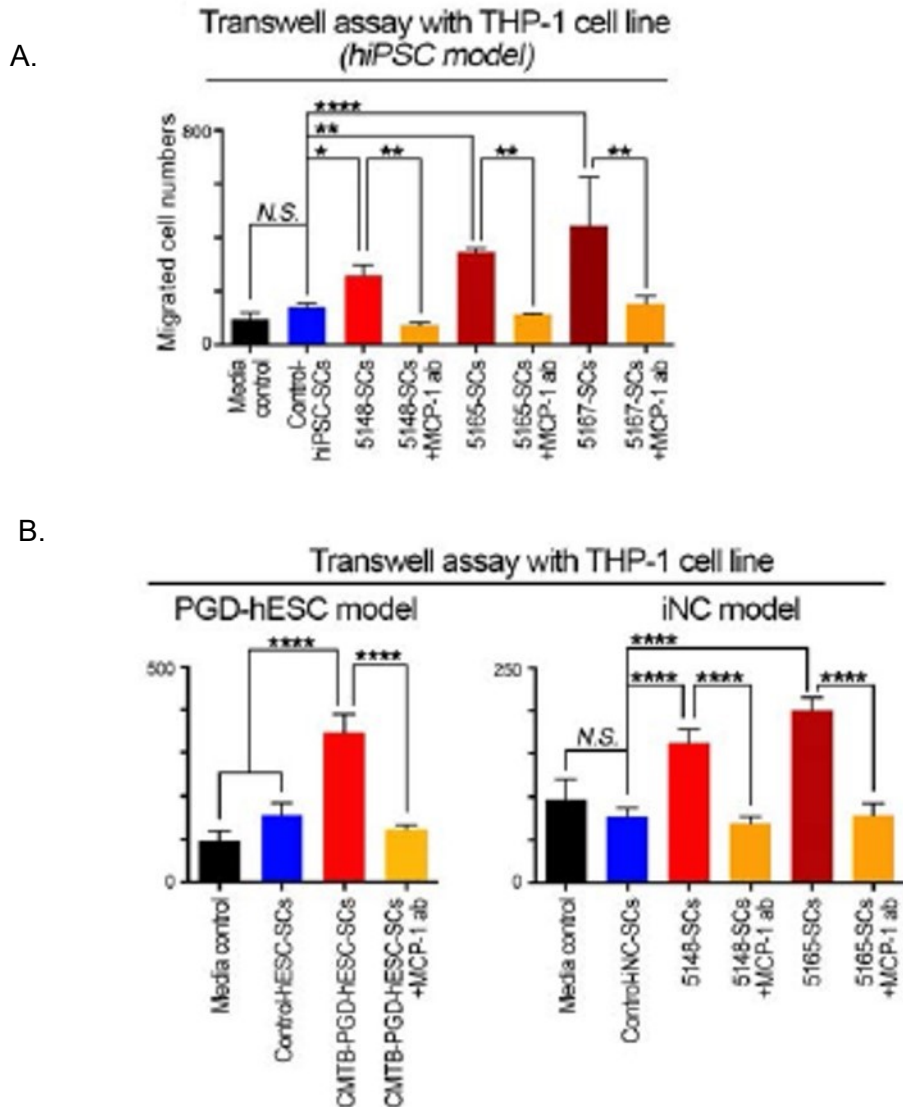


**Figure 4-9. A.** THP-1 human monocyte transwell migration assay results, using conditioned media of Schwann cells derived from different hiPSC lines. Data expressed as mean +/- SD of migrated THP-1 cells, divided by 100. n=3 to 9 per condition. \* p<0.05, \*\* p<0.01, \*\*\*\* p<0.0001, one-way ANOVA. **B.** THP-1 human monocyte transwell migration assay results, using conditioned media of Schwann cells derived from different PGD-hESC and iNC lines. Data expressed as mean +/- SD of migrated THP-1 cells, divided by 100. n=3 to 9 per condition. \* p<0.05, \*\* p<0.01, \*\*\*\* p<0.0001, one-way ANOVA.

**Figure 4-10: Pharmacological treatment can decrease MCP-1 and CXCL1 release in a patient-derived hiPSC line**

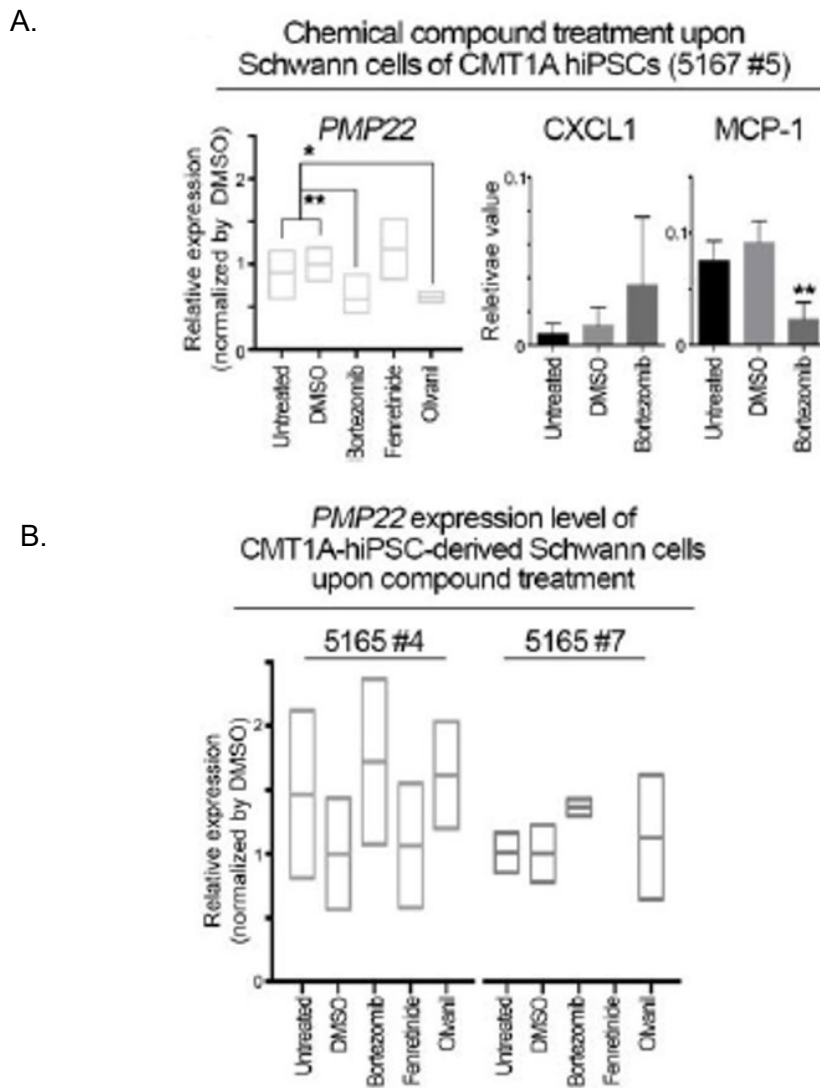


**Figure 4-10. A.** Expression level of *PMP22* transcript and CXCL1 and MCP-1 protein from Schwann cells from a CMT1A hiPSC line (5167 #5) upon three compound treatment. Gene expression data displayed as mean  $\pm$  SD of normalized *PMP22* expression level, and the value of DMSO sample was used for fold change.  $n=3$  to 4 per condition. \*  $p<0.05$ , \*\*  $p<0.01$ , one-way ANOVA. Protein expression data displayed as mean  $\pm$  SD of cytokine dot array intensity.  $n=4$  per condition. \*\*  $p<0.01$ , one-way ANOVA. **B.** Expression level of *PMP22* transcript of Schwann cells of CMT1A hiPSC lines upon three compound treatments. Data expressed as mean  $\pm$  SD of normalized *PMP22* expression level, and the value of the DMSO sample was used for normalization.  $n=3$  to 4 per condition. \*  $p<0.05$ , \*\*  $p<0.01$ , one-way ANOVA.

**Table 4-1: Summary of all genotypes included in this study**

Line name	Genotype	Source	Donor Age (years)	Models used
GM05148	CMT1A	Coriell	17	hiPSC, iNC
GM05165	CMT1A	Coriell	51	hiPSC, iNC
GM05167	CMT1A	Coriell	28	hiPSC
GM05146	CMT1A	Coriell	40	iNC
HUES PGD 11	CMT1A	NIH Stem cell registry	n/a	PGD-hESC
HUES PGD 12	CMT1A	NIH Stem cell registry	n/a	PGD-hESC
GM01582	Control	Coriell	11	hiPSC
GM02623	Control	Coriell	61	hiPSC
GM00498	Control	Coriell	3	iNC
GM05756	Control	Coriell	2 months	iNC
H9	Control	WiCell	n/a	hiPSC, PGD-hESC



## Discussion

Here we report use of CMT1A PGD-hESC Schwann cells and CMT1A iNC-Schwann cells to validate a phenotype previously found in CMT1A hiPSC-Schwann cells. In total six independent CMT1A genotypes and five control genotypes were profiled across three platforms (**Table 4-1**). Use of six independent genotypes and three methodological platforms increases the robustness of our study methodology and provides a model for future disease modeling studies as well.

Consistent features found across all three Schwann cell models include upregulation of the gene *PMP22*, which is duplicated in CMT1A patients. *PMP22* upregulation in CMT1A Schwann cells was anticipated but not with complete certainty, as most previous reports of *PMP22* upregulation in CMT1A patient samples were performed on nerve biopsies consisting of a mixture of Schwann cells, neurons, fibroblasts, and other cell types<sup>13,15</sup>, and only one such study was performed on cultured CMT1A patient Schwann cells<sup>14</sup>. Because *PMP22* is also known to be expressed in Schwann cells, neurons, and fibroblasts, nerve biopsy studies cannot identify which of these cell types are responsible for the increased *PMP22* expression. Our study of CMT1A Schwann cells confirms that Schwann cells are certainly one of the cell types that upregulates *PMP22*, and given that CMT1A is a dysmyelination and demyelination disorder, Schwann cells are likely the most important contributor to CMT1A pathogenesis. Our study does leave open the possibility that CMT1A neurons or fibroblasts may also upregulate *PMP22*, which may easily be addressed in future studies of CMT1A hiPSC-, PGD-hESC-, and iNC-

derived neurons and CMT1A patient primary fibroblasts, both of which are readily available to the lab.

Our study also demonstrates upregulation of the heparan sulfate 3-O-sulfotransferase gene, *HS3ST3B1* in two of the three models of CMT1A (hiPSCs and iNC-Schwann cells). In the CMT1A PGD-hESC model, *HS3ST3B1* is non-statistically significantly upregulated, and perhaps a larger sample size would better clarify whether the gene is also differentially expressed in that system. 3-O-sulfotransferases help create the fine structures of heparan sulfate through sulfation at a 3-OH. The sulfation pattern in turn determines the affinity of heparan sulfate for various growth factors and ligands, which ultimately allows heparan sulfate to regulate a myriad of biological activities from cell growth, differentiation, coagulation, etc. As 3-O-sulfotransferase activity believed to be both rare and rate-limiting, the upregulation of *HS3ST3B1* in CMT1A Schwann cells is likely to be biologically meaningful. Studies in other systems have demonstrated that *HS3ST3B1* plays a role in mediating Herpes simplex virus-1 cell entry<sup>124</sup>, epithelial mesenchymal transition in pancreatic cancer<sup>149</sup>, and dementia development in HIV<sup>133</sup>. The specific physiological role of *HS3ST3B1* in Schwann cells, as in most other tissues, is currently unknown and presents another opportunity for an interesting follow-up study.

Inflammatory protein expression profiling of our three congruent CMT1A Schwann cell models reveal a converged phenotype. In addition to *PMP22* upregulation, several inflammatory proteins were upregulated in three independent human CMT1A models, and CXCL1 and MCP-1 proteins were ultimately commonly

overexpressed (**Fig.4-8A**). CXCL1 has been shown to mediate both neutrophil<sup>100-103</sup> and more recently monocyte<sup>104</sup> chemotaxis in various contexts, and has never been previously implicated in CMT1A pathogenesis. MCP-1, also known as macrophage chemoattractant protein-1, is one of the best studied chemokines and has been shown to robustly induce monocyte migration in a concentration dependent manner<sup>120,122</sup>. While MCP-1 has never previously been reported as upregulated in CMT1A clinical samples, one group has shown its upregulation in a rodent model of CMT1A<sup>22,23</sup>, lending support to our findings.

Whereas hiPSC model data is conventionally validated through genetic correction, the great magnitude of the 1.4Mbp CMT1A duplication makes it challenging to edit CMT1A hiPSCs using currently available genome editing technology. Additionally, another disorder, Hereditary Neuropathy with liability to Pressure Palsies (HNPP), results in patients with only 1 copy of this 1.4Mbp region. Consequently, inadvertent deletion of two copies of the CMT1A duplicated region would model HNPP rather than healthy controls, making the lack of control over copy number editing with CRISPR/Cas9 an additional concern. To circumvent the issues regarding CRISPR/Cas9 editing in the context of CMT1A, CMT1A hiPSC data was validated with two independent models, the PGD-hESC- and iNC-Schwann cells. The resultant CMT1A-specific Schwann cells exhibit phenotypes consistent with those from our CMT1A-hiPSC lines, as well as with nerve biopsy samples from genetically diagnosed CMT1A patients.

Our novel defined protocol for the directed differentiation and prospective isolation of Schwann cell precursors from hPSCs features a chemical compound-

based activation/inhibition of developmentally relevant pathways to enable Schwann cell fate specification in a relatively fast (21-23 days) and efficient (13.62% +/- 1.89 in hESCs, 13.56% +/- 0.8817 in control hiPSCs) manner. The FACS purified cells can also be subsequently replated, allowing for the study of Schwann cell intrinsic properties as well as the potential for *in vitro* maturation along the Schwann cell lineage via extended culture times. Primary human Schwann cells are known for their low myelination efficiency in experimental settings<sup>88</sup>, particularly compared to rodent Schwann cells and human oligodendrocytes. Considering that our CD49d+ cells robustly express *GPR126*<sup>76-78</sup>, a gene critical for initiation of myelination, continued myelination studies should yield positive outcomes under *in vitro* and *in vivo* settings. Given that dysmyelination involves impaired myelination by developmentally immature Schwann cells, and has been demonstrated to play an important role in several CMT1A rodent models<sup>19,150</sup>, our CMT1A Schwann cells should comprise a reliable model for investigating CMT1A pathophysiology during early developmental stages.

CMT1A is not clinically considered to be an inflammatory disorder, although there is some laboratory evidence to support this idea<sup>22,23,118,119</sup>, in addition to our own finding that nerve biopsies from two CMT1A patients upregulate MCP-1 and CXCL1 proteins. Our data might suggest that neutrophils or monocytes can be recruited to nerves of CMT1A patients, potentially in a CXCL1 and MCP-1 mediated manner, as was shown in transwell THP-1 migration experiments. This idea can be corroborated by rodent studies, which have found that CMT1A mouse models overexpressing or mutating *PMP22* have increased macrophage infiltration in peripheral nerves<sup>118,119,151</sup>, and it is largely mediated by MCP-1<sup>22</sup>.

Theories of CMT1A pathogenesis often hypothesize Schwann cell growth and maturation deficits as being responsible for the dysmyelination and demyelination seen in the disorder<sup>14,152-154</sup>. This stems from *PMP22*'s alternate role as a growth arrest gene in fibroblasts<sup>155,156</sup>. However, our own expression profiling of CMT1A-hiPSC-derived Schwann cells in Chapter 3 revealed a robust inflammatory dysregulation, which was then validated using CMT1A PGD-hESC- and CMT1A iNC-Schwann cells in this chapter. Our data suggests that dysregulated immune signaling is not only present in CMT1A Schwann cells, but may also comprise an early and intrinsic feature of CMT1A Schwann cells. It is an early feature because our Schwann cells are likely of the Schwann cell precursor stage, and it is an intrinsic feature because our FACS purification system lends a pure Schwann cell culture.

In addition to modeling disease pathogenesis, our CMT1A Schwann cells can also be used to assess drug efficacy, potentially in a patient-specific manner. Previous rodent model studies have suggested three candidate drugs for the treatment of CMT1A, including ascorbic acid, neurotrophin-3 and progesterone antagonists, yet these drugs either have not appeared successful or their effects are largely unknown in clinical trials<sup>27,29-33,157</sup>. Led by a patient advocacy group, the CMT Association, there has been a renewed effort to identify drugs that can decrease *PMP22* mRNA expression level using a rat Schwann cell line<sup>148</sup>. Such a drug discovery campaign may benefit significantly from performing screens in human CMT1A Schwann cells as well as using them to validate the effects of hit compounds. Although future studies will be required to understand detailed action mechanism of the candidate drugs, our finding that the CMTA's hit compound

bortezomib reduced *PMP22* transcript expression in hiPSCs derived from one patient (GM05167) but not another (GM05165), indicate that there might be genotype-specific drug effects, suggesting that drug validation with individualized human Schwann cells may be particularly beneficial for CMT1A patients.

In addition to the pathological findings, this study also makes paradigmatic contributions to the stem cell field. In contrast to conventional validation methods which require genome editing to demonstrate reproducibility of a given phenotype, here we utilize all three reprogrammed cellular models available to the stem cell community to demonstrate a consistent disease phenotype. Induced pluripotent stem cells have already been widely adopted for disease modeling, and direct conversion of fibroblasts to target cell types is becoming increasingly embraced as more protocols for target cell type induction are being generated. Use of preimplantation genetic diagnosis embryos for disease modeling is also becoming progressively feasible as regulatory burdens are clarified and more lines are added to the NIH Human Embryonic Stem Cell Registry. By taking advantage of the plasticity of cellular identity through multiple reprogramming approaches, our results present an alternative method by which future hiPSC-based studies may also be validated through the use of congruent model systems.

## Conclusion

In this study, Chapter 3 results from profiling CMT1A hiPSC-Schwann cells were validated using CMT1A PGD-hESC-Schwann cells and CMT1A iNC-Schwann cells. Common and novel phenotypes found were upregulation of CMT1A duplicated region gene *HS3ST3B1* in two of the three models, which plays a rate limiting role in heparan sulfate fine structure biosynthesis, and whose specific role in Schwann cells is yet to be determined. In addition, several inflammatory genes and proteins were upregulated in all three CMT1A models, and CXCL1 and MCP-1 were ultimately commonly overexpressed in all three models, and also found to be upregulated in CMT1A patient nerve biopsies. Transwell assay experiments support the idea that THP-1 human monocytes are more readily recruited to CMT1A Schwann cells than controls, in an MCP-1 dependent manner. These results imply dysregulated immune signaling may be an intrinsic and early property of nascent Schwann cells, and that immune dysregulation may be an early contributor to CMT1A pathogenesis, as opposed to a secondary reaction. Finally, the broadest contribution of this study is a methodological one, in which all three reprogrammed Schwann cell models were utilized to demonstrate a converged phenotype. This approach offers a technical alternative to genome editing for disease hiPSC phenotype validation, and comprises a feasible model for future studies.

## CHAPTER 5: DISCUSSION AND CONCLUSIONS



## Wrapping it all up: From *PMP22* to Dysmyelination and Demyelination

### CMT1A: More than just *PMP22*?

The 1.4MB CMT1A microduplication is flanked by two 24bp CMT1A-REP elements. Meiotic misalignment of the CMT1-REP elements leads to unequal crossing over and the formation of either a microduplication (causing CMT1A) or microdeletion (causing HNPP)<sup>158-160</sup>. There is even evidence suggesting that this locus may be a hotspot for such recombination events<sup>159</sup>, but there is also a study disputing its hotspot status<sup>158</sup>.

*PMP22* is accepted to be the causal gene in CMT1A, yet there are many other genes present in the CMT1A duplicated region which may also contribute to CMT1A pathogenesis. As described in Chapter 1, in addition to *PMP22* the region includes six known genes, 13 predicted genes, at least a dozen long non-coding RNAs, a microRNA, and several pseudogenes<sup>12</sup> (**Fig. 3-1B**). Our microarray analysis in Chapter 3 was able to evaluate the presence of some of these genes, and found both *PMP22* and *HS3ST3B1* to be upregulated in CMT1A hiPSC-Schwann cells. The *HS3ST3B1* gene was also found to be significantly upregulated in CMT1A iNC-Schwann cells, and non-significantly upregulated in CMT1A PGD-hESC-Schwann cells, likely due to the small sample number included in that study.

To our knowledge, this is the first report that a non-*PMP22* gene from the CMT1A duplicated region has been aberrantly expressed in CMT1A Schwann cells. Because of the rate limiting role *HS3ST3B1* plays in heparan sulfate fine structure modification and the important regulatory roles heparan sulfate fine structures can play, it's quite plausible that *HS3ST3B1* gene dosage changes might prove

important. Plans are in place to evaluate effects of *HS3ST3B1* by transfecting control hiPSC- and ES-Schwann cells with *PMP22 +/- HS3ST3B1* and determining whether any inflammatory genes are subsequently upregulated.

To evaluate the role of the many non-*PMP22* genes from the CMT1A duplicated region that were not included in our microarray panel, it would be very interesting to use RNA sequencing to assess their expression levels in CMT1A patient-derived Schwann cells vs controls. Given a large enough collection of patient samples and complete data on their clinical characteristics, it might even be possible to correlate expression of some non-*PMP22* genes to clinical outcomes. There is great variability in the clinical manifestations of CMT1A, and they do not particularly correlate with *PMP22* expression levels<sup>13,15</sup>. The idea of interrogating the role of these other genes in a patient-specific manner is an exciting follow-up application of the platform we've developed.

#### Elucidating a mechanism: CXCL1 and MCP-1 in Schwann cells

Our findings add CXCL1 and MCP-1 secretion by CMT1A Schwann cells to an increasing body of work on Schwann cell immunocompetence, as outlined in Chapter 1. Here we hypothesize possible consequences of CXCL1 and MCP-1 upregulation in the context of CMT1A.

CXCL1 is a potent chemokine well-known for its role in neutrophil chemotaxis. Secretion of CXCL1 by pathological cell types and its subsequent binding to the CXCR2 receptor on neutrophils induces neutrophil chemotaxis and appears to mediate inflammatory damage in a number of diseases including Lyme disease<sup>102</sup>, alveolitis<sup>100</sup>, and keratoconjunctivitis<sup>101,103</sup>. There is also one study

suggesting CXCL1 can also act as a monocyte chemoattractant<sup>104</sup>. It is reasonable that CXCL1 may be playing a similar role in CMT1A patient Schwann cells/Schwann cell precursors.

In addition, CXCL1 has been reported to have an analgesic effect relieving inflammatory pain in the nervous system<sup>161</sup>. Leukocytes containing opioid peptides such as B-endorphin, met-enkephalin, dynorphin, and endomorphins enter inflamed peripheral nerves and release opioid peptides in response to certain environmental signals<sup>162</sup>. Specifically, soluble CXCL1 released by inflamed tissues can bind CXCR2 receptors on opioid-containing granulocytes and induce their migration into inflamed tissues as well as their subsequent degranulation<sup>161</sup>.

This suggests a model in which CMT1A Schwann cell-secreted CXCL1 may induce neutrophil migration into the peripheral nerve; there the neutrophils may play one of two potential roles, one pathogenic and one analgesic. Upon chemotaxis and degranulation some neutrophils may release myeloperoxidase, alkaline phosphatase, lactoferrin, lysozyme, and NADPH oxidase, mediating cytotoxic damage to the nascent nerve and contributing to CMT1A pathogenesis. Another population of neutrophils may release endorphins and other opioid peptides upon degranulation, providing local analgesia in the inflamed nerve. Alternatively, it is altogether possible that CXCL1 does not mediate neutrophil chemotaxis in the context of CMT1A, and rather performs an as of yet uncharacterized role in immune signaling or perhaps even developmental signaling.

In addition to CXCL1, our data also demonstrates that CMT1A patient Schwann cells upregulate secretion of MCP-1, as known as Monocyte

Chemoattractant Protein 1, one of the most extensively studied chemokines. MCP-1 robustly induces circulating monocytes to exit the bloodstream and enter foci of active inflammation in the tissues. MCP-1 exerts its effects through signaling to its cognate receptor, CCR2. Whereas MCP-1 can be expressed by a variety of cell types (monocytes, macrophages, endothelium, fibroblasts, epithelium, neurons, microglia, Schwann cells, and others), expression of CCR2 is restricted to monocytes, activated T cells, and dendritic cells<sup>120</sup>.

MCP-1 has been previously shown to mediate inflammation in a number of neurological diseases including multiple sclerosis, stroke, and Alzheimer's disease. MCP-1 is upregulated in the macrophages and astrocytes of acute plaques of multiple sclerosis patients, but attenuates somewhat in chronic MS plaques<sup>120</sup>. In stroke, MCP-1 expression in the post-ischemic brain and is thought to be an early inducer of leukocyte migration and these leukocytes appear to contribute to subsequent post-ischemic injury. Interestingly, overexpression of MCP-1 in rodents appears to increase infarct volume whereas knocking out MCP-1 seems to be neuroprotective during ischemia<sup>120</sup>. In Alzheimer's disease, amyloid-beta activates astrocytes to secrete MCP-1, which then attract microglia. In addition, microvessels of Alzheimer's patients appear to upregulate endothelial expression of MCP-1<sup>163</sup>, and in another study, MCP-1 and other chemokines in combination with amyloid-beta were able to induce monocyte migration across a human model of the blood brain barrier<sup>164</sup>. These studies demonstrate that not only is MCP-1 upregulated in several neurological disorders, but it may also be able to alter the properties of the blood brain barrier.

Similar to the CNS, MCP-1 has been repeatedly implicated in neurodegeneration in the PNS<sup>40,55,121,165</sup>. It appears that during PNS Wallerian degeneration, neuronal injury<sup>40</sup> and Schwann cell denervation<sup>121</sup> results in Schwann cells upregulating MCP-1 and other chemokines that lead to macrophage infiltration. In the context of axotomy, macrophage recruitment is often adaptive, as it facilitates clearance of myelin debris and allows for axonal regeneration.

MCP-1 upregulation in multiple sclerosis, stroke, Alzheimer's disease, and PNS Wallerian degeneration consistently appears to be a secondary response to a primary pathology (ie acute MS plaque formation, ischemia, amyloid-beta overexpression, and axotomy). In our CMT1A Schwann cells, on the other hand, MCP-1 secretion occurs even in the absence of any injury, as our Schwann cells haven't even had the chance to form myelin yet. Our results further the idea that MCP-1 upregulation by Schwann cells may play an early role in CMT1A dysmyelination and demyelination, possibly through monocyte/macrophage recruitment or through yet undefined mechanisms.

The idea that MCP-1 upregulation/macrophage recruitment may be degenerative rather than adaptive in the context of CMT1A patients is supported from data from Rudolf Martini's mouse model of CMT1A. In this model, which expresses four copies of human *PMP22*, macrophages were found to be elevated in CMT1A mouse nerves<sup>23</sup>. Interestingly, knocking out one or both copies of *MCP-1* decreased macrophage infiltration, ameliorated demyelination, and improved grip strength<sup>22</sup>. Whereas the Martini group interprets CMT1A as being a primarily demyelinating disorder, our data that MCP-1 is upregulated even at the Schwann

cell precursor stage suggests that MCP-1 may even be contributing to dysmyelination, prior to the onset of demyelination.

Thus far, we have interpreted the CXCL1 and MCP-1 upregulation seen in our CMT1A Schwann cells as playing an immunopathologic role in CMT1A pathogenesis, as supported by our transwell assay results and other groups' data from CMT1A rodent studies. However, it should be noted that CXCL1 and MCP-1 may have alternate functions in the context of CMT1A, perhaps through modulating developmental signaling cascades, migratory signals, or other yet to be defined biological processes, as many cytokines are now being found to play diverse and varied roles when expressed within the nervous system<sup>166,167</sup>.

#### Reconciling major theories of CMT1A pathogenesis

While there are many theories of how *PMP22* overexpression causes CMT1A, CMT1A is not clinically considered to be an inflammatory disorder. One major model of CMT1A pathogenesis asserts that *PMP22* duplication alters Schwann cell proliferation, differentiation, or apoptosis. Schwann cell proliferation and differentiation are inherently linked as the pro-myelinating Schwann cell can proliferate but has not yet initiated myelination. Upon differentiation to a myelinating Schwann cell, it must exit the cell cycle. Whether *PMP22* overexpression increases or decreases CMT1A Schwann cell proliferation appears to vary based on the experimental context. In general, it appears that *PMP22* overexpression increases Schwann cell proliferation in *in vivo* rodent models, but decreases Schwann cell proliferation in both *in vitro* Schwann cell cultures and in clinical studies of CMT1A patient nerve biopsies<sup>168</sup>. In our *in vitro* studies of CMT1A

and control patient-derived hiPSC/PGD-hESC/iNC-Schwann cells, there were no observed differences in proliferation rates, though more precise analyses should be performed going forward.

Another major theory of CMT1A pathogenesis is that aberrant *PMP22* folding or trafficking is responsible. As a membrane protein, PMP22 must be trafficked from the endoplasmic reticulum to the plasma membrane. Point mutations in the *PMP22* gene, such as those found in some CMT1A patients and the Trembler mouse, result in misfolding of PMP22 protein and impaired trafficking from the ER/Golgi to the membrane<sup>169</sup>. In addition to *PMP22* point mutations leading to misfolding, it appears that wt *PMP22* overexpression can also result in misfolding, as demonstrated in the C22 mouse that harbors 7 copies of *PMP22*<sup>118</sup>. In the context of *PMP22* duplications, it appears that overexpressing *PMP22* may also overwhelm the ubiquitin-proteasome pathway and result in cytoplasmic PMP22 aggregation and activation of autophagosomes and lysosomes. Cytoplasmic PMP22 aggregates decrease the amount of PMP22 that can be targeted to the membrane and can lead to the downstream myelination deficits<sup>170-172</sup>.

A less widely reported theory of CMT1A pathogenesis is that CMT1A (or CMT1, in general) has a substantial inflammatory component. Most of the data supporting this idea have come from Rudolf Martini's mouse models of CMT1A, CMT1B, and CMT1X, and some supporting evidence has come from Lucia Notterpek's mouse models of CMT1A. As mentioned earlier, the Martini lab's C61 mouse model of CMT1A (4 copies of *PMP22*) exhibits increased macrophage infiltration in its peripheral nerves, and knocking out one or both copies of *MCP-1*

substantially decreases the macrophage infiltration and improves myelination<sup>23,117</sup>. Similarly, in their mouse models of CMT1B (P0 +/-) and CMT1X (Cx32 -/-) they see almost normal myelin formation followed by slowly progressing demyelination, with association of T-cells and macrophages in the nerves of the CMT1B and CMT1X mice<sup>151,173</sup>. Common themes across all three of their models were that macrophages were found in contact with myelin sheathes or axons, suggesting that macrophages play an active role in CMT1 demyelination. Similarly, the Notterpek group's C22 (7 copies of *PMP22*) and Trembler-J (*PMP22* point mutation) mouse models of CMT1A both exhibited increased CD11b-positive macrophages infiltration in sciatic nerves, further validating this finding of increased inflammation in two additional models of CMT1A.

Our results that the CMT1A patient hiPSC/PGD-hESC/iNC Schwann cells upregulate CXCL1 and MCP-1 best support an inflammatory model of CMT1A pathogenesis. Although this finding has already been validated in nerve biopsies from two CMT1A patients, a significant finding, more thorough validation efforts must be performed going forward to better determine the role of dysregulated immune signaling in CMT1A. This should be done initially through profiling a broader number of nerve biopsies from CMT1A and control patients for CXCL1 and MCP-1 expression. In addition to evaluating expression of these proteins, it would also be useful to histologically examine macrophage or leukocyte infiltration, and determine whether there are even subtle differences relative to controls. Furthermore, it might also be interesting to determine whether immunomodulatory therapy can alter the dys- and demyelinating phenotype of CMT1A, perhaps



through corticosteroid administration to CMT1A rodents at various time points from birth to adulthood.

There do exist several case reports of CMT1A patients who benefitted from corticosteroid therapy, yet they are generally diagnosed as having an acquired neuropathy superimposed onto a hereditary one<sup>174-177</sup>. Our data implores asking whether inflammation in CMT1A may actually be more common than these occasional case reports would otherwise suggest. Ultimately, if our findings are corroborated in other settings, it might blur the conventional clinical line between acquired demyelinating neuropathies (ie GBS and CIDP) which are thought to be inflammatory, and the hereditary dys- and demyelinating neuropathies which are thought to be structural.

## **Future applications of patient-derived Schwann cells**

### Modeling hereditary and acquired Schwann cell disorders

In this series of studies, we report the successful engineering of patient-derived Schwann cells from three different sources. Fibroblasts were have been de-differentiated in hiPSCs and re-differentiated into Schwann cells, to make CMT1A hiPSC-derived Schwann cells. Embryonic stem cell lines were cultured from blastocysts with the CMT1A duplication and subsequently differentiated into Schwann cells. Fibroblasts were also directly converted into Schwann cells, bypassing the pluripotent stem cell stage.

The three methods of reprogrammed Schwann cell derivation were used in this study to model CMT1A, but going forward they can be used to model a number of disorders. As reviewed in Chapter 1, there are many genetic Schwann cell disorders that might potentially benefit from disease modeling with our platform, including numerous subtypes of CMT1, Hereditary Neuropathy with Liability to Pressure Palsies (HNPP), Dejerine-Sottas disease, Schwannomatosis, and perhaps vestibular schwannomas of Neurofibromatosis Type II (NF2). In all of these disorders, there are still open questions of how associated genetic mutations cause the pathology observed clinically, and modeling them using patient-derived samples will likely add new insights.

In addition to modeling hereditary Schwann cell disorders, it may also be possible to adapt our platform for the modeling of acquired Schwann cell disorders (ie GBS and CIDP). For instance, we may readily collect skin fibroblasts from GBS or CIDP patients and reprogram them into hiPSCs or directly convert them into

Schwann cells. Gene expression profiling of GBS/CIDP patient hiPSC or iNC-derived Schwann cells could allow us to better understand their molecular pathology without performing invasive nerve biopsies. Co-culturing patient hiPSC or iNC-derived Schwann cells with T-cells from peripheral blood of the same patient may also lead to some novel insights. For instance, comparing interactions between different combinations of Schwann cells and T-cells from GBS patients and healthy controls might help shed light on how much pathology is Schwann cell-intrinsic vs T-cell-intrinsic.

Broadening the spectrum further, our patient hiPSC- or iNC-derived Schwann cells might also be used for modeling leukodystrophies that affect both the CNS and PNS, like Krabbe disease<sup>178</sup>. Similar molecular pathology may be present in both the affect Schwann cells and oligodendrocytes in these disorders. Because many other groups have developed methods for hiPSC differentiation into oligodendrocytes and direct conversion towards oligodendrocytes<sup>139,179</sup>, engineered Schwann cells and oligodendrocytes could be generated from Krabbe patient cells and profiled for common molecular pathologies.

### Drug screening

In addition to disease modeling, our three methods of patient-derived Schwann cell development can also be utilized for drug screening. Our hiPSC-Schwann cell and PGD-hESC-Schwann cell differentiation protocols in particular yield Schwann cells that can be expanded in culture for up to two months, making them particularly well suited for high throughput drug screening (HTS). Currently, most high throughput drug screening is performed using rodent cell lines or human

cancer cell lines, which may not share the same characteristics of the tissues involved in disease pathogenesis. Consequently, patient-derived engineered Schwann cells likely better mimic the endogenous diseased Schwann cells and likely have better predictive efficacy in high throughput screens. In this study, we used our CMT1A hiPSC-derived Schwann cells to evaluate the effect of three drugs (bortezomib, fenretinide, and olvanil<sup>148</sup>) on *PMP22* expression on hiPSCs derived from two different patients. Expanding this study to include more hiPSC clones and lines representing a broader number of CMT1A and control genotypes could help better establish the effect these three drugs play on *PMP22* gene expression or CXCL1 and MCP-1 protein expression, particularly as they are evaluated in pre-clinical trials.

#### Cell transplantation therapy

Though still quite distant, therapeutic transplantation of stem cell-derived cells is one of the most highly anticipated applications of stem cell technology. Our system yields three different sources of patient-derived Schwann cells that could potentially be used for transplantation therapy in the future. The advantage of hiPSC-Schwann cells and iNC-Schwann cells is that they can be derived from a patient's own fibroblasts, thereby minimizing immunocompatibility concerns. An advantage of hiPSC-Schwann cells and PGD-hESC-Schwann cells is that they can be expanded *in vitro* prior to transplantation, thereby yielding larger cell numbers. And a major advantage of iNC-Schwann cells is that, by bypassing the pluripotent stem cell stage, these cells have lower tumorigenic potential than their hiPSC and PGD-hESC counterparts.

There are a number of disorders that might potentially benefit from Schwann cell transplantation one day. In a collaboration with Gerald Brandacher's group we are currently evaluating whether transplantation of control hiPSC-derived Schwann cells affects functional neuro-regeneration in rodent models of chronic denervation and limb transplantation surgery. Clinically, in the context of hereditary neuropathies like CMTs, transplantation of patient-matched, genetically corrected Schwann cells to treat demyelination is certainly appealing. Similarly, patient-matched Schwann cell transplantation might also be worth investigating in acquired inflammatory neuropathies (ie GBS and CIDP) and even in spinal cord injury, as Schwann cell transplantation into the spinal cord may aid re-myelination and axonal regeneration<sup>180</sup>.

## **Final perspectives**

As an MD/PhD student, it is currently an exciting time embark on a career as a physician-scientist. Recent advances in stem cell technology in particular make bedside-to-bench experiments readily accessible, and with time, I hope to also translate my findings from the bench back to the bedside. Our lab has created three exciting “disease in a dish” platforms—two of which were the result of this dissertation—to better understand Schwann cell disease biology, screen for drugs, and potentially transplant therapeutically. As I progress through my anticipated career as an academic neurologist, I hope to build upon the techniques learned and knowledge acquired during this dissertation to continue to contribute to our collective understanding of neurological illness and therapy.

## REFERENCES

1. Baggiolini, A. *et al.* Premigratory and Migratory Neural Crest Cells Are Multipotent In Vivo. *Cell Stem Cell* **16**, 314–322 (2015).
2. Fuchs, S. & Sommer, L. The neural crest: understanding stem cell function in development and disease. *Neurodegener. Dis.* **4**, 6–12 (2007).
3. Anderson, R. B., Stewart, a. L. & Young, H. M. Phenotypes of neural-crest-derived cells in vagal and sacral pathways. *Cell Tissue Res.* **323**, 11–25 (2006).
4. Jessen, K. R. & Mirsky, R. The origin and development of glial cells in peripheral nerves. *Nat. Rev. Neurosci.* **6**, 671–82 (2005).
5. Woodhoo, A. & Sommer, L. Development of the Schwann cell lineage: from the neural crest to the myelinated nerve. *Glia* **56**, 1481–90 (2008).
6. Liu, Q. *et al.* Human neural crest stem cells derived from human ESCs and induced pluripotent stem cells: induction, maintenance, and differentiation into functional Schwann cells. *Stem cells ...* **1**, 266–278 (2012).
7. Skre, H. Genetic and clinical aspects of Charcot-Marie-Tooth's disease. *Clin. Genet.* **6**, 98–118 (1974).
8. Klein, C. J., Duan, X. & Shy, M. E. Inherited neuropathies: Clinical overview and update. *Muscle and Nerve* **48**, 604–622 (2013).
9. Saporta, M. A. & Shy, M. E. Inherited Peripheral Neuropathies Inherited Peripheral Neuropathies. *Neurol. Clin.* **31**, 597–619 (2013).
10. Saporta, A. S. D. *et al.* Charcot-marie-tooth disease subtypes and genetic testing strategies. *Ann. Neurol.* **69**, 22–33 (2011).
11. Snipes, G. J., Suter, U., Welcher, a a & Shooter, E. M. Characterization of a novel peripheral nervous system myelin protein (PMP-22/SR13). *J. Cell Biol.* **117**, 225–238 (1992).
12. Inoue, K. *et al.* The 1 . 4-Mb CMT1A Duplication / HNPP Deletion Genomic Region Reveals Unique Genome Architectural Features and Provides Insights into the Recent Evolution of New Genes. 1018–1033 (2001). doi:10.1101/gr.180401.1
13. Hanemann, C. O. *et al.* Peripheral myelin protein-22 expression in Charcot-Marie-Tooth disease type 1a sural nerve biopsies. *J. Neurosci. Res.* **37**, 654–659 (1994).
14. Hanemann, C. O. *et al.* Improved culture methods to expand schwann cells with altered growth behaviour from CMT1a patients. *Glia* **23**, 89–98 (1998).
15. Katona, I. *et al.* PMP22 expression in dermal nerve myelin from patients with CMT1A. *Brain* **132**, 1734–40 (2009).
16. Huxley, C. *et al.* Construction of a mouse model of Charcot-Marie-Tooth disease type 1A by pronuclear injection of human YAC DNA. *Hum. Mol. Genet.* **5**, 563–569 (1996).
17. Huxley, C. *et al.* Correlation between varying levels of PMP22 expression and

- the degree of demyelination and reduction in nerve conduction velocity in transgenic mice. *Hum. Mol. Genet.* **7**, 449–458 (1998).
18. Magyar, J. P. *et al.* Impaired Differentiation of Schwann Cells in Transgenic Mice with Increased PMP22 Gene Dosage. *J. Neurosci.* **16**, 5351–5360 (1996).
  19. Sereda, M. W. & Nave, K. Animal Models of Charcot-Marie-Tooth Disease Type 1A CMT1A: A Gene Dosage Disease. *Neuromolecular Med.* **8**, 1559–1174 (2006).
  20. Magyar, J. P. *et al.* Impaired differentiation of Schwann cells in transgenic mice with increased PMP22 gene dosage. *J. Neurosci.* **16**, 5351–5360 (1996).
  21. Robertson, a M. *et al.* Comparison of a new pmp22 transgenic mouse line with other mouse models and human patients with CMT1A. *J. Anat.* **200**, 377–90 (2002).
  22. Kohl, B., Fischer, S., Groh, J., Wessig, C. & Martini, R. MCP-1/CCL2 modifies axon properties in a PMP22-overexpressing mouse model for Charcot-Marie-tooth 1A neuropathy. *Am. J. Pathol.* **176**, 1390–9 (2010).
  23. Kobsar, I., Hasenpusch-Theil, K., Wessig, C., Müller, H. W. & Martini, R. Evidence for macrophage-mediated myelin disruption in an animal model for Charcot-Marie-Tooth neuropathy type 1A. *J. Neurosci. Res.* **81**, 857–64 (2005).
  24. Perea, J. *et al.* Induced myelination and demyelination in a conditional mouse model of Charcot-Marie-Tooth disease type 1A. *Hum. Mol. Genet.* **10**, 1007–1018 (2001).
  25. Podratz, J. L., Rodriguez, E. & Windebank, a J. Role of the extracellular matrix in myelination of peripheral nerve. *Glia* **35**, 35–40 (2001).
  26. Podratz, J. L., Rodriguez, E. H. & Windebank, A. J. Antioxidants Are Necessary for Myelination of Dorsal Root Ganglion Neurons, In Vitro. *Glia* **45**, 54–58 (2004).
  27. Passage, E. *et al.* Ascorbic acid treatment corrects the phenotype of a mouse model of Charcot-Marie-Tooth disease. *Nat. Med.* **10**, 396–401 (2004).
  28. Kaya, F. *et al.* Ascorbic acid inhibits PMP22 expression by reducing cAMP levels. *Neuromuscul. Disord.* **17**, 248–253 (2007).
  29. Burns, J. *et al.* Ascorbic acid for Charcot-Marie-Tooth disease type 1A in children: a randomised, double-blind, placebo-controlled, safety and efficacy trial. *Lancet Neurol.* **8**, 537–44 (2009).
  30. Verhamme, C. *et al.* Oral high dose ascorbic acid treatment for one year in young CMT1A patients: a randomised, double-blind, placebo-controlled phase II trial. *BMC Med.* **7**, 70 (2009).
  31. Pareyson, D. *et al.* Ascorbic acid in Charcot-Marie-Tooth disease type 1A (CMT-TRIAAL and CMT-TRAUK): a double-blind randomised trial. *Lancet Neurol.* **10**, 320–8 (2011).
  32. Micallef, J. *et al.* Effect of ascorbic acid in patients with Charcot-Marie-Tooth



- disease type 1A: a multicentre, randomised, double-blind, placebo-controlled trial. *Lancet Neurol.* **8**, 1103–1110 (2009).
33. Lewis, R. a *et al.* High-dosage ascorbic acid treatment in Charcot-Marie-Tooth disease type 1A: results of a randomized, double-masked, controlled trial. *JAMA Neurol.* **70**, 981–7 (2013).
  34. Gold, R., Archelos, J. J. & Hartung, H. P. Mechanisms of immune regulation in the peripheral nervous system. *Brain Pathol.* **9**, 343–360 (1999).
  35. Scheinberg, L. C., Kotsilimbas, D. G., Karpf, R. & Mayer, N. Is the Brain an 'Immunologically Privileged Site?' *Arch. Neurol.* **15**, (1966).
  36. Kieseier, B. C., Hu, W. & Hartung, H.-P. in *The Biology of Schwann cells: Development, Differentiation, and Immunomodulation* (ed. Armati, P. J.) 118–125 (2007).
  37. Carson, M. J., Doose, J. M., Melchior, B., Schmid, C. D. & Ploix, C. C. CNS immune privilege: Hiding in plain sight. *Immunol. Rev.* **213**, 48–65 (2006).
  38. Oliveira, R., Ochoa, M. & Sieling, P. Expression of Toll-like receptor 2 on human Schwann cells: a mechanism of nerve damage in leprosy. *Infect. Immun.* **71**, 1427–1433 (2003).
  39. Goethals, S., Ydens, E., Timmerman, V. & Janssens, S. Toll-like receptor expression in the peripheral nerve. *Glia* **58**, 1701–1709 (2010).
  40. Lee, H. *et al.* Necrotic neuronal cells induce inflammatory Schwann cell activation via TLR2 and TLR3: Implication in Wallerian degeneration. *Biochem. Biophys. Res. Commun.* **350**, 742–747 (2006).
  41. Boivin, A. *et al.* Toll-like receptor signaling is critical for Wallerian degeneration and functional recovery after peripheral nerve injury. *J. Neurosci.* **27**, 12565–12576 (2007).
  42. Armati, P. J., Pollard, J. D. & Gatenby, P. Rat and Human Schwann cells in Vitro Can Synthesize and Express MHC molecules. (1990).
  43. Pollard, J. D., McCombe, P. a, Baverstock, J., Gatenby, P. a & McLeod, J. G. Class II antigen expression and T lymphocyte subsets in chronic inflammatory demyelinating polyneuropathy. *J. Neuroimmunol.* **13**, 123–134 (1986).
  44. Pollard, J. D., Baverstock, J. & McLeod, J. G. Class II antigen expression and inflammatory cells in the Guillain-Barré syndrome. *Ann. Neurol.* **21**, 337–341 (1987).
  45. Murata, K. & Dalakas, M. C. Expression of the co-stimulatory molecule BB-1, the ligands CTLA-4 and CD28 and their mRNAs in chronic inflammatory demyelinating polyneuropathy. *Brain* **123** ( Pt 8, 1660–1666 (2000).
  46. Lisak, R. P. & Benjamins, J. A. in *The Biology of Schwann cells: Development, Differentiation, and Immunomodulation* (ed. Armati, P. J.) 100–117 (2007).
  47. Lisak, R. P., Skundric, D., Bealmear, B. & Ragheb, S. The role of cytokines in Schwann cell damage, protection, and repair. *J. Infect. Dis.* **176 Suppl** , S173–S179 (1997).
  48. Bergsteindottir, K., Kingston, a., Mirsky, R. & Jessen, K. R. Rat Schwann cells

- produce interleukin-1. *J. Neuroimmunol.* **34**, 15–23 (1991).
49. Skundric, D. S., Bealmear, B. & Lisak, R. P. Induced upregulation of IL-1, IL-1RA and IL-1R type I gene expression by Schwann cells. *J. Neuroimmunol.* **74**, 9–18 (1997).
  50. Bolin, L. M., Verity, a N., Silver, J. E., Shooter, E. M. & Abrams, J. S. Interleukin-6 production by Schwann cells and induction in sciatic nerve injury. *J. Neurochem.* **64**, 850–858 (1995).
  51. Wagner, R. & Myers, R. Schwann cells produce tumor necrosis factor alpha: expression in injured and non-injured nerves. *Neuroscience* **4522**, 625–629 (1996).
  52. Cheng, C. *et al.* Induction of TNF- $\alpha$  by LPS in Schwann cell is regulated by MAPK activation signals. *Cell. Mol. Neurobiol.* **27**, 909–921 (2007).
  53. Scherer, S. S., Kamholz, J. & Jakowlew, S. B. Axons modulate the expression of transforming growth factor- $\beta$ s in Schwann cells. *Glia* **8**, 265–276 (1993).
  54. Rotshenker, S. Wallerian degeneration: the innate-immune response to traumatic nerve injury. *J. Neuroinflammation* **8**, 109 (2011).
  55. Perrin, F. E., Lacroix, S., Avilés-Trigueros, M. & David, S. Involvement of monocyte chemoattractant protein-1, macrophage inflammatory protein-1 $\alpha$  and interleukin-1 $\beta$  in Wallerian degeneration. *Brain* **128**, 854–866 (2005).
  56. Stoll, G., Griffin, J. W., Li, C. Y. & Trapp, B. D. Wallerian degeneration in the peripheral nervous system: participation of both Schwann cells and macrophages in myelin degradation. *J. Neurocytol.* **18**, 671–683 (1989).
  57. Reichert, F., Saada, a & Rotshenker, S. Peripheral nerve injury induces Schwann cells to express two macrophage phenotypes: phagocytosis and the galactose-specific lectin MAC-2. *J. Neurosci.* **14**, 3231–3245 (1994).
  58. Hirata, K. & Kawabuchi, M. Myelin phagocytosis by macrophages and nonmacrophages during Wallerian degeneration. *Microsc. Res. Tech.* **57**, 541–547 (2002).
  59. Thoma, E. C. *et al.* Chemical Conversion of Human Fibroblasts into Functional Schwann Cells. *Stem Cell Reports* **3**, 539–547 (2014).
  60. Hockemeyer, D. *et al.* Genetic engineering of human pluripotent cells using TALE nucleases. *Nat. Biotechnol.* **29**, 731–734 (2011).
  61. Lee, G., Chambers, S. M., Tomishima, M. J. & Studer, L. Derivation of neural crest cells from human pluripotent stem cells. *Nat. Protoc.* **5**, 688–701 (2010).
  62. Thomson, J. *et al.* Embryonic stem cell lines derived from human blastocysts. *Science (80-. ).* **282**, 1145–1147 (1998).
  63. Scott, C. T., McCormick, J. B. & Owen-Smith, J. And then there were two: use of hESC lines. *Nat. Biotechnol.* **27**, 696–697 (2009).
  64. Perrier, A. L. *et al.* Derivation of midbrain dopamine neurons from human

- embryonic stem cells. *Proc. Natl. Acad. Sci.* **101**, 12543–12548 (2004).
65. Zhang, S. C., Wernig, M., Duncan, I. D., Brüstle, O. & Thomson, J. a. In vitro differentiation of transplantable neural precursors from human embryonic stem cells. *Nat. Biotechnol.* **19**, 1129–1133 (2001).
  66. Kriks, S. *et al.* Dopamine neurons derived from human ES cells efficiently engraft in animal models of Parkinson's disease. *Nature* **480**, 547–551 (2011).
  67. Chambers, S. M. *et al.* Combined small-molecule inhibition accelerates developmental timing and converts human pluripotent stem cells into nociceptors. *Nat. Biotechnol.* **30**, 715–20 (2012).
  68. Chambers, S. M. *et al.* Highly efficient neural conversion of human ES and iPS cells by dual inhibition of SMAD signaling. *Nat. Biotechnol.* **27**, 275–280 (2009).
  69. 0006899386913946.
  70. Kim, H. a, Ratner, N., Roberts, T. M. & Stiles, C. D. Schwann cell proliferative responses to cAMP and Nf1 are mediated by cyclin D1. *J. Neurosci.* **21**, 1110–1116 (2001).
  71. Stewart, H. J., Eccleston, P. a, Jessen, K. R. & Mirsky, R. Interaction between cAMP elevation, identified growth factors, and serum components in regulating Schwann cell growth. *J. Neurosci. Res.* **30**, 346–352 (1991).
  72. Monje, P. V., Athauda, G. & Wood, P. M. Protein kinase A-mediated gating of neuregulin-dependent ErbB2-ErbB3 activation underlies the synergistic action of cAMP on schwann cell proliferation. *J. Biol. Chem.* **283**, 34087–34100 (2008).
  73. Morgan, L., Jessen, K. R. & Mirsky, R. The effects of cAMP on differentiation of cultured schwann cells: Progression from an early phenotype (04+) to a myelin phenotype (P<sub>0</sub>+, GFAP-, N-CAM-, NGF-receptor-) depends on growth inhibition. *J. Cell Biol.* **112**, 457–467 (1991).
  74. Eldridge, C. F., Bunge, M. B. & Bunge, R. P. Differentiation of axon-related Schwann cells in vitro: II. Control of myelin formation by basal lamina. *J. Neurosci.* **9**, 625–638 (1989).
  75. Takahashi, M. & Osumi, N. Identification of a novel type II classical cadherin: Rat cadherin19 is expressed in the cranial ganglia and Schwann cell precursors during development. *Dev. Dyn.* **232**, 200–208 (2005).
  76. Monk, K. R. *et al.* A G protein-coupled receptor is essential for Schwann cells to initiate myelination. *Science* **325**, 1402–1405 (2009).
  77. Mogha, A. *et al.* Gpr126 functions in Schwann cells to control differentiation and myelination via G-protein activation. *J. Neurosci.* **33**, 17976–85 (2013).
  78. Monk, K. R., Oshima, K., Jörs, S., Heller, S. & Talbot, W. S. Gpr126 is essential for peripheral nerve development and myelination in mammals. *Development* **138**, 2673–2680 (2011).
  79. Lindsley, A. *et al.* Identification and characterization of a novel Schwann and

- outflow tract endocardial cushion lineage-restricted periostin enhancer. *Dev. Biol.* **307**, 340–355 (2007).
80. Conti, L. *et al.* Niche-independent symmetrical self-renewal of a mammalian tissue stem cell. *PLoS Biol.* **3**, 1594–1606 (2005).
  81. Ludwig, T. E. *et al.* Derivation of human embryonic stem cells in defined conditions. *Nat. Biotechnol.* **24**, 185–187 (2006).
  82. Lu, J., Hou, R., Booth, C. J., Yang, S.-H. & Snyder, M. Defined culture conditions of human embryonic stem cells. *Proc. Natl. Acad. Sci. U. S. A.* **103**, 5688–5693 (2006).
  83. Yao, S. *et al.* Long-term self-renewal and directed differentiation of human embryonic stem cells in chemically defined conditions. *Proc. Natl. Acad. Sci. U. S. A.* **103**, 6907–6912 (2006).
  84. Liu, Y. *et al.* A novel chemical-defined medium with bFGF and N2B27 supplements supports undifferentiated growth in human embryonic stem cells. *Biochem. Biophys. Res. Commun.* **346**, 131–139 (2006).
  85. Shaltouki, A., Peng, J., Liu, Q., Rao, M. S. & Zeng, X. Efficient generation of astrocytes from human pluripotent stem cells in defined conditions. *Stem Cells* **31**, 941–952 (2013).
  86. Swistowski, A. *et al.* Xeno-free defined conditions for culture of human embryonic stem cells, neural stem cells and dopaminergic neurons derived from them. *PLoS One* **4**, (2009).
  87. Martin, M. J., Muotri, A., Gage, F. & Varki, A. Human embryonic stem cells express an immunogenic nonhuman sialic acid. *Nat. Med.* **11**, 228–232 (2005).
  88. Lehmann, H. C. *et al.* Human Schwann Cells Retain Essential Phenotype Characteristics After Immortalization. *Stem Cells Dev.* **21**, 423–431 (2012).
  89. Pearse, D. D. *et al.* cAMP and Schwann cells promote axonal growth and functional recovery after spinal cord injury. *Nat. Med.* **10**, 610–616 (2004).
  90. Blakemore, W. F. Remyelination of CNS axons by Schwann cells transplanted from the sciatic nerve. *Nature* **266**, 68–69 (1977).
  91. Jones, J. W., Gruber, S. a, Barker, J. H. & Breidenbach, W. C. Successful hand transplantation. One-year follow-up. Louisville Hand Transplant Team. *N. Engl. J. Med.* **343**, 468–473 (2000).
  92. Khalifian, S. *et al.* Stem Cell-Based Approaches to Improve Nerve Regeneration: Potential Implications for Reconstructive Transplantation? *Arch. Immunol. Ther. Exp. (Warsz)*. **63**, 15–30 (2014).
  93. Best, C. M. Hand and Upper Extremity Fellowship. 53213 (2013). doi:10.1097/PRS.0000000000000892
  94. Hu, B.-Y. *et al.* Neural differentiation of human induced pluripotent stem cells follows developmental principles but with variable potency. *Proc. Natl. Acad. Sci. U. S. A.* **107**, 4335–4340 (2010).
  95. Choi, I. Y., Lim, H. & Lee, G. Efficient Generation Human Induced Pluripotent

- Stem Cells from Human Somatic Cells with Sendai-virus. *J. Vis. Exp.* e51406 (2014). doi:10.3791/51406
96. Martins-Taylor, K. & Xu, R.-H. Concise review: Genomic stability of human induced pluripotent stem cells. *Stem Cells* **30**, 22–7 (2012).
  97. Kim, H. *et al.* miR-371-3 expression predicts neural differentiation propensity in human pluripotent stem cells. *Cell Stem Cell* **8**, 695–706 (2011).
  98. Koyanagi-Aoi, M. *et al.* Differentiation-defective phenotypes revealed by large-scale analyses of human pluripotent stem cells. *Proc. Natl. Acad. Sci. U. S. A.* **110**, 20569–74 (2013).
  99. Kim, H. *et al.* miR-371-3 expression predicts neural differentiation propensity in human pluripotent stem cells. *Cell Stem Cell* **8**, 695–706 (2011).
  100. Trujillo, G. *et al.* Neutrophil recruitment to the lung in both C5a- and CXCL1-induced alveolitis is impaired in vitamin D-binding protein-deficient mice. *J. Immunol.* **191**, 848–56 (2013).
  101. Chintakuntlawar, A. V & Chodosh, J. Chemokine CXCL1/KC and its receptor CXCR2 are responsible for neutrophil chemotaxis in adenoviral keratitis. *J. Interferon Cytokine Res.* **29**, 657–666 (2009).
  102. Ritzman, A. M. *et al.* The chemokine receptor CXCR2 ligand KC (CXCL1) mediates neutrophil recruitment and is critical for development of experimental lyme arthritis and carditis. *Infect. Immun.* **78**, 4593–4600 (2010).
  103. Lin, M., Carlson, E., Diaconu, E. & Pearlman, E. CXCL1/KC and CXCL5/LIX are selectively produced by corneal fibroblasts and mediate neutrophil infiltration to the corneal stroma in LPS keratitis. *J. Leukoc. Biol.* **81**, 786–792 (2007).
  104. Vries, M. H. M., Wagenaar, A. & Post, M. J. CXCL1 promotes arteriogenesis through enhanced monocyte recruitment into the peri-collateral space. 163–171 (2015). doi:10.1007/s10456-014-9454-1
  105. Clahsen, T. & Schaper, F. Interleukin-6 acts in the fashion of a classical chemokine on monocytic cells by inducing integrin activation, cell adhesion, actin polymerization, chemotaxis, and transmigration. *J. Leukoc. Biol.* **84**, 1521–1529 (2008).
  106. Chomarat, P., Banchereau, J., Davoust, J. & Palucka, a K. IL-6 switches the differentiation of monocytes from dendritic cells to macrophages. *Nat. Immunol.* **1**, 510–514 (2000).
  107. Kaplanski, G., Marin, V., Montero-Julian, F., Mantovani, A. & Farnarier, C. IL-6: A regulator of the transition from neutrophil to monocyte recruitment during inflammation. *Trends Immunol.* **24**, 25–29 (2003).
  108. Fielding, C. a *et al.* IL-6 regulates neutrophil trafficking during acute inflammation via STAT3. *J. Immunol.* **181**, 2189–2195 (2008).
  109. de Oliveira, S. *et al.* Cxcl8 (IL-8) mediates neutrophil recruitment and behavior in the zebrafish inflammatory response. *J. Immunol.* **190**, 4349–59 (2013).

110. Mukaida, N., Harada, A. & Matsushima, K. Interleukin-8 (IL-8) and monocyte chemotactic and activating factor (MCAF/MCP-1), chemokines essentially involved in inflammatory and immune reactions. *Cytokine Growth Factor Rev.* **9**, 9–23 (1998).
111. Kilgore, K. S., Flory, C. M., Miller, B. F., Evans, V. M. & Warren, J. S. The membrane attack complex of complement induces interleukin-8 and monocyte chemoattractant protein-1 secretion from human umbilical vein endothelial cells. *Am. J. Pathol.* **149**, 953–961 (1996).
112. Niu, J., Azfer, A., Zhelyabovska, O., Fatma, S. & Kolattukudy, P. E. Monocyte chemotactic protein (MCP)-1 promotes angiogenesis via a novel transcription factor, MCP-1-induced protein (MCPIP). *J. Biol. Chem.* **283**, 14542–14551 (2008).
113. Huffnagle, G. B. *et al.* The role of monocyte chemotactic protein-1 (MCP-1) in the recruitment of monocytes and CD4+ T cells during a pulmonary *Cryptococcus neoformans* infection. *J. Immunol.* **155**, 4790–4797 (1995).
114. Ylä-Herttua, S. *et al.* Expression of monocyte chemoattractant protein 1 in macrophage-rich areas of human and rabbit atherosclerotic lesions. *Proc. Natl. Acad. Sci. U. S. A.* **88**, 5252–5256 (1991).
115. Matsukawa, a *et al.* Endogenous monocyte chemoattractant protein-1 (MCP-1) protects mice in a model of acute septic peritonitis: cross-talk between MCP-1 and leukotriene B4. *J. Immunol.* **163**, 6148–6154 (1999).
116. Bouchon, a, Dietrich, J. & Colonna, M. Cutting edge: inflammatory responses can be triggered by TREM-1, a novel receptor expressed on neutrophils and monocytes. *J. Immunol.* **164**, 4991–4995 (2000).
117. Neuropathy, C. *et al.* MCP-1 / CCL2 Modifies Axon Properties in a PMP22-Overexpressing Mouse Model for. **176**, 1–10 (2010).
118. Chittoor, V. G. *et al.* Biochemical characterization of protein quality control mechanisms during disease progression in the C22 mouse model of CMT1A. *ASN Neuro* **5**, e00128 (2013).
119. Misko, a., Ferguson, T. & Notterpek, L. Matrix metalloproteinase mediated degradation of basement membrane proteins in Trembler J neuropathy nerves. *J. Neurochem.* **83**, 885–894 (2002).
120. Conductier, G., Blondeau, N., Guyon, A., Nahon, J. L. & Rovère, C. The role of monocyte chemoattractant protein MCP1/CCL2 in neuroinflammatory diseases. *J. Neuroimmunol.* **224**, 93–100 (2010).
121. Tofaris, G. K., Patterson, P. H., Jessen, K. R. & Mirsky, R. Denervated Schwann cells attract macrophages by secretion of leukemia inhibitory factor (LIF) and monocyte chemoattractant protein-1 in a process regulated by interleukin-6 and LIF. *J. Neurosci.* **22**, 6696–6703 (2002).
122. Deshmane, S. L., Kremlev, S., Amini, S. & Sawaya, B. E. Monocyte chemoattractant protein-1 (MCP-1): an overview. *J. Interferon Cytokine Res.* **29**, 313–326 (2009).
123. Gasimli, L. *et al.* Structural remodeling of proteoglycans upon retinoic acid-

- induced differentiation of NCCIT cells. *Glycoconj. J.* **30**, 497–510 (2013).
124. Shukla, D. *et al.* A novel role for 3-O-sulfated heparan sulfate in herpes simplex virus 1 entry. *Cell* **99**, 13–22 (1999).
  125. Structures, S., But, E., Is, H. & Regulated, S. Perspectives Series : Cell Adhesion in Vascular Biology Heparan Sulfate Proteoglycans of the Cardiovascular System. *Society*
  126. Xu, D., Moon, A. F., Song, D., Pedersen, L. C. & Liu, J. Engineering sulfotransferases to modify heparan sulfate. *Nat. Chem. Biol.* **4**, 200–202 (2008).
  127. Shworak, N. W. *et al.* Molecular cloning and expression of mouse and human cDNAs encoding heparan sulfate D-glucosaminyl 3-O-sulfotransferase. *J. Biol. Chem.* **272**, 28008–28019 (1997).
  128. Lawrence, R. *et al.* The principal neuronal gD-type 3-O-sulfotransferases and their products in central and peripheral nervous system tissues. *Matrix Biol.* **26**, 442–455 (2007).
  129. Copeland, N. G. *et al.* Multiple Isoforms of Heparan Sulfate. **274**, 5170 –5184 (1999).
  130. Moon, A. F. *et al.* Structural analysis of the sulfotransferase (3-O-sulfotransferase isoform 3) involved in the biosynthesis of an entry receptor for herpes simplex virus 1. *J. Biol. Chem.* **279**, 45185–45193 (2004).
  131. Song, K., Li, Q., Jiang, Z. Z., Guo, C. W. & Li, P. Heparan sulfate D-glucosaminyl 3-O-sulfotransferase-3B1, a novel epithelial-mesenchymal transition inducer in pancreatic cancer. *Cancer Biol. Ther.* **12**, 388–398 (2011).
  132. Salehi, L. B. *et al.* Assignment of a locus for autosomal dominant idiopathic scoliosis (IS) to human chromosome 17p11. *Hum. Genet.* **111**, 401–4 (2002).
  133. Boven, L. a *et al.* Brain-derived human immunodeficiency virus-1 Tat exerts differential effects on LTR transactivation and neuroimmune activation. *J. Neurovirol.* **13**, 173–184 (2007).
  134. Davis, R. L., Weintraub, H. & Lassar, a B. Expression of a single transfected cDNA converts fibroblasts to myoblasts. *Cell* **51**, 987–1000 (1987).
  135. Zhou, Q., Brown, J., Kanarek, A., Rajagopal, J. & Melton, D. a. In vivo reprogramming of adult pancreatic exocrine cells to beta-cells. *Nature* **455**, 627–32 (2008).
  136. Vierbuchen, T. *et al.* Direct conversion of fibroblasts to functional neurons by defined factors. *Nature* **463**, 1035–41 (2010).
  137. Lujan, E., Chanda, S., Ahlenius, H., Sudhof, T. C. & Wernig, M. Direct conversion of mouse fibroblasts to self-renewing, tripotent neural precursor cells. *Proc. Natl. Acad. Sci.* **109**, 2527–2532 (2012).
  138. Son, E. Y. *et al.* Conversion of mouse and human fibroblasts into functional spinal motor neurons. *Cell Stem Cell* **9**, 205–218 (2011).

139. Najm, F. J. *et al.* Transcription factor-mediated reprogramming of fibroblasts to expandable, myelinogenic oligodendrocyte progenitor cells. *Nat. Biotechnol.* **31**, 426–33 (2013).
140. Yang, N. *et al.* Generation of oligodendroglial cells by direct lineage conversion. *Nat. Biotechnol.* **31**, 434–9 (2013).
141. Kim, Y. J. *et al.* Generation of Multipotent Induced Neural Crest by Direct Reprogramming of Human Postnatal Fibroblasts with a Single Transcription Factor. *Cell Stem Cell* **15**, 497–506 (2014).
142. Szabo, E. *et al.* Direct conversion of human fibroblasts to multilineage blood progenitors. *Nature* **468**, 521–526 (2010).
143. Meyer, K. *et al.* Direct conversion of patient fibroblasts demonstrates non-cell autonomous toxicity of astrocytes to motor neurons in familial and sporadic ALS. *Proc. Natl. Acad. Sci. U. S. A.* **111**, 829–32 (2014).
144. Caiazzo, M. *et al.* Direct generation of functional dopaminergic neurons from mouse and human fibroblasts. *Nature* **476**, 224–227 (2011).
145. Stephenson, E. L., Mason, C. & Braude, P. R. Preimplantation genetic diagnosis as a source of human embryonic stem cells for disease research and drug discovery. *BJOG* **116**, 158–65 (2009).
146. Niclis, J. C. *et al.* Human embryonic stem cell models of Huntington disease. *Reprod. Biomed. Online* **19**, 106–113 (2009).
147. Eiges, R. *et al.* Developmental Study of Fragile X Syndrome Using Human Embryonic Stem Cells Derived from Preimplantation Genetically Diagnosed Embryos. *Cell Stem Cell* **1**, 568–577 (2007).
148. Jang, S., Lopez-anido, C., Macarthur, R., Svaren, J. & Inglese, J. Identification of Drug Modulators Targeting Gene-Dosage Disease CMT1A. *ACS Chem. Biol.* 1205–1213 (2012).
149. Song, K., Li, Q., Jiang, Z.-Z., Guo, C.-W. & Li, P. Heparan sulfate D-glucosaminyl 3-O-sulfotransferase-3B1, a novel epithelial-mesenchymal transition inducer in pancreatic cancer. *Cancer Biol. Ther.* **12**, 388–398 (2011).
150. Robaglia-Schlupp, a *et al.* PMP22 overexpression causes dysmyelination in mice. *Brain* **125**, 2213–21 (2002).
151. Kobsar, I., Mäurer, M., Ott, T. & Martini, R. Macrophage-related demyelination in peripheral nerves of mice deficient in the gap junction protein connexin 32. *Neurosci. Lett.* **320**, 17–20 (2002).
152. Hanemann, C. O. & Müller, H. W. Pathogenesis of Charcot-Marie-Tooth 1A (CMT1A) neuropathy. *Trends Neurosci.* **21**, 282–6 (1998).
153. Hanemann, C. O., Gabreëls-Festen, a a, Stoll, G. & Müller, H. W. Schwann cell differentiation in Charcot-Marie-Tooth disease type 1A (CMT1A): normal number of myelinating Schwann cells in young CMT1A patients and neural cell adhesion molecule expression in onion bulbs. *Acta Neuropathol.* **94**, 310–5 (1997).



154. Nobbio, L. *et al.* Impairment of PMP22 transgenic Schwann cells differentiation in culture: implications for Charcot-Marie-Tooth type 1A disease. *Neurobiol. Dis.* **16**, 263–73 (2004).
155. Fabbretti, E., Edomi, P., Brancolini, C. & Schneider, C. Apoptotic phenotype induced by overexpression of wild-type gas3/PMP22: its relation to the demyelinating peripheral neuropathy CMT1A. *Genes Dev.* **9**, 1846–1856 (1995).
156. Karlsson, C., Afrakhte, M., Westermark, B. & Paulsson, Y. Elevated level of gas3 gene expression is correlated with G0 growth arrest in human fibroblasts. *Cell Biol. Int.* **23**, 351–358 (1999).
157. Jerath, N. U. & Shy, M. E. Hereditary motor and sensory neuropathies: Understanding molecular pathogenesis could lead to future treatment strategies. *Biochim. Biophys. Acta* **1852**, 667–678 (2014).
158. Han, L. L., Keller, M. P., Navidi, W., Chance, P. F. & Arnheim, N. Unequal exchange at the Charcot-Marie-Tooth disease type 1A recombination hot-spot is not elevated above the genome average rate. *Hum. Mol. Genet.* **9**, 1881–1889 (2000).
159. Timmerman, V. *et al.* Detection of the CMT1A/HNPP recombination hotspot in unrelated patients of European descent. *J. Med. Genet.* **34**, 43–49 (1997).
160. Keller, M. P., Seifried, B. a & Chance, P. F. Molecular evolution of the CMT1A-REP region: a human- and chimpanzee-specific repeat. *Mol. Biol. Evol.* **16**, 1019–1026 (1999).
161. Rittner, H. L., Brack, a. & Stein, C. Pain and the immune system. *Br. J. Anaesth.* **101**, 40–44 (2008).
162. Stein, C., Schäfer, M. & Machelska, H. Attacking pain at its source: new perspectives on opioids. *Nat. Med.* **9**, 1003–1008 (2003).
163. Grammas, P. & Ovase, R. Inflammatory factors are elevated in brain microvessels in Alzheimer’s disease. *Neurobiol. Aging* **22**, 837–842 (2001).
164. Fiala, M. *et al.* Amyloid-beta induces chemokine secretion and monocyte migration across a human blood--brain barrier model. *Mol. Med.* **4**, 480–489 (1998).
165. Martini, R., Fischer, S., López-Vales, R. & David, S. Interactions between schwann cells and macrophages in injury and inherited demyelinating disease. *Glia* **56**, 1566–1577 (2008).
166. Deverman, B. E. & Patterson, P. H. Cytokines and CNS Development. *Neuron* **64**, 61–78 (2009).
167. Stolp, H. B. Neuropoietic cytokines in normal brain development and neurodevelopmental disorders. *Mol. Cell. Neurosci.* **53**, 63–68 (2013).
168. Li, J., Parker, B., Martyn, C., Natarajan, C. & Guo, J. The PMP22 gene and its related diseases. *Mol. Neurobiol.* **47**, 673–98 (2013).
169. Kamholz, J. *et al.* Charcot-Marie-Tooth disease type 1: molecular pathogenesis to gene therapy. *Brain* **123** ( Pt 2, 222–233 (2000).

170. Notterpek, L., Ryan, M. C., Tobler, a R. & Shooter, E. M. PMP22 accumulation in aggresomes: implications for CMT1A pathology. *Neurobiol. Dis.* **6**, 450–460 (1999).
171. Fortun, J. *et al.* Impaired proteasome activity and accumulation of ubiquitinated substrates in a hereditary neuropathy model. *J. Neurochem.* **92**, 1531–1541 (2005).
172. Fortun, J. *et al.* Alterations in degradative pathways and protein aggregation in a neuropathy model based on PMP22 overexpression. *Neurobiol. Dis.* **22**, 153–164 (2006).
173. Carenini, S. *et al.* The role of macrophages in demyelinating peripheral nervous system of mice heterozygously deficient in P0. *J. Cell Biol.* **152**, 301–308 (2001).
174. Desurkar, a. *et al.* Charcot-Marie-Tooth (CMT) disease 1A with superimposed inflammatory polyneuropathy in children. *Neuropediatrics* **40**, 85–88 (2009).
175. Vital, A. *et al.* Inflammatory demyelination in a patient with CMT1A. *Muscle and Nerve* **28**, 373–376 (2003).
176. Ginsberg, L. *et al.* Coexistent hereditary and inflammatory neuropathy. *Brain* **127**, 193–202 (2004).
177. Carvalho, A. a S. *et al.* Charcot-Marie-Tooth disease type 1A: clinicopathological correlations in 24 patients. *J. Peripher. Nerv. Syst.* **10**, 85–92 (2005).
178. Schlaepfer, W. W. & Prensky, A. L. Quantitative and qualitative study of sural nerve biopsies in Krabbe's disease. *Acta Neuropathol.* **20**, 55–66 (1972).
179. Wang, S. *et al.* Human iPSC-derived oligodendrocyte progenitor cells can myelinate and rescue a mouse model of congenital hypomyelination. *Cell Stem Cell* **12**, 252–264 (2013).
180. Williams, R. R. & Bunge, M. B. *Schwann cell transplantation: A repair strategy for spinal cord injury?* *Progress in Brain Research* **201**, (Elsevier B.V., 2012).

## Appendix 1: Protocol for Schwann cell differentiation from human pluripotent stem cells

### 1. Purpose

Derivation of Schwann cells has enormous implications for the study of peripheral neuropathies. Here we describe a defined method to directly differentiate human pluripotent stem cells into Schwann cells, followed by antibody based FACS purification and culture.

## 2. Materials

### 2.1 Equipment

1. Cell culture disposables: Cell culture dishes, multiwell plates, centrifuge tubes, pipettes, pipette tips, sterile filter units.
2. Nylon mesh cell strainers, 45  $\mu\text{m}$  pore size (BD Falcon, cat. no. 352340).
3. Glass Pasteur pipettes, sterilized by autoclaving and dry heat monitored with indicator tape.
4. Bench-top laminar flow hood with a HEPA filter.
5. Inverted microscope.
6. Picking hood.
7. Dissecting microscope.
8. CO<sub>2</sub> incubator with CO<sub>2</sub>, humidity, and temperature control.
9. Cell culture centrifuge.
10. Glass hemocytometer.

### 2.2 hPSC culture

1. Human embryonic stem cells or induced pluripotent stem cells (see *Note 1*)
2. MEF CF-1 mitomycin-C treated mouse embryonic fibroblasts (MEFs; Applied StemCell, Inc., ASF-1223).
3. MEF medium containing 900 mL of Dulbecco's modified Eagle medium (Life Technologies, cat. no. 11965-118), 100 mL fetal bovine serum (Life Technologies, cat. no. 26140-095). The medium is sterile-filtered before use.
4. Recombinant FGF2 (R&D, cat. no. 233-FB-001MG/CF) prepared as 100 $\mu\text{g}/\text{ml}$

stock in 1x DPBS containing 0.1% BSA (see *Note 2* about growth factors).

5. hESC medium containing 800 mL of DMEM/F12 hESC medium (Life Technologies, cat. no. 11330-032), 200 mL knockout serum replacement (KSR; Life Technologies, cat. no. 10828-028), 5 mL L-glutamine (200 mM, Life Technologies, cat. no. 25030-081), 10 mL MEM non-essential amino acids (MEM NEAA; Life Technologies, cat. no. 11140-050), and 1 mL of 2-mercaptoethanol (Life Technologies, cat. no. 21985-023). The medium is sterile filtered in a hood and 60  $\mu$ L of FGF2 stock is added after filtration to a final concentration of 6 ng/mL.
6. Sterile 1x DPBS (Gibco/Life Technologies, cat. no. 14190)
7. Gelatin coated dishes made by adding enough gelatin to coat the bottom of the dish (0.1% gelatin in PBS, Chemicon/Millipore, cat. no. ES-006-B). Allow gelatin to incubate for at least 15 minutes prior to plating cells. Remove gelatin before plating.
8. Dispase (5U/ml, Stem Cell Technologies, cat. no. 07913)
9. MEF conditioned medium (CM) is harvested from MEF coated flasks. MEFs are plated at a density of 50,000 cells/cm<sup>2</sup> in a T225 flask in MEF medium. The next day, the cells are washed once with PBS before adding 100 mL of hESC medium. Incubate medium with MEFs for 24 hours before removal. The medium is now known as "conditioned medium" (CM) and can be directly used or stored at 4 °C for less than two weeks. Additional hESC medium can be conditioned daily for up to ten days on the same flask of feeders. Just before using, FGF2 is added to CM to a final concentration of 10 ng/mL, hereafter called complete CM (cCM).

### 2.3 Schwann cell differentiation

1. Accutase (Innovative Cell Technologies, cat. no. AT104)
2. Nylon mesh cell strainers, 45  $\mu\text{m}$  pore size (BD Falcon, cat. no. 352340)
3. Matrigel Basement Membrane Matrix (BD Bioscience; cat. no. 354234: we only use lots that contain over 10 mg/ml protein). Thaw the frozen vial of Matrigel on ice overnight in a 4°C refrigerator. Prepare 1 mL aliquots in a 50 mL centrifuge tube using chilled pipettes and freeze at -20°C. Matrigel must be thawed slowly to prevent gelatinization. Chilled pipettes and 50 mL centrifuge tubes should be used when making aliquots of the Matrigel.
4. KSR medium, containing 820 mL of Knockout DMEM (Life Technologies; cat. no. 10829-018), 150 mL KSR (Life Technologies, cat. no. 10828-028), 10 mL L-glutamine (200 mM, Life Technologies, cat. no. 25030-081), 10 mL MEM NEAA (Life Technologies, cat. no. 11140-050), and 1 mL of 2-mercaptoethanol (Life Technologies, cat. no. 21985-023).
5. NB medium, containing 1000 mL of Neurobasal medium (Life Technologies, cat no. 21103-049), 10 mL L-glutamine (Life Technologies, cat. no. 25030-081), 20 mL B27 supplement (Life Technologies, cat. no. 12587-070), and 10 mL N2 supplement (Life Technologies, cat. no. 17502-048)
6. SB-431542 (Tocris Bioscience, cat. no. 1614) prepared at 10 mM in 100% ethanol (1000x stock).
7. LDN-193189 (Stemgent, cat. no. 04-0074) prepared at 500  $\mu\text{M}$  in DMSO (1000x stock).
8. Y-27632 dihydrochloride (Tocris Bioscience, cat. no. 1254) prepared at 10

mM in sterile water (1000x stock).

9. CHIR 99021 (Tocris Bioscience, cat. no. 4423) prepared at 6 mM in DMSO (2000x stock).
10. DAPT (R&D Systems, cat. no. 2634) prepared at 10 mM in DMSO (1000x stock.)
11. Dibutyl cAMP (Sigma, cat. no. D0627) prepared at 100 mM in sterile water (500x stock).
12. Sodium L-ascorbate (Sigma, cat. no. A4034) prepared at 100 mM in sterile water (500x stock).

#### 2.4 Schwann cell purification and culture

13. 1mg/ml mouse laminin I solution (LAM; Cultrex, R&D Systems, cat. no. 3400-010-1, 1000x stock).
14. 2mg/ml human fibronectin (FN; R&D Systems, cat. no. 1918-FN-02M, 1000x stock)
15. FN/LAM-coated dishes: Add 1ug/ml LAM and 2ug/mL FN (in PBS) to 12 well cell culture plates. Incubate at least two hours, preferably overnight – longer incubation improves adhesion. Before using plates, aspirate medium.
16. DMEM with 10% FBS, containing 450 mL DMEM high glucose (Life Technologies, cat. no. 11965-118) and 50 mL fetal bovine serum (Hyclone, cat. no. SH30070.03).
17. DNase1 (Roche applied science, cat. no. 10104159001) prepared at 10 mg/mL in sterile water.
18. FACS buffer, containing 40 mL DPBS (Corning, cat. no. 21-031-CV), 10 mL DMEM with 10% FBS, and 100 uL of 10 mg/mL DNase1 solution.

19. Human Integrin alpha 4/CD49d Phycoerythrin MAb (Clone 7.2R) (R&D Systems, cat. no. FAB1354P).
20. NB medium with 1% FBS, containing 49.5 mL NB medium and 0.5 mL fetal bovine serum (Hyclone, cat. no. SH30070.03).
21. Trypsin EDTA, 0.25% (Life Technologies, 25200-114)

### 3. Methods

#### 3.1 Grooming and preparation of hPSCs for differentiation

1. Groom pluripotent cells (hESCs or hiPSCs) using the picking hood, objective microscope and 200  $\mu$ L pipette with sterile filter tips. Remove any pluripotent colonies that have the appearance of differentiated cells, irregular borders, or transparent centers.
2. Aspirate hESC medium and add minimal Accutase to coat the dish and let sit at 37°C until all colonies are rendered to single cells (approximately 20 minutes). Amount used: 1 ml for a 6 well dish, 2 ml for a 6 cm dish, or 5 ml for a 10 cm dish.
3. Avoiding bubbles, triturate the cells in the dish using a pipette with additional hESC medium until there is a single cell suspension and filter using a 45  $\mu$ m nylon cell strainer to remove clumps.
4. Wash and centrifuge cells (200 x g for 5 minutes) twice in hESC medium to remove all traces of Accutase.
5. While washing, prepare Matrigel-coated dishes. Add 19 mL of DMEM:F12



to the frozen Matrigel aliquot (see equipment setup) and pipette until thawed. Work quickly and do not let the Matrigel warm up or it will polymerize. A 45  $\mu\text{m}$  nylon cell strainer can be used to remove any insoluble clumps. Coat 24 well cell culture plates with the diluted Matrigel solution and incubate for 1 hour at 37 degrees Celsius.

6. After washing hPSCs, resuspend the cells in hESC medium containing 10  $\mu\text{M}$  Y-27632 and plate on a gelatin-coated dish 2-3x the area as step 2 (e.g. 10 cm gelatin-coated dish for a 6 cm dish of Accutase treated cells). (*Y-27632 prevents single hPSCs from dying*)
7. Incubate dish at 37°C for 30 minutes in a cell incubator.
8. After 30 minutes, collect the non-adherent cells and wash the dish with hESC medium containing 10  $\mu\text{M}$  Y-27632 and centrifuge cells.
9. Resuspend the cells in cCM + 10  $\mu\text{M}$  Y-27632.
10. Determine the cell concentration using a hemocytometer and add cCM + 10  $\mu\text{M}$  Y-27632 to the appropriate cell volume to achieve 70,000 to 120,000 cells/well in a 24 well plate.
11. Aspirate Matrigel solution.
12. Plate pluripotent cells on Matrigel-coated dishes at 70,000 to 120,000 cells/well in a 24 well plate.
13. Twenty-four hours after plating, aspirate medium and add fresh cCM + 10  $\mu\text{M}$  Y-27632.
14. Forty-eight hours after plating, aspirate the medium and add fresh cCM – from this point on, Y-27632 is no longer necessary. Cells can be maintained for additional days in cCM until the ideal differentiation density is obtained

(~70%-80% confluence for schwann cell differentiation).

### 3.2 Schwann cell differentiation

10. Prepare hPSCs for neural induction as described above in 3.1 and maintain until 70-80% confluence is reached.
11. To initiate differentiation, aspirate the medium and add KSR medium containing 10  $\mu$ M SB-431542 and 500 nM LDN-193189 (day 0).
12. On day 2 of differentiation, aspirate the medium and add KSR medium containing 10  $\mu$ M SB-431542, 500 nM LDN-193189, 3  $\mu$ M CHIR 99021, 10  $\mu$ M DAPT. (*activates WNT while blocking gamma secretase/Notch*)
13. On day 4 of differentiation, aspirate the medium and add KSR/NB (3:1) medium containing 3  $\mu$ M CHIR 99021 and 10  $\mu$ M DAPT (final concentrations are for the combined KSR/NB mixture).
14. On day 6 of differentiation, aspirate the medium and add KSR/NB (1:1) medium containing 3  $\mu$ M CHIR 99021 and 10  $\mu$ M DAPT.
15. On day 8 of differentiation, aspirate the medium and add KSR/NB (1:3) medium containing 3  $\mu$ M CHIR 99021 and 10  $\mu$ M DAPT. Some toxicity may be observed that is inversely correlated with efficiency of SOX10 induction.
16. On day 10 of differentiation, aspirate the KSR/NB and add NB medium containing 200  $\mu$ M dibutyrl cAMP and 200  $\mu$ M sodium L-ascorbate.
17. On day 14 of differentiation, aspirate the NB and add NB medium containing 200  $\mu$ M dibutyrl cAMP and 200  $\mu$ M sodium L-ascorbate.
18. On day 18 of differentiation, aspirate the NB and add NB medium containing 200  $\mu$ M dibutyrl cAMP and 200  $\mu$ M sodium L-ascorbate.

19. Maintain in this manner until day 21-23 of differentiation, when the cells are ready for purification.

### 3.3 Schwann cell purification using CD49d antibody

1. Prepare hPSCs for schwann cell induction as described above in 3.1
2. Aspirate hESC medium and add minimal Accutase with 50  $\mu\text{g}/\text{mL}$  DNase1 to coat the dish and let sit at 37°C until all colonies are rendered to single cells (approximately 30 minutes). Amount used: 0.25 mL for each well of a 24 well plate
3. Avoiding bubbles, triturate the cells in the dish using a pipette with additional DMEM + 10% FBS medium until there is a single cell suspension.
4. Centrifuge cells (200 x g for 4 minutes) to remove Accutase.
5. Resuspend cells in FACS buffer to a concentration of approximately 10 million cells/mL, and filter using a 45  $\mu\text{m}$  nylon cell strainer to remove clumps. Dilute 50  $\mu\text{L}$  of these cells in 500  $\mu\text{L}$  FACS buffer to serve as an unstained control for FACS.
6. Stain the remaining cells with the CD49d-PE antibody, diluted in a 1:100 volumetric ratio of antibody to cells. Incubate on ice, covered from light, for 10-15 minutes, tapping occasionally.
7. Wash the cells with two volumes of FACS buffer, and centrifuge (200 g for 4 minutes).
8. Resuspend cells in FACS buffer at a concentration of approximately 10 million cells/mL.

9. Perform FACS and collect CD49d-PE+ (Schwann cell) and CD49d-PE- (non-Schwann cell) populations.
10. For culturing of Schwann cells after FACS, two approaches may be employed. Method A: Use a 2 mL pipet to pipet 50,000 cells into each well of a 12 well plate coated in FN/lam. Add at least 1 mL of NB + 1% FBS medium to each well. Change medium once cells adhere, typically 2-4 days. Method B: Centrifuge freshly sorted cells (200 g for 5 min) and gently tap to resuspend in NB + 1% FBS. Plate 50,000 cells into each well of a 12 well plate coated in FN/lam.
11. Passage cultured Schwann cells after several days upon confluency, using a 5 min trypsin incubation. Wash with DMEM + 10% FBS, centrifuge (200 g for 4 min), and resuspend in NB + 1% FBS.

## Notes:

1. Human pluripotent stem cells differ in their properties, so optimization might be required for a cell line of interest. These protocols were primarily derived using H9 hESCs although studies have also demonstrated their utility with hiPSCs. The plating efficiency, the optimal NC-inducing cell density and the concentration and timing of growth factors are all variables that might need adjustment to find the best yield for a given pluripotent stem cell source.
2. We generally purchase growth factors in bulk as lyophilized protein. Most factors are reconstituted in 1x DPBS containing 0.1% BSA at a concentration recommended by the manufacturer: storing recombinant proteins at too low of a concentration promotes instability. We do not sterile filter recombinant proteins because protein can adhere to the membrane, lowering the effective concentration of the preparation. Single-use aliquots are stored at  $-80^{\circ}\text{C}$ . After thawing, we store aliquots at  $4^{\circ}\text{C}$  for up to two weeks.

Appendix 2A: Table of qRTPCR Primers used

Primer name	Sequence (5' to 3')
LincROR fwd	GCTTAGCGGCTGAAGACTGA
LincROR rev	CTTAGCGACAATGCCATCAA
HHLA1 fwd	AAAGTTTGTGGTGGTTTTTT
HHLA1 rev	AAAAAATTAATCTCCTCCATATACCTT
S100B fwd	AGGGAGACAAGCACAAGCTG
S100B rev	CGTGGCAGGCAGTAGTAACC
Periostin fwd	CTGCCATCACATCGGACATA
Periostin rev	GCGTCTCAAAGACTGCTCCT
GPR126 fwd	CGAATGAGATGCATGTGTCC
GPR126 rev	CTTCATGGCCAACTTTGGTT
TGFBI fwd	GTCCACAGCCATTGACCTT
TGFBI rev	ACCGCTCACTTCCAGAGAGA
IL1R1 fwd	GATTGTGAGCCCAGCTAATGAG
IL1R1 rev	AGCACTGTGATGAGGGTACTCC
HS3ST3B1 fwd	TATTCAGCCTTCAGTCACCGTC
HS3ST3B1 rev	GGTACACAGGCAGGAAGAGACA
PMP22 fwd	CTGGTCTGTGCGTGATGAGT
PMP22 rev	AGATGACACCGCTGAGAAGG
TNFAIP2 fwd	TTCAAGAGGTTACGCACAC
TNFAIP2 rev	CCCTTGCTGAGTTGGATGAT
IL-6 fwd	GGTACATCCTCGACGGCATCT
IL-6 rev	GTGCCTCTTTGCTGCTTTTAC
IL-8 fwd	ATGACTTCCAAGCTGGCCGT
IL-8 rev	TCCTTGGCAAACCTGCACCT
CCL2/MCP-1 fwd	AGGTGACTGGGGCATTGAT
CCL2/MCP-1 rev	GCCTCCAGCATGAAAGTCTC
TGFB1 fwd	GCCCTGGACACCAACTATTGC
TGFB1 rev	GCTGCACTTGCAGGAGCGCAC
CXCL12 fwd	CTGGGCAAAGCCTAGTGA
CXCL12 rev	GTCCTGAGAGTCCTTTTGCG
Cxcl1 fwd	AACCGAAGTCATAGCCACAC
Cxcl1 rev	GTTGGATTTGTC ACTGTTTCAGC
Cxcl14 fwd	GTACCGAGGTCAGGAGCACT
Cxcl14 rev	TTGCACAAGTCTCCCAACTG
Mip1a/CCL3 fwd	ATGCAGGTCTCCACTGCTGCCCTT
Mip1a/CCL3 rev	GCACTCAGCTCCAGGTCGCTGACAT
CDH19 fwd	ATTGGTCAGCCAGGAGCGTTGT
CDH19 rev	GCAGATTGAGAGACAGTCAAGCG
Sox10 fwd	ATACGACACTGTCCCGGCCCTAAA
Sox10 rev	TTCTCCTCTGTCCAGCCTGTTCTC
DHH fwd	AGGATGAGGAGAACAGTGGAGC
DHH rev	TCAGTCACTCGTAGGCGCACTC

Appendix 2B: Table of primary antibodies used

<b>Antigen</b>	<b>Species</b>	<b>Company</b>
GFP	Rabbit	Cell Signaling 2956
GFP	Chicken	Abcam 13970
TUJ1	Rabbit	Covance MRB-435P
TUJ1	Mouse	Covance MMS-435P
GFAP	Rabbit	Pierce PA3-16727
GFAP	Rabbit	DAKO Z0334
S100B	Rabbit	DAKO Z0311
GalC	Mouse	EMD Millipore MAB342
Nanog	Rabbit	Cell Signaling 3580
SSEA3	Rat	DSHB MC-631
SSEA4	Mouse	DSHB MC-813-70
Tra1-60	Mouse	Cell Signaling 4746
Tra1-81	Mouse	Cell Signaling 4745
Periaxin	Rabbit	Sigma HPA001868
MPZ	Chicken	Novus NB100-1607

## **Bipasha Mukherjee-Clavin**

### **Birth Date and Place**

April 24, 1985 in Seattle, Washington, USA

### **Education**

- Ph.D. Neuroscience Graduate Program, 2011-2015  
Thesis title, "Modeling Charcot Marie Tooth 1A with Human Pluripotent Stem Cells"  
Johns Hopkins University School of Medicine  
Research Advisor: Gabsang Lee, Assistant Professor of Neurology and Neuroscience
- M.D. In progress, 2009-present  
Johns Hopkins University School of Medicine
- B.A. Molecular and Cell Biology, 2007  
University of California, Berkeley  
Emphasis in Biochemistry  
Minor in BioEngineering  
GPA 3.77, Graduation with Distinction

### **Experience**

PhD Candidate Oct 2011-May 2015  
Lab of Gabsang Lee, DVM/PhD, Assistant Professor of Neurology and Neuroscience  
Johns Hopkins University School of Medicine

As part of my dissertation, I first developed a methodology for differentiating human embryonic stem cells (hESCs) and human induced pluripotent stem cells (hiPSCs) into Schwann cells. This methodology was then applied to the creation of an in vitro model of Charcot Marie Tooth 1A, a genetic peripheral neuropathy caused by Schwann cell



dysmyelination and demyelination. Skin fibroblasts from CMT1A patients were epigenetically reprogrammed into hiPSCs and subsequently differentiated into Schwann cells. Gene expression profiling and protein expression profiling experiments then revealed a very interesting phenotype of dysregulated immune signaling, which is not classically considered to play a role in CMT1A pathogenesis, but has been reported in multiple CMT1A animal models by other investigators. Results from our CMT1A hiPSC-derived Schwann cells were validated using CMT1A hESC-derived Schwann cells as well as CMT1A skin fibroblasts that were directly converted into Schwann cells without entering a pluripotent state. hiPSCs, hESCs, and direct lineage converted cells represent the three models currently available, and this work is notably the first report utilizing all three models to demonstrate a consistent phenotype.

PhD Rotation Student

Jun 2010 – Aug 2010

Lab of Michael Caterina, MD/PhD, Professor of Biological Chemistry and Neuroscience  
Johns Hopkins University School of Medicine

I helped investigate the role of TRPV3 in regulating skin inflammation, and also explored the role of skin (keratinocytes) in mediating heat sensation by trying to determine whether signaling can occur between keratinocytes and sensory neurons.

Staff Research Associate/Lab Manager

Jun 2007 – May 2009

Lab of Robert Edwards, MD, Professor of Neurology and Physiology  
University of California, San Francisco

Performed functional and structural studies of the synaptic vesicle protein, Vesicular Monoamine Transporter 2 (VMAT2). (See Zhang H, et al. and Gubernator NG, et al.)

Paid Research Intern

Jun 2005 – May 2007

Lab of Frank Fanqing Chen, PhD, Staff Scientist  
Lawrence Berkeley National Labs

Paid Research Intern

Jun 2006 – Aug 2006

Gene Technologies Group

Berlex Laboratories, Richmond, CA (now Bayer)

Paid Research Intern

Summer 2003, 2004

Lab of Mitchell Singer, Professor of Microbiology  
University of California, Davis

### Honors and Awards

Medical Scientist Training Program Fellowship 2011-present  
Johns Hopkins University School of Medicine

Recipient, Foundation for Advanced Research in the 2013-2014  
Medical Sciences (FARMS) Fellowship

Dean's List, College of Letters and Sciences, UC Berkeley 2003-2007  
Awarded 6 of 8 semesters; acknowledges the top 4% of students in the  
College of Letters and Sciences

### Academic Publications

**Mukherjee-Clavin B**, Kim Y, Lim H, Choi I, Oh Y, Lannon B, Eggan K, Hoke A, Studer L, and Lee G. Three congruent human Schwann cell models of CMT1A 1 reveal a converged phenotype. (Under revision for resubmission)

**Mukherjee-Clavin B**, Tomishima M, Lee G. Current approaches for efficient genetic editing in human pluripotent stem cells. *Frontiers in Biology*. 2013 Oct; 8(5): 461-467.

Lee G, Ramirez CN, Kim H, Zeltner N, Liu B, Radu C, Bhinder B, Kim YJ, Choi IY, **Mukherjee-Clavin B**, Djaballah H, Studer L. Large-scale screening using familial dysautonomia induced pluripotent stem cells identifies compounds that rescue IKBKAP expression. *Nature Biotechnology*. 2012 Dec; 30(12):1244-8

Sun C, Su KH, Valentine J, Rosa-Bauza YT, Ellman JA, Elboudwarej O, **Mukherjee B**, Craik CS, Shuman MA, Chen FF, Zhang X. Time-resolved single-step protease activity quantification using nanoplasmonic resonator sensors. *ACS Nano*. 2010 Feb 23; 4(2):978-84.

Zhang H, Gubernator NG, Yue M, Staal RG, Mosharov EV, Pereira D, Balsanek V, Vadola PA, **Mukherjee B**, Edwards RH, Sulzer D, Sames D. Dopamine release at individual presynaptic terminals visualized with FFNs. *J Vis Exp*. 2009 Aug 31;(30).

Gubernator NG, Zhang H, Staal RG, Mosharov EV, Pereira DB, Yue M, Balsanek V, Vadola PA, **Mukherjee B**, Edwards RH, Sulzer D, Sames D. Fluorescent false neurotransmitters visualize dopamine release from individual presynaptic terminals. *Science*. 2009 Jun 12; 324(5933):1441-4.

Tang YJ, Ashcroft JM, Chen D, Min G, Kim C, **Mukherjee B**, Larabell C, Keasling JD, Chen FF. Charge-associated effects of fullerene derivatives on microbial structural integrity and central metabolism. *Nano Letters*. 2007 Mar; 7(3): 754-60.

Liu GL, Yin Y, Kunchakarra S, **Mukherjee B**, Gerion D, Jett SD, Bear DG, Gray JW, Alivisatos AP, Lee LP, Chen FF. A nanoplasmonic molecular ruler for measuring nuclease activity and DNA footprinting. *Nature Nanotechnology*. 2006 Oct; 1(1): 47-52.

Pham VD, Shebelut CW, **Mukherjee B**, Singer M. 2005. RasA is required for *Myxococcus xanthus* development and social motility. *J Bacteriol*. 2005 Oct; 187(19): 6845-8.

## **Public outreach**

**Bipasha Mukherjee-Clavin**, Carolina Montañó, Neil M. Neumann and Wan R. Yang. U.S. must restore biomedical research funding. *Baltimore Sun*. Sep 17, 2013.

Anirudh Ramesh, Karlo Perica, Meghana Desale, **Bipasha Mukherjee**, Stephanie McLaughlin. A great victory, but the work is not done. *Baltimore Sun*. Jul 2, 2012.

## **Leadership**

Founder and co-leader, Association of Women Student MD/PhDs Mar 2012 - present

Longitudinal attrition of women physician-scientists across all stages of training and career development is a well-established phenomenon, yet the factors leading contributing to this phenomenon are often not well understood. Several colleagues, faculty, and I came together to found an organization dedicated to addressing barriers to women's advancement and promoting women's important roles as leaders and vital contributors to the fields of science and medicine. My roles includes mentorship and outreach to undergraduates considering pursuing an MD/PhD, organizing networking events with junior and senior female faculty, and recruiting male peer and faculty allies.

In Feb 2016, I am also chairing a full day event in which Jo Handelsman, Associate Director of Science at the White House, interfaced with Johns Hopkins graduate students, faculty, and senior leadership to discuss her research findings regarding unconscious bias in academia as well as her policy efforts to promote gender equality. This was part of the annual Catherine DeAngelis Lectureship to recognize women in science, and event became one of the capstone events of the Johns Hopkins School of Medicine Office of Women in Science and Medicine and of the Office of Faculty Affairs.

Founder and co-leader, MD/PhD Student Advisory Board Jan 2012 - present

Out of a desire to promote greater student involvement in the MD/PhD program, several students and I came together to form this advisory board. Together, we have implemented a faculty-student mentorship program, increased the diversity of our invited speakers, created programming on professional development for physician-scientists, and succeeding in fostering a collegial and inclusive atmosphere within our program.

Leadership Board, Maryland Doctors for America Sep 2009 - 2014

Doctors for America is an organization dedicated to promoting health care access for all, as well as educating the public about the Affordable Care Act (ACA). Prior to the passage of the ACA, I attended town halls, organized phone banks, lobbied my representatives, wrote op-eds in local papers, and spoke to the media to encourage the passage of a comprehensive health care reform bill. After passage of the ACA, I lead a committee that created a

series of educational materials to better inform both patients and health care providers about the effects of health care reform.

### **Teaching**

Neuroanatomy dry and wet labs, JHUSOM	2015
Cell Physiology, JHUSOM	2012
Neuroanatomy wet lab, JHUSOM	2012

### **Extracurricular**

Bharatanatyam (classical Indian) dancer for 14 years  
Sourdough yeast culture and baking  
Traveling domestically and internationally